Natural remanent magnetization acquisition in bioturbated sediments

Insights from redeposition experiments in a biologically-active environment and general theory

Xiangyu Zhao

München 2015

Natural remanent magnetization acquisition in bioturbated sediments

Insights from redeposition experiments in a biologically-active environment and general theory

Xiangyu Zhao

Dissertation

an der Fakultät für Geowissenschaften

der Ludwig-Maximilians-Universität

München

vorgelegt von

Xiangyu Zhao

aus Qingdao, China

München, den 23.07.2015

Erstgutachter: Prof. Dr. Stuart Gilder

Zweitgutachter: Prof. Dr. Tilo von Dobeneck

Tag der mündlichen Prüfung: 29.10.2015

Contents

List of Figures

Lists of Tables

Summary

Sedimentary rocks are commonly found on the Earth's surface. Their relatively continuous coverage in time and space provides a detailed record of the evolution of the Earth system, and the magnetic signals preserved within them serve as useful tools for Earth scientists, not only to understand the evolution of the geomagnetic field, but also for geochronology, tectonic reconstructions, paleoclimate studies, etc. Despite intense research, several details remain unclear just how sediments acquire their magnetic remanences. One major obstacle concerns reproducing in laboratory the essential process of acquisition in nature. Most redeposition experiments use crushed or disaggregated sediments, where living organisms are completely eliminated. This becomes a critical issue when studying sediments naturally subjected to bioturbation, which as it will be shown in this thesis, can be driven by microorganisms to an extent that affects the acquisition of a natural magnetization. Among such microorganisms, an important role is played by magnetotactic bacteria with chains of nanometer-sized iron oxide and iron sulfide crystals (magnetosomes). These crystals have been recently considered as an important contributor to the magnetic remanence in a wide range of sediments, yet the knowledge of the underlying mechanism remains incomplete. Three key missing elements are (1) the structure of the remanence carriers; (2) the acquisition efficiency of magnetosomes with respect to detrital (or primary) magnetic minerals; (3) the influence of living organisms that stir up (randomize) the sediment through bioturbation. This thesis addresses these problems.

We conducted a research program concentrating on natural sediments rich in microfauna including magnetotactic bacteria. First, the rock magnetic experiments show that ~87% of the magnetization in these sediments is carried by single domain magnetite that likely comes from magnetosomes derived from bacteria. However, the relative contribution of live magnetotactic bacteria to the total magnetic signal is negligible, on the order of 1‰, as estimated from cell counts. This suggests that the fossil magnetosomes (magnetofossils) dominate the remanence in the sediment. Next, two main types of redeposition experiments were performed with such sediments in their original form thereby preserving the living microorganisms (mainly non-magnetic bacteria). The first concerns in-field deposition as the sediment settles, which is called a depositional remanent magnetization (DRM). In the second type, the sediments are fully settled in a zero magnetic field and then the field is turned on. This is known as a post-depositional remanent magnetization (PDRM). We also measured the decay of the acquired remanence after the field was turned off. All experiments were carried out in triplicate and were repeated using sediments with different concentrations of biomass and in different field strengths.

We demonstrate that both DRM and PDRM carriers are mainly single domain magnetic minerals, attached to larger sediment particles, as a consequence of a flocculation process occurring directly inside the sediment. We can further demonstrate that the magnetic structure of PDRM carriers experience negligible magnetic interactions, as seen by the insensitivity of PDRM

to magnetic pre-treatments that would change the magnetic moment of non-single domain or interacting single-domain particles. Given the magnetofossil-bearing nature of the sediment used for the experiments, flocs involved in PDRM acquisition likely consist of single intact magnetosome chains adhering to one or more sediment particles. The efficiency of DRM acquisition in our sediments is comparable with previous redeposition experiments, however, PDRM can easily reach ~50% of DRM, significantly exceeding the previously assumed limit of 10%. We also observed a drastic loss of remanence after leaving the sediments in a zero field. Through control experiments, we discovered that these characteristics in fact result from bioturbation. The acquisition/decay rate of the remanences is sensitive to the biomass which in turn modulates the intensity of bioturbation. Finally, we found the acquisition of (P)DRM depends nonlinearly on the field intensity in most cases.

Classic theories and models could not explain the experimental findings. This thesis therefore develops a new theory to account for remanence acquisition in sediment under the influence of (a) magnetic torques, (b) randomizing torques, and (c) torques resulting from inter-particle forces. In the framework of the general theory, DRM and PDRM are no longer exclusive processes. Dynamic equilibrium between (a) and (b) in the water column and at the sediment-water interface generates a DRM, while much stronger randomizing torques may occur through bioturbation inside the mixed layer resulting in a PDRM, which is stabilized by mechanical interaction forces. Both processes are governed by a lock-in function that depends on rotational diffusion, mixed layer thickness and sedimentation rate. This model explains (1) lock-in delays that can be matched with empirical reconstructions from paleomagnetic records, (2) the existence of small lock-in depths that lead to DRM preservation, (3) specific acquisition efficiencies of magnetofossil-rich sediments, and (4) some relative paleointensity artifacts. The model can quantitatively explain the observed data, supporting the experimental discovery of the effect of microbial bioturbation on remanence acquisition.

This study confirms that bioturbation is responsible for the acquisition of a PDRM inside the surface mixed layer, which eventually replaces the initial DRM if rotational diffusion is fast enough with respect to the mean residence time of particles in this layer. These experiments support the conclusion that DRM and PDRM represent two stages of a statistical equilibrium between magnetic and perturbing torques: DRM is the first stage that applies to the sediment-water interface, and PDRM is the later stage developing inside the more strongly perturbed mixed layer. The kinetics of particle reorientation, which is dictated by a rotational diffusion coefficient, determines whether DRM survives the new equilibrium or it is replaced by a PDRM. The difference between DRM and PDRM intensities might be larger in naturally deposited sediment owing to higher shear strengths that must be overcome by perturbing torques. This new quantitative understanding of how sediment becomes magnetized in the Earth's field will hopefully facilitate the development of better techniques for paleointensity reconstructions, especially if proxies for bioturbation activity can be used.

Chapter 1 Introduction and overview

The Earth's gravity and magnetic fields reflect the distributions of mass and electric currents inside our planet, therefore providing essential information about internal dynamic processes [e.g. Blakely, 1996]. These fields also affect living organisms: gravity in an obvious manner, and magnetism for navigation purposes. Besides humans, the most evident example is that of magnetotactic bacteria [e.g. Blakemore, 1975; Bellini, 2009a, b; Frankel, 2009; Mao et al., 2014b]. More evolved species, such as bees [Kuterbach et al., 1982], trouts [Eder et al., 2012], birds [Wiltschko and Wiltschko, 2005] and whales [Walker et al., 2002] appear to use magnetic navigation as well. The Earth magnetic field plays an important role as a shield against the solar wind, drastically reducing the radiation exposure of living organisms [Elsasser et al., 1956; Black, 1967; Hays, 1971; Raup, 1985]. Furthermore, planetary magnetic field might be essential for a long-term protection against atmospheric erosion from the solar wind, although the quantification of such effects is controversial [e.g. McCormac and Evans, 1969; Lundin, 2001; Seki et al., 2001; Lundin et al., 2004].

Although magnetic forces were known by the ancient Greeks through loadstone (magnetite), the geomagnetic field was discovered much later. First observations through a form of magnetic compass can be dated back to the ancient Chinese as reported in the book *Lun Heng* (Critical Essays) published in AD 83 [Kono, 2007]. An ancient Chinese work, *Meng Xi Bi Tan* (The Dream Pool Essays, ca. AD 1088), also states that the magnetic south seen by compass slightly deviates from the geographic South: this may be the earliest report about the declination of the Earth's magnetic field [Needham et al., 1962; Kono, 2007]. Systematic declination measurements for navigation purposes began after the voyage of Columbus in 1493. Declination measurements were also performed to provide the correct orientation of sun compasses [Jonkers et al., 2003]. The measurements of the other two important elements of the geomagnetic field, i.e. inclination and intensity, began with Georg Hartmann and Robert Norman in the 16th century and with Carl Friedrich Gauss in 1832, respectively. Carl Friedrich Gauss and Alexander von Humboldt organized the Göttingen Magnetic Union which initiated global standardized observations among 50 observatories [Jonkers, 2007; Kono, 2007]. Nowadays, satellites significantly improve the global data coverage that eventually facilitates the harmonic spherical analysis of the field developed by Gauss [e.g. Cain, 1971; Barraclough, 1976; Langel and Hinze, 1998; Lowe et al., 2001; Neubert et al., 2001].

Modern and historical geomagnetic field measurements cover only few centuries and record the most recent variations of the geomagnetic field (secular variations). Longer records must rely on indirect observations based on the magnetization acquired in the Earth's magnetic field by pottery during firing (archaeomagnetism), and by rocks and sediments during their formation (paleomagnetism) [Butler, 1992; Tauxe, 1998]. Such records revealed a succession of polarity reversals, during which the dominantly dipolar signature of the geomagnetic field is switched. Such reversals separate periods of consistent magnetic poarity (chrons) and occur irregularly in time, the last being the Brunhes/Matuyama reversal occurred 0.7 Myr ago. The sequence of

polarity reversals led to the development of the Geomagnetic Polarity Time Scale (GPTS) [Cande and Kent, 1992; Cande and Kent, 1995; Opdyke and Channell, 1996]. The GPTS is an essential tool for geochronology, enabling relative dating of polarity sequences of unknown ages. The resolution of this dating technique is limited by chron duration. With this regard, field intensity variations within chrons have a global or regional coherence which makes intensity estimates useful for higher resolution (millennial scale) geochronology [Valet and Meynadier, 1993; Roberts et al., 2013]. The reconstruction of field intensity variations benefit from continuous records that can only be provided by sediments and sedimentary rocks.

While the determination of paleofield directions is quite straightforward, being based on a stepwise demagnetization of the natural remanent magnetization (NRM), the reconstruction of field intensities from the NRM is an extremely challenging task that requires some understanding of the physical mechanisms by which the NRM was acquired. All paleointensity techniques are based on the comparison of NRM with a magnetization acquired in the laboratory in known fields. Ideally, the laboratory magnetization should be acquired in the same manner as NRM was, although this is only rarely possible. The only fully quantitative theory of NRM acquisition deals with the thermoremanent magnetization (TRM) acquired by rocks containing single-domain (SD) particles upon cooling from above their Cure temperature (e.g. 580 ℃ for magnetite) [Néel, 1949]. Provided that no chemical alteration took place since rock formation, TRM can be reproduced in the laboratory with heating/cooling cycles in controlled fields. The protocol developed by Thellier and Thellier [1959], and improved Thellier-type methods including alteration and domain state checks [e.g. Coe, 1967; Aitken et al., 1988; Tauxe and Staudigel, 2004; Yu et al., 2004] are widely used for absolute paleointensity determinations on igneous rocks [Biggin, 2010]. Although fully quantitative models for the TRM acquisition in non-SD particles are not available, absolute paleointensity protocols have been developed, which are relatively insensitive to the domain state of remanence carriers [e.g. Dekkers and Böhnel, 2006].

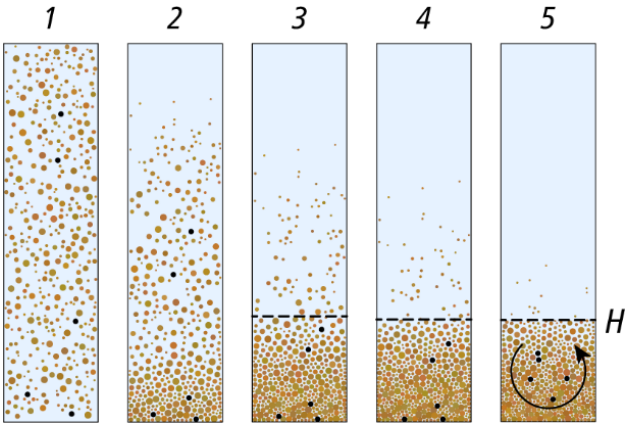

Figure 1-1 Schematic representation of sediment redeposition in five time frames. A homogeneous sediment suspension settles in a magnetic field, forming a clear sediment-water interface (dashed) after some time. The same five particles are highlighted by black dots in each frame. A DRM is acquired by alignment of magnetized particles in the ambient field during deposition (frames 1-4). This magnetization is stabilized by inter-particle forces developing at contact points (frames 3-4). Sediment mixing (arrow in frame 5) is responsible for particle realignment after deposition and generates a PDRM.

The NRM acquisition mechanism in sediments is completely different and relies on partial mechanical alignment of magnetic particles in the Earth field during or after deposition, which generate a depositional remanent magnetization (DRM) and a post-depositional remanent magnetization (PDRM), respectively. Because (P)DRM acquisition cannot be replicated under identical conditions in the laboratory, sedimentary paleointensity reconstructions are based on indirect methods that capture field intensity variations (so-called relative paleointensity), rather than absolute intensity values [Tauxe, 1993]. DRM acquisition begins in the water column (Figure 1-1), where settling particles with a magnetic moment m are aligned by the magnetic torque $\mathbf{m} \times \mathbf{B}$ exerted by the geomagnetic field $\mathbf{B}$. This alignment is counteracted by the viscous drag, which is proportional to the particle volume, and by random fluctuations of particle orientations due to the collision with water molecules (Brownian motion). Viscous drag torques determine the time required to attain the final alignment, which is of the order of 1 s for magnetite particles [Stacey, 1972], and thus sufficiently small to reach full equilibrium during settling. On the other hand, Brownian motion control the extent of the alignment at full equilibrium, which is given by the Langevin law $\langle\cos\theta\rangle = L(mB/k_BT)$, where θ is the angle between $\mathbf{m}$ and $\mathbf{B}$, $\langle\cos\theta\rangle$ is the average alignment, L is the Langevin function, k_B is the Boltzmann constant, and T the absolute temperature. The magnetic moment of magnetite particles capable of carrying a stable remanence is sufficiently large to produce equilibrium alignments that, if maintained inside the sediment, would yield much larger NRMs that generally observed. This is a well-known problem of simple DRM acquisition models that cannot be attributed to inaccuracies in the description of magnetic particle alignment and Brownian motion, since accurate experimental validations have been obtained for the case of magnetotactic bacteria swimming in water [Frankel and Blakemore, 1980; Steinberger et al., 1994]. Therefore, other mechanisms acting against magnetic alignment, such as turbulence [Heslop, 2007], particle rolling at the sediment surface [Bilardello et al., 2013], and particle aggregation [Tauxe et al., 2006], must be invoked. Widely accepted modern DRM acquisition theories rely on particle aggregation (flocculation) mechanisms [Shcherbakov and Sycheva, 2010], where magnetic moments of individual constituents are added almost randomly in large flocs. The resulting net magnetic moment is no longer proportional to floc volume, so that large flocs with small magnetic moments will not have the time to fully align with the field during deposition [Tauxe et al., 2006]. The importance of flocculation is demonstrated by the influence of salinity on redeposition experiments [Katari and Tauxe, 2000].

Once a DRM has been acquired by particles that were just incorporated in the sediment/water interface, other processes occurring inside the sediment can lead to further alignment of magnetic moments with the Earth's field, leading to the acquisition of a delayed PDRM. Differences between sediment age, dated for instance with ^{10}Be, and the age deduced from paleomagnetic records, prove that PDRM can be the dominant NRM acquisition mechanism in some cases [e.g. Suganuma et al., 2011]. The sedimentation rate ω links a time delay t with a mean depth $z = \omega t$ of PDRM of acquisition below the sediment-water interface, which is called lock-in depth. Empirical PDRM acquisition models assume a certain distribution of lock-in depths below the top mixed layer of the sedimentary column, so that original field variations are convoluted with

the lock-in distribution, yielding smoothed and delayed paleomagnetic records [Roberts and Winklhofer, 2004].

All models proposed so far to explain PDRM acquisition proved to be unsatisfactory [Roberts et al., 2013]. For example, further passive alignment of magnetic grains by a long-term viscous process that overcomes inter-particle forces [Shcherbakov and Shcherbakova, 1987] is too slow to enable significant PDRM acquisition before compaction definitively locks the acquired magnetization. This conclusion is supported by redeposition experiments. When sediment deposited in a null field is successively exposed to a controlled field, it acquires only small fractions of the DRM resulting from deposition in the same field [Shcherbakov and Shcherbakova, 1987]. On the other hand, post-depositional alignment of magnetic grains could be facilitated by bioturbation, i.e. the mixing process occurring in the topmost ~10 cm of the sedimentary column (the so-called benthic mixed layer, Figure 1-1). Laboratory simulations of bioturbation, realized by stirring sediments in an applied field, led to the acquisition of a DRM-like stable magnetization [Kent, 1973; Løvlie, 1976]. However, the magnetization was measured on dried sediments, whereby it is known that the drying process itself can lead to significant magnetizations [Henshaw and Merrill, 1979]. The role of bioturbation was questioned by experiments of Katari et al. [2000], where a bulk of marine sediment exposed to the burrowing activity of polychaete worms did not acquire a new magnetization in a reversed field.

Further complication for the understanding of sedimentary NRM comes from the recent discovery that magnetofossils (i.e. the fossil remnants of magnetotactic bacteria) are widespread and can be preserved over geological times [Roberts et al., 2012]. Because magnetofossils form directly in the uppermost sediment layers, where marine magnetotactic bacteria live and die [Petermann and Bleil, 1993], magnetofossil would not contribute to DRM acquisition but could possibly acquire a “biogenic remanent magnetization” [Heslop et al., 2013], which is equivalent to a PDRM. In this case, given the important magnetic and structural differences existing between magnetotactic bacteria first and magnetofossils at a later stage on one hand, and other magnetic particles or aggregates on the other hand, important questions arise about the efficiency of magnetofossil PDRM acquisition vs. DRM and other PDRM sources. For example, the common assumption that magnetotactic bacteria are well aligned with the Earth magnetic field [Frankel and Blakemore, 1980], which is considered a fundamental requirement for maintaining a biological advantage over other organisms, would lead to full saturation of the resulting PDRM, which contrasts with much lower NRM intensities usually observed in magnetofossil-rich sediments [e.g. McNeill and Kirschvink, 1993]. On the other hand, chain collapse after bacteria dissolution [Kobayashi et al., 2006] would drastically reduce or completely randomize any acquired magnetization, making magnetofossil contributions extremely sensitive to chain preservation and therefore erratic and unreliable. However, recent relative paleointensity investigations suggest that magnetofossils carry a consistent NRM that is far from saturation and yet different from the NRM component corresponding to detrital remanence carriers [Ouyang et al., 2014].

Again, as with conventional PDRM models, postulated acquisition mechanisms do not provide a satisfactory explanation of observed paleomagnetic records and apparent rock-magnetic

artifacts therein [e.g. Yamazaki et al., 2013]. This is a crucial problem, since future improvements of relative paleointensity records must rely on a better understanding of processes leading to NRM acquisition and their dependence on the type of remanent magnetization carrier involved, as well as other factors such as bioturbation and physical/chemical properties of the sediment. Any variation of these parameters can lead to NRM intensity changes that could be erroneously attributed to the Earth magnetic field. However, only the role of remanent magnetization carriers in the NRM normalization process has been addressed until now [Tauxe, 1993].

Some of the abovementioned shortcomings of PDRM acquisition models, especially in magnetofossil-rich sediments, have been addressed in Mao et al. [2014b]. For example, the role of bioturbation was discussed in relation with existing estimates of solid diffusion rates in the mixed layer, which, if extrapolated to the rotational diffusion of magnetic remanence carriers, would lead to complete randomization of the initial DRM in unrealistically short times. On the other hand, living magnetotactic bacteria appear to be very poorly aligned with the Earth's magnetic field ($<\cos\theta> < 0.01$), providing a more realistic starting point for magnetofossil PDRMs, which does not require chain collapses to explain observed NRM intensities. Yet, an appropriate PDRM acquisition model backed by convincing experimental proofs was missing at the time this dissertation was started.

The aim of the present work was to develop a new theory of PDRM acquisition backed with suitable experimental verification. The first two chapters describe PDRM acquisition experiments conducted on freshly collected sediment containing living magnetotactic bacteria communities that have been extensively investigated in the past [e.g. Mao et al., 2014b]. The long-term presence of such bacteria in laboratory-stored sediment ensures that microscopic bioturbation – the only form of bioturbation that can be studied in samples that must fit in a rock magnetometer – is sustained by a stable community of microorganisms during PDRM acquisition experiments, eliminating the need for artificial simulations of sediment mixing, such as stirring. These experiments can therefore be considered as the closest possible analogue to post-depositional processes occurring in a natural sediment. On the other hand, the presence of magnetofossils enables a semi-quantitative derivation of mean particle alignments from measured magnetizations, providing precious constraints to PDRM acquisition theories. Experiments demonstrate that bioturbation is essential to the acquisition of a PDRM, and that the efficiency of the acquired PDRM is smaller than that of a DRM, but not negligible.

A general theory for (P)DRM is developed in Chapter 4 on the basis of experimental results discussed in Chapters 2-3. This theory uses a statistical approach to describe acquired magnetizations in terms of dynamic equilibrium between aligning and randomizing torques acting on magnetic particles subjected to additional forces representing mechanical interactions between particles. Accordingly, the initially acquired DRM is progressively lost in favor of a new equilibrium representing the conditions of the mixed layer, where randomizing torques are created by bioturbation. The newly acquired PDRM eventually replaces – totally or in part – the initial DRM, depending on the bioturbation rate and on the total time spent by sediment particles inside the mixed layer. In case of partial PDRM acquisition, NRM intensity fluctuations reflect DRM/PDRM proportions, which are in turn modulated by bioturbation intensity and

sedimentation rate. This theory is consistent with experimental observations and makes testable predictions about the effects of changes in the depositional environment that can be explored in future work. Chapter 5 demonstrates a quantitative analysis of experimental data introduced in Chapters 2-3 based on theory developed in Chapter 4.

Parts of the thesis have been published or submitted. The magnetic stability of acquired (P)DRM against AF demagnetization is part of the content in the paper by Mao et al. [2014b]. The reference is: *Mao, X., R. Egli, N. Petersen, M. Hanzlik, and X. Zhao (2014), Magnetotaxis and acquisition of detrital remanent magnetization by magnetotactic bacteria in natural sediment: First experimental results and theory, Geochem. Geophys. Geosyst., 15, 255–283, doi:10.1002/2013GC005034*. My contribution includes (1) designing experimental protocol for (P)DRM acquisition; (2) performing parts of the (P)DRM acquisition experiments and AF demagnetization; (3) analyses and discussion of data. The content of Chapter 4 has been published in G-cubed (Geochemistry, Geophysics, Geosystems). The reference is: *Egli, R., and X. Zhao (2015), Natural remanent magnetization acquisition in bioturbated sediment: General theory and implications for relative paleointensity reconstructions, Geochem. Geophys. Geosyst., 16, 995–1016, doi:10.1002/2014GC005672.* My contribution consists of (1) preliminary modelling of the decay of PDRM in zero field using the Fokker-Planck equation; (2) discussion and (3) composing the manuscript. Chapter 5 is based on the manuscript "*Microbially-assisted recording of the Earth's magnetic field in sediment*" by *Zhao, X., R. Egli, S. Gilder, X. You, K. He and S. Müller*, which has been submitted to Nature Communications. My contribution involves (1) the design of the experimental protocols; (2) performing experiments; (3) data analyses and (4) composition.

Some work done during the PhD are not included in the thesis due to the little relevance to the main theme. One work considers how secondary magnetite produced in the absolute paleointensity experiments affects the estimates, which has been published in G-cubed. The reference is: *Zhao, X., Q. Liu, G. A. Paterson, H. Qin, S. Cai, Y. Yu, and R. Zhu (2014), The effects of secondary mineral formation on Coe-type paleointensity determinations: Theory and simulation, Geochem. Geophys. Geosyst., 15, 1215–1234, doi:10.1002/2013GC005165*. My contribution consists of (1) modelling; (2) discussion and (3) composition. A second published work investigates the rock magnetic property of aluminum-substituted hematite: *Jiang, Z., Liu, Q., Zhao, X., Jin, C., Liu, C., and Li, S. (2015). Thermal magnetic behaviour of Al-substituted haematite mixed with clay minerals and its geological significance. Geophysical Journal International, 200(1), 130-143.* I was involved in (1) experimental design; (2) data analysis and (3) composition. Another work deals with the identification of magnetofossils in the Cambrian carbonaceous rocks where fossils of microorganisms have been found. Comprehensive rock magnetic experiments were performed, however, signals of magnetofossil, were not able to be distinguished, if any, due to the presence of dominant hard magnetic minerals (hematite and pyrrhotite).

Chapter 2 A case study on the acquisition of natural remanent magnetizations in magnetofossil-rich sediments

2.1 Introduction

Sedimentary strata bear continuous records of past geomagnetic field variations, through the natural remanent magnetization (NRM) acquired during and shortly after deposition. The directional information of NRM has been widely applied to tectonic reconstruction [Klootwijk et al., 1992; Acton and Gordon, 1994] and geochronology [e.g. Gilder et al., 2001; Zhu et al., 2001; Zhu et al., 2004]. Variations in relative paleointensity (RPI) derived from sedimentary NRM [King, 1955; Levi and Banerjee, 1976; Tauxe, 1993] are often globally coherent because of the dominating dipolar component of geomagnetic filed. Therefore, RPI supports high-resolution geochronology on millennial scales [Guyodo and Valet, 1996, 1999; Laj et al., 2000; Stott et al., 2002; Channell et al., 2009] that cannot be obtained from the chronology of geomagnetic reversals [Roberts et al., 2013]. Relative paloeintensity also possesses potential importance for understanding the dynamics of the geodynamo [e.g. Valet and Meynadier, 1993] and the geomagnetic field's role as a shield against cosmic rays [e.g. Elsasser et al., 1956]. While more RPI data can nowadays be obtained at higher resolution, due to instrumental advancements, robust interpretation of the fine-scaled variations becomes crucial in order to discriminate dipolar geomagnetic variations (global signals) from artifacts related to changes of the magnetic mineralogy, depositional environment, and sediment properties [Roberts et al., 2013]. For this purpose, many efforts have been devoted to understanding acquisition of sedimentary NRM since Johnson et al. [1948], which will be briefly reviewed in the following. A detailed review can be found in Tauxe and Yamazaki [2007].

The magnetization acquired by settling or resuspended sediment particles at and shortly after deposition is called depositional remanent magnetization (DRM). Nagata [1961] describes the DRM acquisition mechanism as a rotation of magnetic particles subjected to magnetic and viscous drag torques. In case of isolated magnetite particles, full alignment with external magnetic fields of the order of 50 μT is reached in less than a second [Stacey, 1972]. In this case, DRM acquired in typical geomagnetic field intensities would be close to the saturation remanent magnetization (M_{rs}), regardless of the actual field intensity, providing a useless signal for paleointensity reconstructions. Such alignment is never observed in redeposition experiments, where the acquired DRM depends, in some cases almost linearly, on the applied field intensity, although DRM/M_{rs} values obtained in this manner are about one order of magnitude larger than NRM/M_{rs} [e.g. Tauxe et al., 2006]. Furthermore, an error in inclination of laboratory DRM, termed as inclination shallowing, is oftentimes documented [e.g. King, 1955; Tauxe and Kent, 1984; Bilardello et al., 2013]. Differences between NRM acquired in nature and DRM acquired in redeposition experiments have been attributed to flocculation [Shcherbakov and Shcherbakova,

1983; van Vreumingen, 1993; Tauxe et al., 2006; Shcherbakov and Sycheva, 2010]. Flocculation is the aggregation of colliding particles during settling, due to attractive electrostatic and Van der Waals forces. During this process, the volume of aggregates, termed as floc, increases more rapidly than the net magnetic moment resulting from the vector sum of randomly or almost randomly oriented elemental contributions [Tauxe et al., 2006; Heslop, 2007]. As a result, larger flocs require more time to align with the geomagnetic field than available during (re)deposition. Most importantly, large flocs are more sensitive to hydrodynamic torques developing around settling particles in the water column [Heslop, 2007]. Redeposition experiments and numerical simulations confirm that DRM intensity drops when flocculation increases [Tauxe et al., 2006; Shcherbakov and Sycheva, 2010]. The DRM obtained from redeposition experiments is often non-linearly related to the external magnetic field, depending on the size of flocs [Tauxe et al., 2006; Mitra and Tauxe, 2009]. Lack of proportionality between NRM and geomagnetic field would further complicate the application of RPI.

NRM acquisition can continue after deposition, generating what is known as a post-depositional remanent magnetization (PDRM). The exact PDRM acquisition mechanism is not known: the two main hypotheses rely on passive alignment of particles that are not fully blocked, and on bioturbation. These processes have been simulated by laboratory experiments with unstirred [Irving, 1957; Irving and Major, 1964; Tucker, 1979] and stirred sediments[Kent, 1973; Løvlie, 1976]. Laboratory PDRM is generally characterized by (1) negligible inclination shallowing and (2) linear relationship between magnetization and the magnetizing field [Kent, 1973; Verosub et al., 1979; Barton et al., 1980; Tucker, 1980; Spassov and Valet, 2012; Mao et al., 2014b]. On the other hand, the PDRM acquired by unstirred sediment represents a negligible fraction of the DRM, and is considered irrelevant in natural sediments. Shcherbakov and Shcherbakova [1987] estimated that PDRM could reach at most only ~10% of DRM, in agreement with some experimental results [Tauxe, 1993]. On the other hand, experiments conducted with stirred sediment led to the acquisition of non-negligible magnetizations [Kent, 1973], which, however, might have originated from sample drying before measurement [Henshaw and Merrill, 1979]. Katari et al. [2000] argued that most reported laboratory PDRM experiments overestimate PDRM acquisition efficiencies, since the shear strength of remolded sediments used in experiments are significantly reduced. Higher shear strength corresponds to stronger inter-particle forces, which prevents particle rotation [Verosub et al., 1979; Payne and Verosub, 1982].

Physical properties of the sediment, such as grain size, might also influence PDRM acquisition. For instance, clay and silty sediments are characterized by smaller pores where magnetic particles can rotate [Payne and Verosub, 1982], as well as more important flocculation effects than sands and carbonates [Spassov and Valet, 2012].

New challenges for sedimentary NRM acquisition theories are introduced by the recently gained knowledge on magnetofossils, i.e. the fossil magnetic remainders of magnetotactic bacteria. Since their discovery [Blakemore, 1975], magnetotactic bacteria have been found to be ubiquitous in sedimentary environments [Bazylinski et al., 1988; Farina et al., 1990; Petermann and Bleil, 1993; Flies et al., 2005; Faivre and Schüler, 2008], leaving fossil chains of magnetite

or greigite particles – so called magnetofossils – inside the sediment matrix upon death [Kirschvink and Chang, 1984; Petersen et al., 1986; Stolz et al., 1986]. Because magnetotactic bacteria live inside the sediment, the natural magnetization possibly acquired by magnetofossils is by definition a PDRM, so that magnetotactic bacteria could be an important NRM source that might differ substantially from the contribution of other remanence carriers. However, the paleomagnetic role of magnetofossils has long been considered irrelevant, due to the widespread belief that they would not withstand reductive diagenesis and be preserved over geological times [Karlin, 1990; Leslie et al., 1990].

This point of view changed recently with development of rock magnetic techniques [Egli, 2004; Egli et al., 2010; Heslop et al., 2014] which enable reliable magnetofossil detection in a wide range of sediments with different ages and provenances [Roberts et al., 2012]. In many cases, magnetofossil contribute to >50% of the saturation remanence [Ludwig et al., 2013], so that their role as possible PDRM carriers can no longer be neglected. Heslop et al. [2013] coined the term "biogenic remanent magnetization" for designating magnetofossil contributions to the NRM.

Magnetofossil PDRM acquisition might be substantially different from the NRM acquired by other remanence carriers. One possible reason is that magnetotactic bacteria are expected to be well aligned with the Earth magnetic field, as seen in water, because this alignment is required for navigation purposes in what is known as magnetotaxis [Frankel and Blakemore, 1980]. In this case, magnetofossils would inherit this initial alignment, and a strong randomization mechanisms is required to reduce the corresponding magnetization by ~4 orders of magnitudes in order to match NRM intensities of magnetofossil-bearing sediments [McNeill and Kirschvink, 1993; Ouyang et al., 2014]. If such randomization action is associated with bioturbation, it would affect other remanence carriers as well, resulting in unrealistically large differences between NRM acquisition efficiencies of magnetofossils and detrital particles, which are not observed [Ouyang et al., 2014]. Magnetosome chain collapse after dissolution of supporting cell structures [Kobayashi et al., 2006] could provide a selective mechanism of NRM randomization acting only on magnetofossils. However, this mechanism require all chains to be affected by structural collapse, while Ludwig et al. [2013] set <50% as an upper limit. These simple thoughts demonstrate that PDRM acquisition might be far more complicated than suggested by our current understanding about sedimentary processes affecting the orientation of magnetic particles. Therefore, an experimental approach is needed to improve our understanding of NRM acquisition in sediment.

Paterson et al. [2013] performed redeposition experiments with pure suspensions of cultured magnetotactic bacteria which were allowed to dry in a magnetic field. The resulting magnetization was parallel to the applied field and proportional to its intensity, leading to the conclusion that magnetofossils could provide NRM contributions suited to RPI studies. The remanence acquired in these experiments, however, is carried by whole cells, instead of fossil chains dispersed in a non-magnetic matrix, and could result from drying [Henshaw and Merrill, 1979], rather than PDRM acquisition.

Mao et al. [2014b] used magnetofossil-rich freshwater sediments to investigate the NRM acquisition behavior under more realistic conditions, focusing on the relation between the

alignment of living magnetotactic bacteria and their fossil remainders. They found that bacteria living in sediment are very poorly aligned (<1%) with the Earth magnetic field. This finding challenges existing models of magnetic navigations, but, on the other hand, it provides a less critical starting point for magnetofossil NRM. In fact, the observed alignment is similar to that of magnetic particles in redeposition experiments [Tauxe et al., 2006], so that PDRM would start from similar initial conditions for all remanence carriers. Mao et al. [2014b] also documented a linear dependence of PDRM on magnetizing fields with a PDRM/M_{rs} ratio that is comparable to that of geological records. The poor alignment of magnetotactic bacteria and PDRM acquisition in the same sediment were interpreted as being the result of an equilibrium between magnetic torques and randomizing forces arising from bioturbation. The experiments of Mao et al. [2014b], however, were not based on full sediment deposition in a water column, so that the obtained magnetization might not fully represent a PDRM.

In order to address the possible role of bioturbation in the acquisition of a PDRM in a realistic manner that is as close as possible to real conditions in sediments, we performed redeposition experiments with freshly collected, magnetofossil-rich sediment known to host stable magnetotactic bacteria populations during laboratory storage [Mao et al., 2014b]. Magnetotactic bacteria are not by themselves necessary for these experiments, since they represent a negligible fraction of the living biomass, and, most importantly, a negligible fraction of the total magnetofossil concentration deduced from magnetic measurements. However, their presence means that the sediment is hosting a stable microbial community during the redeposition experiments, where motile organisms can provide the required driving forces for bioturbation. Mao et al. [2014a] showed that magnetotactic bacteria can displace vertically by several cm/week inside the same type of sediment used here for the PDRM experiments, ensuring us about microbial motility and associated bioturbation on a microscopic scale. These conditions have been never realized in previous redeposition experiments, since old sediment retrieved from cores and subjected to treatments typically used to disperse sediment particles can be considered as lifeless.

In this chapter, we discuss the results of (P)DRM acquisition/decay experiments in the framework of diffusive processes associated with bioturbation, while a proof of the role of microorganisms in these experiments is provided in Chapter 3.

2.2 Materials and Methods

2.2.1 Sediment collection

Sediment material for this study was collected from the top ~10 cm sediment layer in a small pond with ~1 m maximum water depth, located next to our paleomagnetism laboratory in Niederlippach (Bavaria, Germany, 48°35’14.98’’ N, 12°04’43.71’’ E) in October of 2012. The pond sediment is known to contain abundant magnetotactic bacteria populations, including the rod-shaped *M. bavaricum* and round cocci [Jogler et al., 2010; Mao et al., 2014b]. The sediment is dominantly made of clay and silt, with only 10% of particles > 63 μm based on sieve analysis. Grain size distributions (Figure 2-1) was measured with a Beckman Coutler LS230 laser

diffractometer on aqueous suspensions that were not subjected to dispersion treatments, owing to the fact that only the size of grains and grain aggregates behaving as solid units is relevant in PDRM experiments.

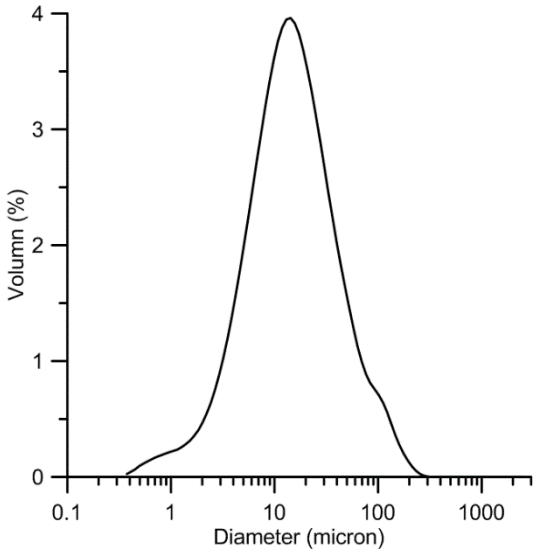

Figure 2-1 Grain size distribution of untreated sediments.

Sediments were transferred to glass aquaria at ambient temperature as described in Blakemore et al. [1979]. A stable chemical stratification with a well-defined oxygen gradient is re-established within one week of laboratory storage. After this initial stabilization, magnetotactic bacteria populations have been characterized with the hanging drop assay with a specially equipped optical microscope (Magnetodrome) as described in Mao et al. [2014b]. A few weeks after the sampling, *M. Bavaricum* was predominant, while round cocci became more numerous after 7 months. Such cycles are commonly observed with this type of sediment, while the average concentration of magnetotactic bacteria remains on the order of 10^5 cells/mL.

2.2.2 Rock magnetic properties

Bulk magnetic properties of the pond sediment are typical of many magnetofossil-bearing sediments, with hysteresis parameters ($M_{rs}/M_s \approx 0.33$, $H_{cr}/H_c = 2.273$) typical for pseudo-single domain (PSD) particles (Figure 2-2a). On the other hand, comparison of the stepwise acquisition of an isothermal remanent magnetization (IRM) with the DC demagnetization of the saturation IRM, known as Wohlfarth-Cisowski test [Cisowski, 1981], suggests that the magnetization is dominated by single-domain (SD) particles with little magnetostatic interactions (Figure 2-2b). A similar magnetic composition is also suggested by the ratio χ_{ARM}/IRM between the anhysteretical remanent magnetization (ARM) susceptibility, χ_{ARM} and IRM, which is >0.15, as expected for non-interacting SD particles [Egli and Lowrie, 2002; Egli, 2004]. The contribution of high-coercivity minerals (e.g. hematite and goethite) to the saturation remanence is small, as seen from $IRM_{0.3T}/M_{rs} \approx 95\%$.

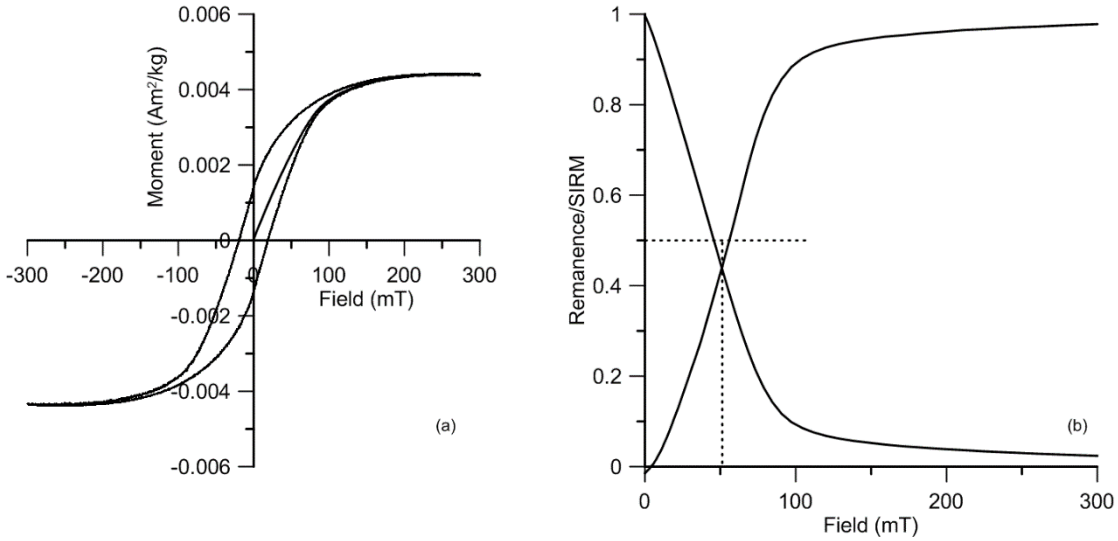

Figure 2-2 Rock magnetic measurements. (a) The typical hysteresis loop after slope correction is characterized by Mrs/Ms ≈ 0.33 and B_c = 19 mT. (b) IRM acquisition and backfield demagnetization are presented as a Wohlfarth-Cisowski test [Cisowski, 1981], suggesting the magnetic minerals have negligible magnetic interaction. Both data demonstrate high coercivity minerals have negligible contribution.

The nature of remanence carriers in the sediment used for (P)DRM acquisition experiments has been further investigated with a combination of selective dissolution of SD magnetite and high-resolution measurements of first-order reversal curves (FORC) using the procedure described in Ludwig et al. [2013]. For this analysis, dried and homogenized sediment has been divided into two aliquots: the first aliquot was used directly for measurements, while the second aliquot was treated with a citrate-bicarbonate-dithionite (CBD) solution optimized for magnetofossil dissolution according to the receipt given in Ludwig et al. [2013]: about 30 g of sediment were added to 200 ml of water containing 5 g sodium dodecyl sulphate (a detergent for cell dissolution), 15 g sodium citrate, and 4 g sodium bicarbonate. After heating the sediment suspension to 50 ℃, 6 g sodium dithionite were added and the suspension was stirred at constant temperature for ~ 1 h. Afterwards, the remaining sediments were separated by stepwise vacuum filtration with decreasing pore size of the filters down to 100 nm for magnetic analysis. The treated sediment, referred to as CBD-residue in the following, was then measured with the same protocol as the original sample (bulk sediment). As shown by Ludwig et al. [2013], the difference between identical measurements untreated and treated material corresponds to the in-situ magnetic signature of CBD-extractable magnetite, i.e. crystals <0.5 μm in size, which are directly dispersed in the sediment matrix. Larger crystals, or SD magnetite inclusions in silicate host minerals, which are protected from dissolution, are unaffected by the CBD treatment. Therefore, the CBD treatment selectively removes secondary SD magnetite, i.e. magnetofossils and authigenic particles.

High-resolution FORC measurements [Egli et al., 2010], on the other hand, are now widely used as a standard tool for magnetofossil detection [Roberts et al., 2013]. Single magnetofossil chains, as well as isolated SD particles, have a characteristic FORC signature consisting of a

horizontal ridge along $H_b = 0$. The intrinsic sharpness of this ridge is a diagnostic signature with respect to other magnetic contributions characterized by a continuous FORC function, so that the magnetic contribution of particles contributing to the central ridge can be quantified [Egli, 2013]. Collapsed magnetosome chains [Kobayashi et al., 2006], on the other hand, do not contribute to the central ridge because of strong and random magnetostatic interactions occurring within the dense particle clusters resulting from chain collapse. The whole magnetic signature of secondary magnetite particles is captured only by comparison of bulk and CBD-residue. The analysis of a magnetofossil-rich pelagic carbonate by Ludwig et al. [2013] shows that the contributions of the central ridge and remaining parts of the FORC diagram to the total FORC magnetization are almost equal, suggesting that 50% of all CBD-extractable particles were isolated or arranged in isolated linear chains, while the other 50% formed clusters of interacting particles.

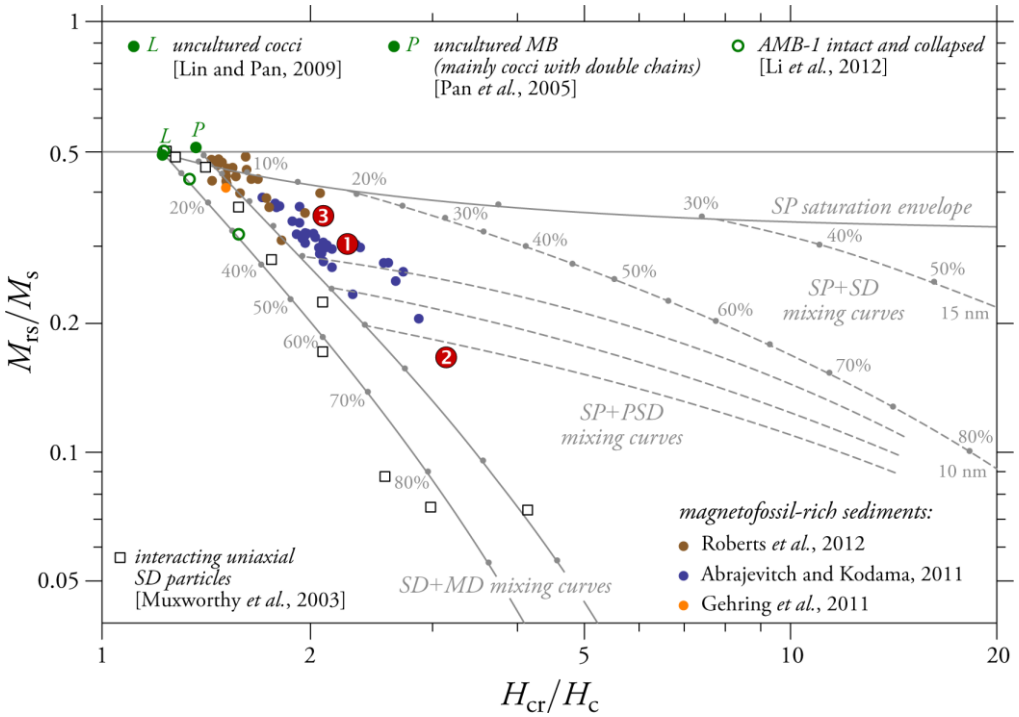

Figure 2-3 Day plot with theoretical mixing lines between superparamagnetic (SP), single-domain (SD) and multidomain (MD) magnetite particles (gray lines, after Dunlop [2002]). Circled numbers indicate the hysteresis parameters of untreated sediment (1), CBD-residue (2), and the difference between untreated sediment and residue (3). Bulk properties of magnetofossil-bearing sediments, cultured magnetotactic bacteria and interacting SD particles are shown for comparison.

High-resolution FORC measurements in field steps of ~0.5 mT have been performed with a Princeton Measurement Corporation VSM at the University of Minnesota and processed with VARIFORC [Egli, 2013]. The CBD treatment has a clear effect on bulk hysteresis properties (Figure 2-3), which are located near the SD-MD mixing line of the Day plot [Dunlop, 2002], with the CBD-residue being more close to the MD end-member and the CBD-extractable fraction being more close to the SD end-member. The mixing line defined by the CBD treatment is compatible by the trend formed by magnetofossil-rich sediments as expected from mixtures of

MD-like primary minerals and SD-like secondary minerals. The SD end-member of this trend coincides with the ideal hysteresis of non-interacting SD particles with uniaxial anisotropy. On the other hand, CBD-extractable minerals in our sediments are relatively far from this end-member.

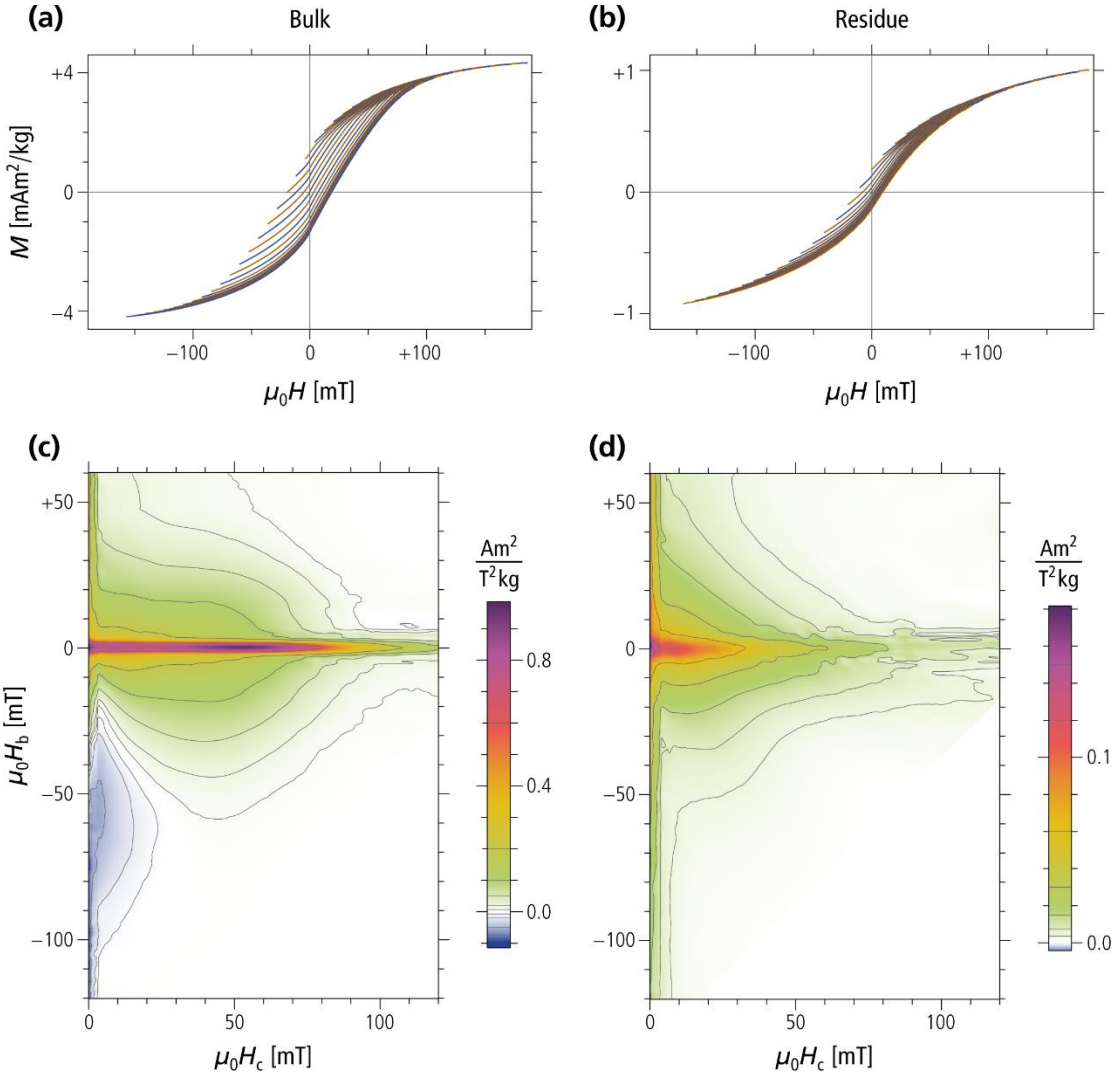

Figure 2-4 High-resolution FORC measurements of the untreated sediment (a), and the corresponding CBD residue (b). Notice the difference in scale. Every 16th curve in (a) and every 20th curve in (b) are shown for clarity. (c) FORC diagram of the untreated sediment. The following VARIFORC processing parameters have been used. Reference smoothing factor: 12; increase rate of the smoothing factor: 0.2; smoothing factor limitation along $H_c = 0$ and $H_b = 0{:}6$. (d) FORC diagram of the CBD-treated sediment. The following VARIFORC processing parameters have been used. Reference smoothing factor: 13; increase rate of the smoothing factor: 0.3; smoothing factor limitation along $H_c = 0$ and $H_b = 0{:}7$. See the VARIFORC manual (www.conrad-observatory.at/cmsjoomla/en/download) for more details about the parameters.

The saturation remanence of the CBD residue is ~13% of the untreated sediment (Figure 2-4), which means that only a minor fraction of all remanence carriers consists of magnetic particles that are resistant to the CBD treatment. As discussed before, these remanence carriers

are >500 nm in size, or of smaller sizes but protected from dissolution by inclusion in a silicate matrix. The FORC diagram of untreated sediment contains a central ridge superimposed to continuous positive and negative contributions over the remaining FORC space (Figure 2-4c). Negative contributions near the vertical axis in the lower quadrant are the typical signature of reversible magnetic moment rotation in SD particles [Newell, 2005]. On the other hand, the FORC signature of the CBD-residue is characterized by triangular contour lines with maximum vertical extension at $H_c = 0$, which is typical for PSD particles [Roberts et al., 2000; Muxworthy and Dunlop, 2002]. With these measurements we conclude that ~13% of the saturation remanence is carried by PSD particles of primary origin, while remaining remanence carriers are associated with SD minerals.

The FORC diagram of CBD-extractable particles is very similar to that of the untreated sediment (Figure 2-5), due to the limited contribution of non-extractable particles. FORC contributions over the upper quadrant (Figure 2-5b) are incompatible with non-interacting SD particles [Newell, 2005] or isolated magnetosome chains [Egli et al., 2010] and must therefore be associated with interacting SD particles, possibly from collapsed magnetosome chains [Ludwig et al., 2013]. The central ridge has been isolated from other FORC contributions using VARIFORC (Figure 2-5c). This ridge defines a clearly bimodal coercivity distribution f_{cr} peaking at $H_c = 0$ and $H_c = 60$ mT (Figure 2-5d). The second peak is compatible with the magnetofossil coercivity component 'BH' often seen in freshwater sediments [Egli, 2004]. This component has been attributed to chains of elongated magnetosomes. The peak at $H_c = 0$, on the other hand, could be compatible with nearly equidimensional SD particles similar to pedogenic magnetite found in soils [Egli, 2004]. A bimodal coercivity distribution is also obtained from backfield demagnetization data contained in a subset f_{bk} of the FORC measurements. About 30% of the total FORC magnetization is carried by the central ridge: for comparison, this proportion was ~50% in the pelagic carbonate analyzed in Ludwig et al. [2013].

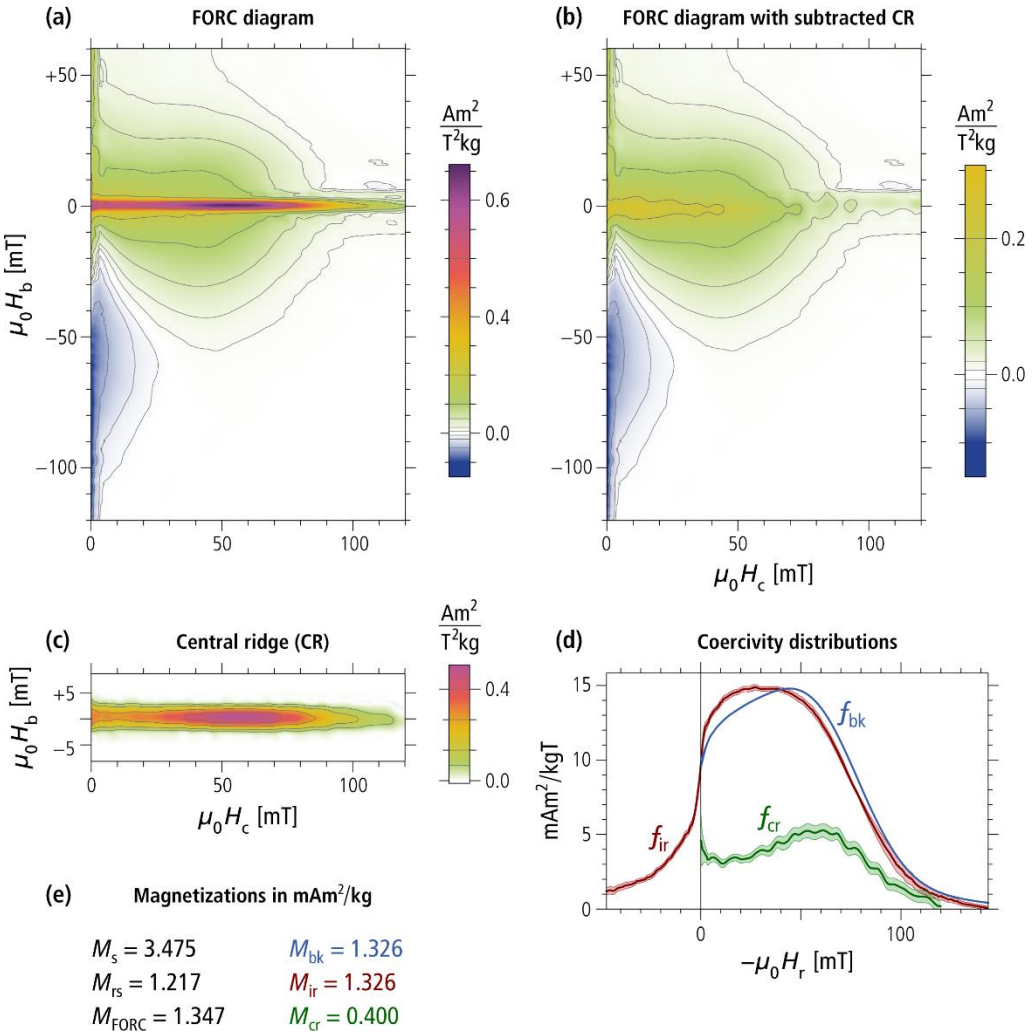

Figure 2-5 FORC diagrams and coercivity distributions. (a) FORC diagram of CBD-extractable particles obtained with VARIFORC. Same processing parameters as in Figure 2-4c have been used. (b) FORC diagram remaining after subtraction of the central ridge with VARIFORC. The isolated central ridge is shown in (c) with a 2× vertical exaggeration, which highlights a small upward shift of the whole ridge. The shift is due to thermal activation effects and is a common feature for all sedimentary materials featuring a central ridge. All FORC diagrams share the same color scale. (d) Three types of coercivity distribution derived from FORC measurements, with shaded bands around each curve representing the 2σ confidence level. The first two distributions, f_{bk} and f_{ir}, originate from FORC measurements in $H = 0$ and from the irreversible component of the lower branch of the hysteresis loop, respectively. These coercivity distributions are generated by VARIFORC as part of the standard output. The third distribution, f_{cr}, is associated with the central ridge. f_{ir} is the only distribution that exists for positive and negative fields, like the hysteresis loop from which it is derived. Negative arguments of f_{ir} originate from irreversible magnetization processes that occur without reversing the field direction. Only non-interacting, uniaxial single-domain particles produce a strictly positive f_{ir}. (e) Total magnetizations derived from FORC measurements (M_s and M_{rs}), integration of the FORC diagram (M_{FORC}), and integration of the coercivity distributions shown in (d) (M_{bk}, M_{ir}, and M_{cr}).

FORC analysis of untreated and CBD-treated sediment suggest the following conclusions. Remanence carriers in the sediment are mainly SD particles of magnetofossil origin. The central ridge indicates that ~30% of the particles occur in isolated form or as isolated magnetosome chains in the sediment matrix. The remaining SD particles are clustered, probably as a consequence of chain collapse. If clusters originate from magnetosome chain collapse, they are expected to be isolated from each other as the original chains were. About ~13% of the saturation remanence originates from PSD particles as part of a detrital component. These findings are similar to those obtained for a pelagic carbonate from the equatorial Pacific [Ludwig et al., 2013], where, however, the proportion of SD particles contributing to the central ridge was larger.

2.2.3 Redeposition Experiments

2.2.3.1 General set-up

Redeposition (DRM) experiments have been performed in glass vials with an inner diameter of 22 mm and a volume of 15 ml as the container (Figure 2-6a), which have negligible remanent magnetization (~0.26 nAm^2 on average), in comparison with the magnetic moment acquired by the sediment (>20 nAm^2 in 20 μT). Each sample consists of ca. 5 ml of slurry and 10 ml of tap water. Loaded vials were sealed and vigorously shaked in order to fully randomize the sediment suspension before the acquisition of magnetization. Magnetic field was provided by Helmholtz coils that is ~ 1m on each side with good homogeneity (with < 1% standard deviation) in the sample region (Figure 2-6c). The remanent magnetization acquired after given amount of time (T_{DRM_f}, see Table 2-1 at the end of this chapter for the summary of parameters used in the experiments) in the applied field was measured with a superconducting rock magnetometers. For this purpose, vials were transferred to the magnetometer very gently to keep the mechanical disturbance as low as possible. The vials were then lowered down into the optimum measurement position of the magnetometer by a non-magnetic sample holder very carefully. After a measurement which takes ~ 3 minutes/sample, samples were then randomized for acquisition with a different T_{DRM_f}. Triple samples were used in each acquisition for the concern of reproducibility.

For PDRM experiments, sediments were prepared in the same way as were in DRM experiments except that before the acquisition starts samples were placed in the shielded room to settle for a certain time (T_{PDRM_0}) after the initial randomization. Afterwards, samples were transferred to the applied field very gently. Acquired PDRM were then measured periodically during the course of acquisition (T_{PDRM_f}) in a same manner as that in DRM experiments except that samples were returned to identical position and orientation for experiment continuation without any deliberate mechanical disturbances. After T_{PDRM_f} was reached, samples were carefully transferred to null field and the subsequent changes in their previously acquired PDRM were periodically measured for a few days.

The values for the aforementioned parameters used in (P)DRM experiments are as follows. T_{DRM_f} was set to be 2, 4, 8, 16, 36 48, 80 hours, 6, 8.5 and 9 days. For most samples, T_{PDRM_0} is 4.5 days when the porosity becomes stabilized at 80.8% ± 3.5%, which was deduced from the difference in volume before and after consolidation. T_{PDRM_0} is 16 hours for only one control

group to demonstrate the effect of initial porosity on the PDRM acquisition. T_{PDRM_f} is mostly 1 week. The field intensity (B) was set to be B = 60 ± 0.4 μT with inclination I_c = 50 ° for the (P)DRM acquisition except for tests for inclination shallowing and field dependence. In the inclination shallowing test, field inclination was set to 0 °, 20 °, 50 °, 80 ° with constant B = 60 μT. For field dependence of (P)DRM, B was set to 20, 40, 60, 80,100 and 150 μT with constant I_c = 50 °.

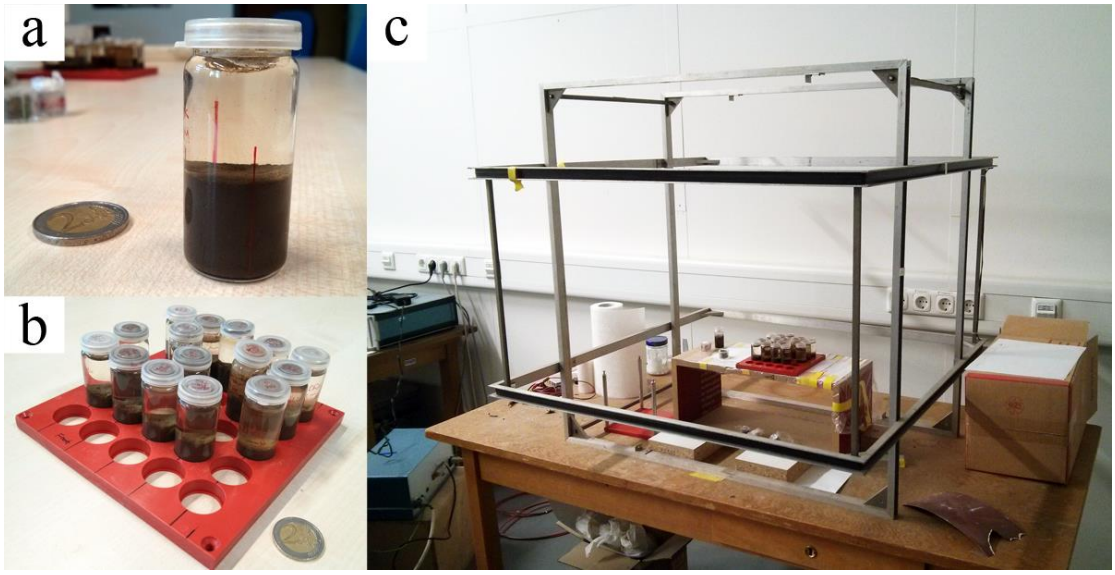

Figure 2-6 The apparatus for redeposition experiments.(a) Snap cap vials are used to contain sediments and water. It allows NRM measurements without drying sediments. Red lines on the vials mark the orientation. (b) Loaded vials are mounted on a substrate. The marks of vials are aligned with marks of the substrate. (c) The substrate is fixed in the Helmholtz coils which provide a homogeneous magnetic field for NRM acquisition, with its marks parallel to the north of the magnetic field.

2.2.3.2 Pre-treatments

In order to determine the structure and domain state of remanence carriers involved in the (P)DRM acquisition experiments, we prepared 4 types of control samples subjected to different magnetic treatments. Three treatments were applied before each redeposition experiment: (1) IRM at 100 mT, which saturates all low-coercivity magnetic minerals (2) ARM (peak AC = 100 mT with DC = 100 μT), which selectively saturates SD particles and (3) AF demagnetization with a peak field of 100 mT. The fourth treatment was an AF demagnetization applied after redeposition but before PDRM acquisition.

Another control group of samples was prepared by desiccating and disaggregating some sediment, which was successively rehydrated with distilled water. The resulting batch of control samples, called “crushed sediment” in the following, served two purposes: (1) check if disaggregated sediments is suitable for redeposition studies, and (2) eliminate bioturbation in the same manner as it is done with “classical” redeposition experiments.

The last control group consists of desiccated sediments that are AF-demagnetized before acquisition. This batch of samples were then subjected to magnetic field and measured in the

same manner as other groups. The resulting remanent magnetization will be compared with PDRMs of wet samples.

2.2.4 AF demagnetization of acquired magnetizations

Three samples were manually AF demagnetized in the originally wet condition after (P)DRM acquisition. These samples acquired (1) a DRM with T_{DRM_f} = 7 days, (2) a PDRM with T_{PDRM_f} = 7 days, and (3) a PDRM with T_{PDRM_f} = 1 day, respectively. High-resolution AF demagnetization was also performed with SUSHIBAR [Wack and Gilder, 2012] after complete drying. The dried samples were successively used for measuring detailed AF demagnetization curves of ARM and SIRM. The samples were demagnetized every 1 or 2 mT in the range of 1 mT to 50 mT and every 5 or 10 mT in the range from 50 to 90 mT.

2.3 Results and discussions

2.3.1 DRM acquisition

Results of DRM acquisition experiments as a function of time elapsed (i.e. T_{DRM_f}) in a given field are shown in Figure 2-7. The maximum DRM intensity is obtained with the first measurement in < 20 minutes, long before a stable height of the sediment column is approached (Figure 2-7c). Unlike classical redeposition experiments with lifeless sediment, initial rapid DRM acquisition in <20 minutes is followed by a steady decrease of DRM intensity in a constant applied field. Inclination, on the other hand, did not change significantly with time, and was ~6 ° shallower than the magnetizing field (Figure 2-7b). This corresponds to a shallowing factor ($f_{shallow}$) [King, 1955] of 0.81.

DRM intensity did not reach an equilibrium with the applied field after 9 days, however, the rate of change decreased significantly. DRM at T_{DRM_f} = 16 hours (DRM_{16hrs}) is used to investigate the dependence of inclination shallowing on the field direction and for later comparison with PDRM acquisition experiments. DRM intensity and inclination depend on the field inclination (I_f). As seen in Figure 2-8a, the moment of DRM acquired at I_f = 80 ° is ~ 80% of that acquired at I_f = 0 ° (Figure 2-8b). On the other hand, a maximum inclination shallowing of ~7 ° is observed for I_f = 50 °. These results are a characteristic feature of DRM, as found in previous studies [Tauxe and Kent, 1984; Bilardello et al., 2013], and can be explained with the classic inclination shallowing model of King [1955].

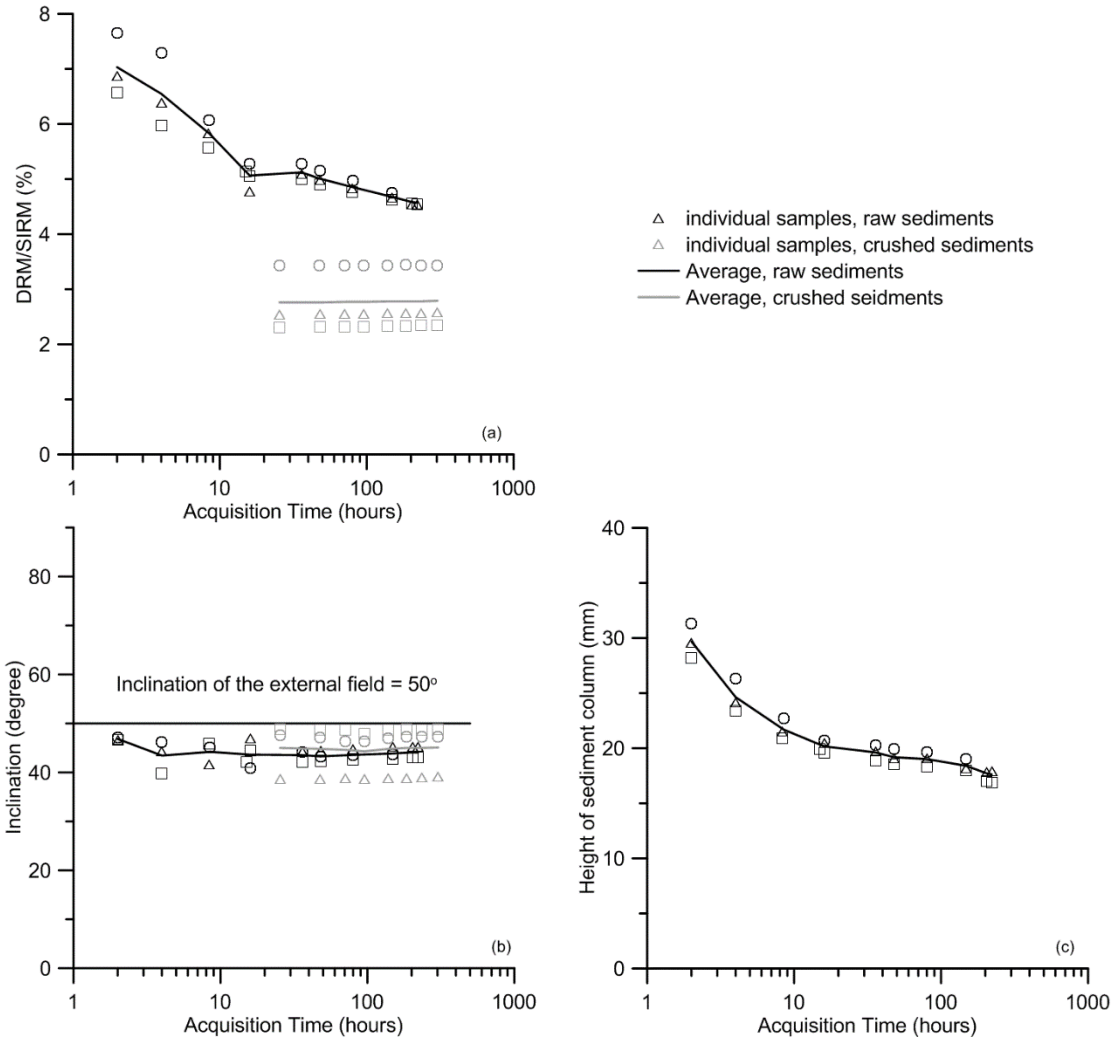

Figure 2-7 DRM acquisition versus time. (a) The intensity of DRM of raw sediments (black symbols) decreases with increasing acquisition time after the maximum is reached within < 2 hours. On the other hand, DRM of crushed sediments (gray symbols) is constant with acquisition time, though with larger scatters. (b) Inclination of DRM of raw sediments is constantly lower than that of the magnetizing field independent of acquisition time, corresponding to a shallowing factor [King, 1955] of 0.81. The scatter in inclination of crushed sediments is still higher, but the average inclination is similar to that of raw sediments. (c) The height of raw sediment column is measured as a function of settling time which is identical to the acquisition time for DRM. During the first 2 hours of redeposition, sediments are mere in suspension state. After 4 hours, a clear interface between water and sediment has formed. After 8 hours, water suspension becomes clear, but the sediments still feels like suspensions. The change in height becomes insignificant after 16 hours when sediments become sensibly stiffer.

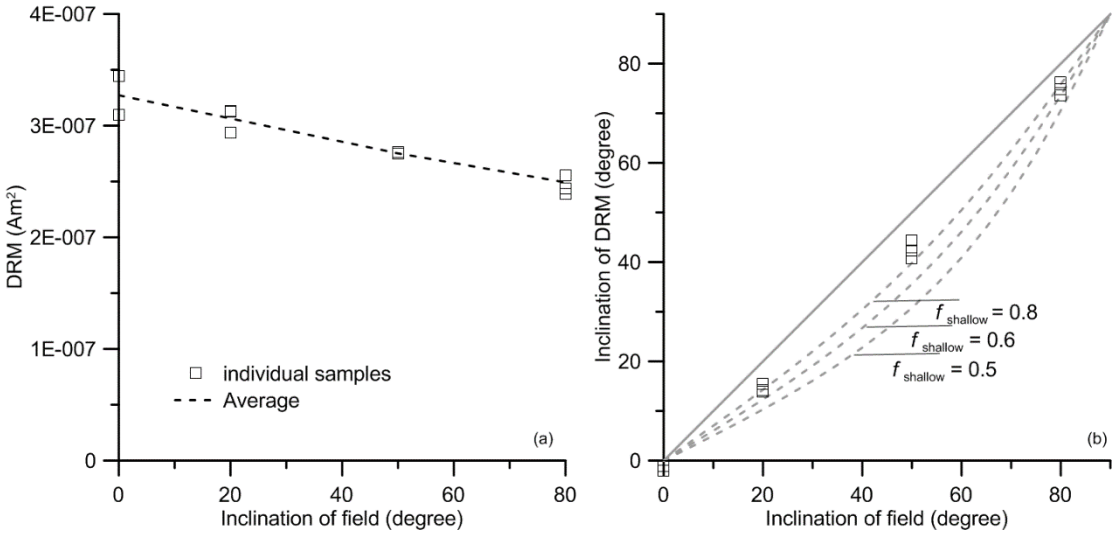

Figure 2-8 Dependence of DRM on field direction. DRM (16 hours long) of raw sediments is obtained in fields with different inclination (I_f) but with same intensity of 60 μT. (a) The average of the intensity declines with increasing inclination of the field. (b) Inclination of DRM is slightly dependent on the field inclination with a relatively higher deviation at I_f = 50 °. The dependence suggests the shape of DRM carriers are anisotropic with prevent them aligning at higher I_f.

2.3.2 PDRM acquisition

Results of PDRM acquisition experiments are shown in Figure 2-9. PDRM is acquired progressively with time, with a more rapid growth during the first days, followed by what appears to be the asymptotic approach to a final equilibrium that is not reached in 26 days (Figure 2-9a). Therefore, most PDRM acquisition experiments have been interrupted after a 7 day field exposure (T_{PDRM_f} = 7 days), at which point ~67% of the 26-day PDRM value is reached. Control experiments with dried sediments where particle rotation is not possible are characterized by the acquisition of a much smaller magnetization (Figure 2-9), so that a significant viscous contribution to the PDRM acquisition can be excluded.

Another important parameter controlling PDRM acquisition is the time elapsed since beginning of deposition before the field is turned on (T_{PDRM_0}). In general, the rate at which PDRM is acquired decreases with increasing T_{PDRM_0}: for example the initial PDRM acquisition rate for T_{PDRM_0} = 16 hours is twice as large as that corresponding to T_{PDRM_0} = 4.5 days (Figure 2-9b). On the other hand, the PDRM increase rate after ~5 days is the same for the two cases. These results suggest that the PDRM acquisition capability of the sediment decreases during the initial stages of deposition, probably because of compaction and buildup of inter-particle forces. In our experiments, most changes in the PDRM acquisition capability occur during the first 5 days. Therefore, all subsequent PDRM acquisition experiments have been performed with T_{PDRM_0} = 5 days, so that quasi-stationary sediment properties can be assumed.

PDRM directions coincide with the magnetizing field vector (Figure 2-9d) and no systematic inclination shallowing is observed. The absence of inclination shallowing is a typical characteristics of PDRM [e.g. Irving and Major, 1964; Kent, 1973; Tucker, 1979].

Unlike most PDRM acquisition experiments without active stirring [Tauxe and Kent, 1984; Shcherbakov and Shcherbakova, 1987], the PDRM acquired in our experiments is a significant fraction of a DRM acquired in the same field, in any case >30% (Figure 2-9c). Considering that PDRM experiments were interrupted before a final equilibrium is reached, and that the PDRM acquired in nature replaces a DRM, as shown later, PDRM acquisition can no longer be considered a negligible NRM source.

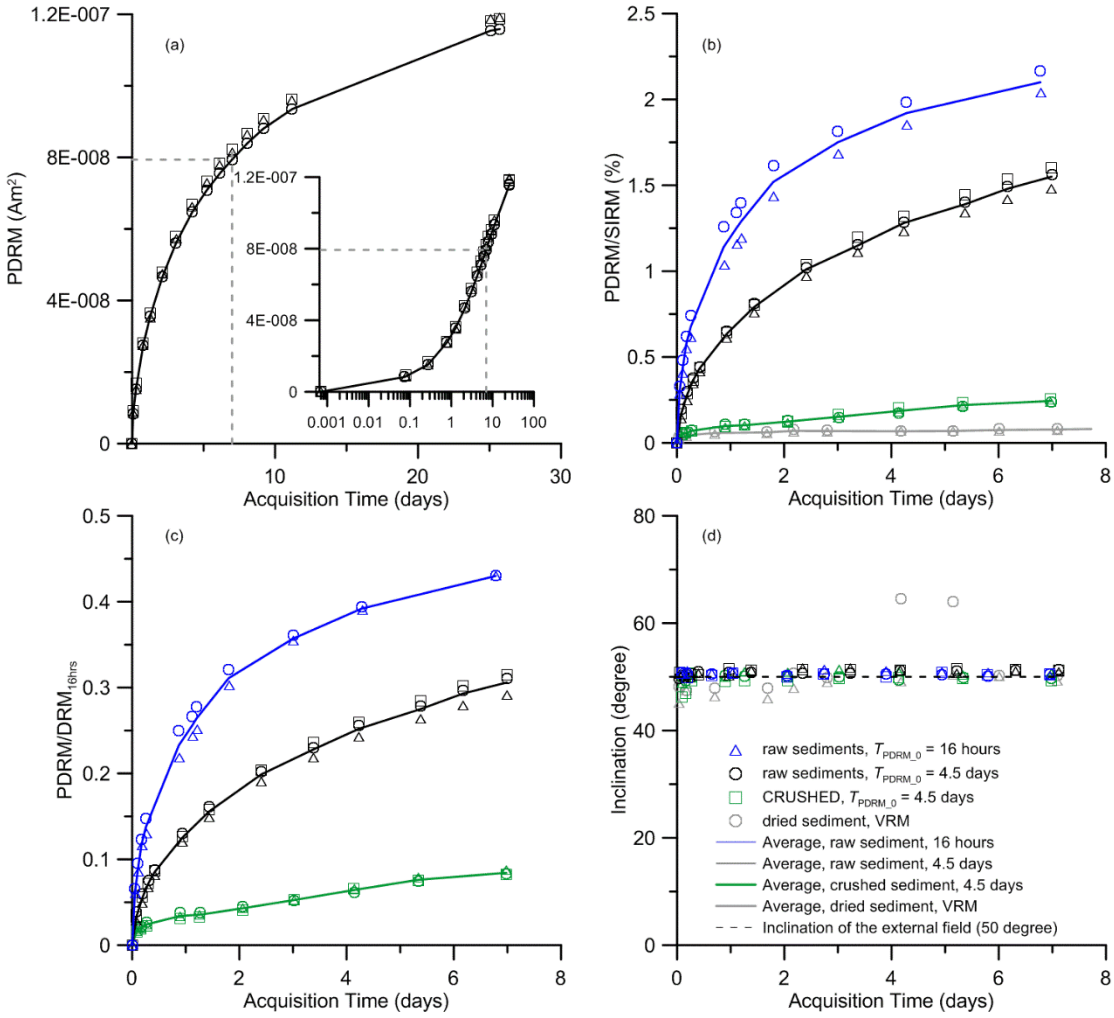

Figure 2-9 PDRM acquisition versus time. (a) PDRM of raw sediments is continuously acquired in 26 days with varying rates. PDRM acquisition started with a settling time in zero field (T_{PDRM_0}) = 4.5 days before acquisition ($PDRM_{4.5days}$). The initial segment represents a faster increase but lasts just < 1 day. The increase proceeds with a constant rate on the logarithmic time scale after 1 day of acquisition (inset). (b) PDRM with T_{PDRM_0} = 16 hours ($PDRM_{16hrs}$, blue symbols) have higher acquisition efficience than that of $PDRM_{4.5days}$. None of them is viscous remanent magnetization (VRM) as evidenced by comparison with consolidated samples (gray symbols) which acquire pure VRM. Crushed samples that were prepared by rehydrating powders of mechanically milled raw sediments, however, acquired very weak remanence which could be a combination of PDRM and VRM. (c) $PDRM_{16hrs}$ and $PDRM_{4.5days}$ are significant compared to their DRM which are acquired in 16 hours. (d) Inclination of PDRM agrees well with the magnetizing field.

A series of PDRM acquisition experiments have been conducted with sediment that was previously dried, crushed, and rehydrated (referred in the following as “crushed sediment”). This treatment mimics the experimental procedure commonly used in redeposition experiments, transforming the original fresh sediment with its community of microorganisms into a lifeless reprocessed material. This treatment reduces the PDRM acquisition capability of the original sediment by more than one order of magnitude (Figure 2-9b), and reproduces the typical results obtained by redeposition experiments [Katari et al., 2000]. This example shows that unaltered sediment properties are of paramount importance for the correct reproduction of NRM acquisition processes, therefore crushed sediments are not suitable for reproducing the natural PDRM acquisition.

2.3.3 (P)DRM carriers

As deduced from rock magnetic experiment, remanence carriers in the sediment can be divided into three main categories: (1) isolated SD particles or isolated, intact chains of SD particles (magnetofossils), (2) interacting SD particles (clusters, collapsed magnetosome chains or multiple chains), and (3) negligible amounts of PSD particles. How are these particles, and especially magnetofossils, arranged inside the sediment? Mao et al. [2014b] discussed the initial fate of magnetosome chains once dead magnetotactic bacteria and their supporting structures are dissolved. They excluded the possibility that such chains could remain freely suspended in the pore water, because in this case they would become completely aligned with the Earth magnetic field, yielding a saturated NRM. Instead, chains would adhere electrostatically to other sediment particles, forming for example magnetite-clay aggregates, such as those observed by Galindo-Gonzalez et al. [2009]. This aggregation process, which can be considered as a sort of flocculation occurring inside the sediment column rather than in the water, would probably stabilize magnetosome chains against complete collapse, preserving the original magnetic moments. This hypothesis is supported by the fact that the central ridge of FORC diagrams obtained from magnetofossil-bearing sediments contributes significantly to the total magnetization.

Remanence carriers can thus be imagined as intact or collapsed magnetosome chains adhering to larger non-magnetic sediment particles. The elevated magnetic moment of intact chains would contribute to NRM acquisition, while collapsed chains with a small resulting moment would be less important remanence carriers. During PDRM acquisition, magnetic flocs can thus be imagined as aggregates of one or more chains attached to non-magnetic sediment particles that behave as discrete elastic units during bioturbation. The nature of the remanence carriers and floc structure has been investigated with two types of experiments, as described in the following.

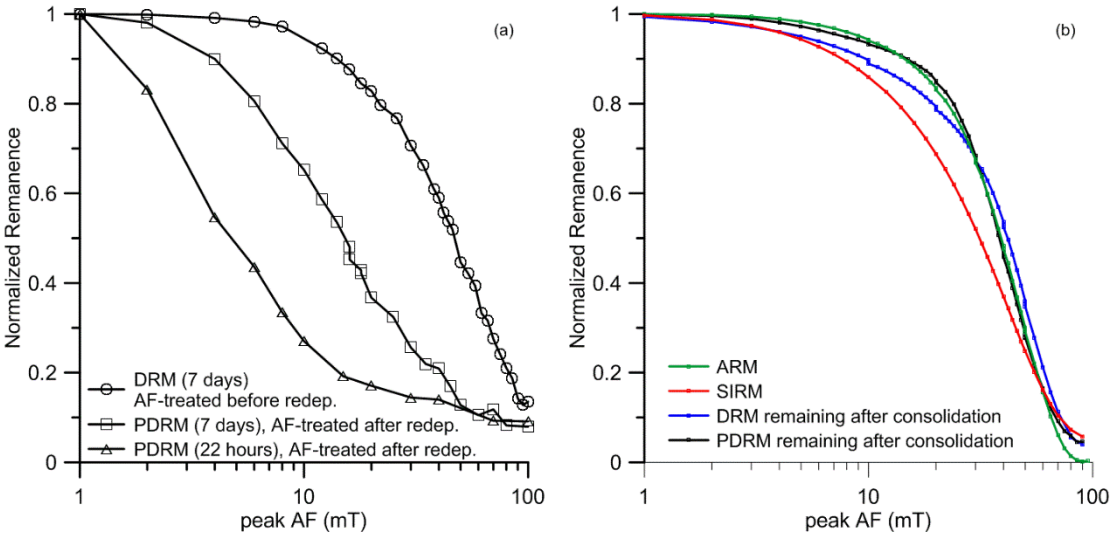

Figure 2-10 AF demagnetization of remanent magnetization of wet and dry sediments. (a) Results of wet samples. DRM was acquired in field of 60 μT for 7 days. For PDRM acquisition, the sample was first kept in zero field for > 1 month and was AF demagnetized at 90 mT shortly before the PDRM acquisition. After a certain time of acquisition (7 days or 22 hours), the acquired PDRM was AF demagnetized. (b) Raw sediments were consolidated after acquisition of (P)DRM. The demagnetization of NRM are compared with that of ARM and IRM of the same sample.

2.3.3.1. AF demagnetization curves

The shape of AF demagnetization curves of PDRM depend on the time T_{PDRM_0} elapsed before acquisition was started (Figure 2-10a). In particular, the median destructive field, defined as the AF peak field required to erase 50% of the initial magnetization, increases with T_{PDRM_0} and the curve shape changes from exponential (T_{PDRM_0} = 22 hours) to sigmoidal (T_{PDRM_0} = 7 days). A similar phenomenon has been documented by Mao et al. [2014b] with experiments on the same type of sediment. By changing the direction of the applied field during PDRM acquisition, Mao et al. [2014b] could show that exponential AF demagnetization curves with small median descructive fields are controlled by mechanical unblocking of magnetic particles or flocs in the alternating field. This phenomenon tends to disappear with increasing time from deposition, due to the buildup of inter-particle forces that prevent mechanical unblocking. The AF stability of DRM, on the other hand, changes little with time, as expected from particles or flocs that become rapidly blocked during the early stages of deposition.

In order to avoid possible biases introduced by mechanical unblocking processes, a set of high-resolution AF demagnetization curves has been obtained with dried sediment samples. In this case, sediment has been allowed to dry in the (P)DRM acquisition field. AF demagnetization curves of ARM and IRM acquired by the dried sediment have been measured after (P)DRM acquisition to provide a term of comparison (Figure 2-10b). AF demagnetization curves of DRM and PDRM are similar in shape to the AF demagnetization of ARM, rather than IRM. In particular, the ARM and PDRM curves are practically identical. These results suggest that (1) (P)DRM remanence carriers are mainly SD, given the high selectivity of ARM towards SD particles [Egli and Lowrie, 2002], and (2) the natural magnetic moments of flocs are best reproduced by an ARM,

rather than an IRM. The nature of (P)DRM remanence carriers can be further explored by combining the AF demagnetization results with the magnetic composition of the sediment deduced from FORC measurements (section 2.2.2). Three main groups of remanence carriers can be distinguished: (a) PSD particles of detrital origin, (b) non-interacting SD particles (isolated crystals or isolated, single magnetosome chains), and (c), strongly interacting SD particles (clusters or collapsed chains) with relative contributions to the total FORC magnetization listed in Table 2-2. Because the FORC magnetization is similar to a saturation remanence, these results can be considered as rough approximations for the relative contributions of the three groups to M_{rs}. ARM contributions, on the other hand, can be deduced from M_{rs} through expected χ_{ARM}/M_{rs} values (Table 2-2). These estimates indicate that ~80% of the ARM is carried by non-interacting SD particles or magnetosome chains. A similar proportion is also expected for the PDRM, given the identical shape of the corresponding AF demagnetization curves. The shape of the DRM demagnetization curve, on the other hand, is intermediate between the ARM and IRM curves over the low-coercivity range (0-20 mT), which is dominated by PSD and interacting SD contribution, as seen from coercivity distribution curves deduced from FORC measurements (section 2.2.2).

Overall, it appears that the most important contribution to the (P)DRM acquired during redeposition experiments comes from non-interacting SD particles, probably in form of intact magnetosome chains. The nature of such carriers is explored in detail with experiments described in the next section.

2.3.3.2. Redeposition experiments with magnetic pre-treatments

The magnetic structure of magnetic flocs has been further investigated by subjecting the sediment to different magnetic treatments before and during redeposition experiments. These treatments were aimed at changing the net magnetic moment of the flocs and observe the consequences for PDRM acquisition. Predicted consequences for different floc configurations and magnetic treatments are summarized in Table 2-3.

The following scenarios can be envisaged:

1. Each floc consists of a single magnetosome chain or a single SD particle. In this case, the floc magnetic moment coincides with the saturation moment m_s, reagardless of the magnetic pre-treatment. A natural consequence of this scenario is that the SD magnetic carriers are well dispersed in the sediment matrix, being separated by at least one sediment particle diameter (i.e. ~20 μm on average in our sediment). As a result, rock magnetic properties are dominated by the signature of non-interacting SD particles. We know from FORC measurements (see section 2.2.2), that this condition is met by up to ~33% of the remanence carriers.

2. Each floc consists of several unaligned magnetosome chains or SD particles. This scenario is similar to the previous one, except that flocs contain more than one SD magnetic carrier (magnetosome chain or particle), as a result of an aggregation process. Because the original alignment of the individual remanence carriers is small, this property is transferred to the whole floc, which behaves as a miniature sample containing (almost randomly) oriented SD particles. The natural net magnetic moment of flocs is thus given by the vector sum of individual moments with a small residual alignment, which is dictated by the intensity of the geomagnetic field during aggregation. The net magnetic moment remains small after AF or ARM pre-treatments, so that

the (P)DRM acquired during redeposition experiments is not expected to exceed the values obtained from the untreated sediment. On the other hand, the application of a large saturating field (IRM treatment), will switch individual magnetic moments in the flocs to <90 °angles to the applied field, so that each floc will acquire a magnetic moment corresponding to a saturation remanence. Because these flocs can be imagined as aggregates of weakly interacting SD particles, the resulting magnetic moment is ~50% of the saturation moment m_s. Accordingly, redeposition experiments performed with IRM-treated sediment should yield significantly larger (P)DRM intensities with respect to the untreated sediment. This scenario can be expected in cases where the local concentration of SD particles or magnetosome chains was sufficiently large to produce repeated events where a magnetic carrier adheres to a sediment particle.

3. Each floc consists of SD particle clusters or collapsed magnetosome chains. In this case, flocs contain strongly interacting SD particles, either formed directly by chemical precipitation, induced for instance by metal-reducing bacteria [Moskowitz et al., 1989], or as a result of chain collapse. In the latter case, the original saturated moment of individual magnetosome chains is almost completely nullified, as deduced from the structure of collapsed chains [Kobayashi et al., 2006]. On the other hand, chemical precipitation of SD particles in dense clusters produces a chemical remanent magnetization (CRM) whose intensity is strongly depressed by magnetostatic interactions [Shcherbakov et al., 1996]. In both cases, the magnetic moment of individual flocs is only a small fraction of the saturation moment. The same is true after AF or ARM treatments, which are not expected to change the sediment's (P)DRM acquisition capability during redeposition experiments. On the other hand, a strong magnetic field will induce a saturation remanence state in each floc, which, due to magnetostatic interactions is expected to be comprised between 20% and 50% of the saturation moment m_s [Muxworthy et al., 2003; Li et al., 2010], and in any case significantly larger than the original magnetic moment. Accordingly, the IRM pre-treatment is expected to significantly enhance (P)DRM intensities acquired in redeposition experiments, while other magnetic treatments should produce only minor effects.

4. Each floc consists of multiple magnetosome chains inherited from a single magnetotactic bacterium. Several magnetotactic bacteria species produce double or multiple parallel magnetosome chains [Spring et al., 1995; Jogler et al., 2010], and possess, as a whole, a saturated magnetic moment [Hanzlik et al., 2002; Simpson et al., 2005]. As demonstrated by magnetic moment measurements of individual bacteria, multiple chains, unlike single ones, possess intermediate magnetic states and therefore do not behave, as a whole, like isolated SD particles. In particular, multiple chains can exist in a demagnetized state. If, in analogy to case 1, the original magnetic moment is maintained after cell dissolution and transferred to individual flocs, these flocs will be characterized by a saturation moment that can be demagnetized by AF and ARM treatments, and re-created by application of a strong magnetic field (IRM). Accordingly, (P)DRM intensities obtained from redeposition experiments with untreated and IRM-treated sediment are expected to be similar, while AF and ARM treatments are expected to reduce (P)DRM intensities significantly.

5. Each floc contains one or more PSD or MD particles. This case describes the expected (P)DRM contribution of primary minerals. The magnetic moment of these remanence carriers

corresponds to the NRM acquired by the parent rock, which has often a TRM in origin. Accordingly, the natural magnetic moment of such particles, as well as the whole flocs, is only a fraction of the saturation moment m_s. These particles possess multiple magnetic states and are therefore affected by magnetic pre-treatments. Resulting magnetic moments, and therefore (P)DRM intensities, will be proportional to the type of remanence acquired with the magnetic treatment. The following (P)DRM intensity ranking can therefore be expected: AF < ARM < NRM << IRM.

As shown by Table 2-3, each of the five categories of magnetic flocs has its own signature in terms of (P)DRM sensitivity to the magnetic pre-treatment. Thus we could infer the structure of flocs by comparing the (P)DRM with different magnetic pre-treatments.

Magnetic pre-treatments have been applied to the sediment suspension before redeposition experiments were started. The application of a saturating field (IRM pre-treatment) rotates the individual flocs and saturates their magnetic moment. On the other hand, the effect of alternating fields on suspended flocs is less straightforward, because particle rotation could prevent changes of their magnetic state. In the following, the effect of an alternating field $H = H_0\sin(2\pi\nu t)$ with amplitude H_0 and frequency n on a floc with radius R, which behaves as a SD particle with uniaxial anisotropy, is illustrated. In this case, the angle j between the floc's magnetic moment m and H_0 minimizes the total magnetic free energy given by:

$$E(\varphi,\beta) = \frac{1}{2}\mu_0 m H_K \sin^2(\varphi-\beta) - \mu_0 m H_0 \sin(2\pi\nu t)\cos\varphi,$$

where H_K is the microcoercivity and b the angle between the easy axis and H_0. Floc rotation, on the other hand, is governed by the equilibrium between magnetic torque and viscous drag [Steinberger et al., 1994], i.e.:

$$8\pi\eta f R^3\dot{\beta} = \mu_0 m H_0 \sin(2\pi\nu t)\sin\varphi,$$

where $\eta \approx 1$ mPa s is the dynamic viscosity of water, and f a viscous resistance factors that depends on the floc shape ($f = 1$ for a sphere). Numerical solutions of the coupled equations with initial condition $\beta(t = 0) = \beta_0$ and $\varphi(t = 0) = 0$ give the angle φ-β between magnetic moment and easy axis. Two examples with $\beta_0 = 45$ °, $n = 200$ Hz (corresponding to the frequency of the ASC demagnetizer used for the experiments), $H_0 = 0.1$ T (corresponding to the AF peak field used in the experiments), $H_K = 0.08$ T (corresponding to twice the median destructive field of ARM) and $m = 2 \times 10^{-16}$ Am^2 (corresponding to a chain of 12 magnetosomes with a diameter of 40 nm) are shown in Figure 2-11. In general, moment switching occurs with floc radii >1 μm for most values of β_0. Because the mean grain size of sediment used for the experiments is ~10 μm, the AF field is expected to affect the magnetic moments in a similar manner as for fully blocked particles.

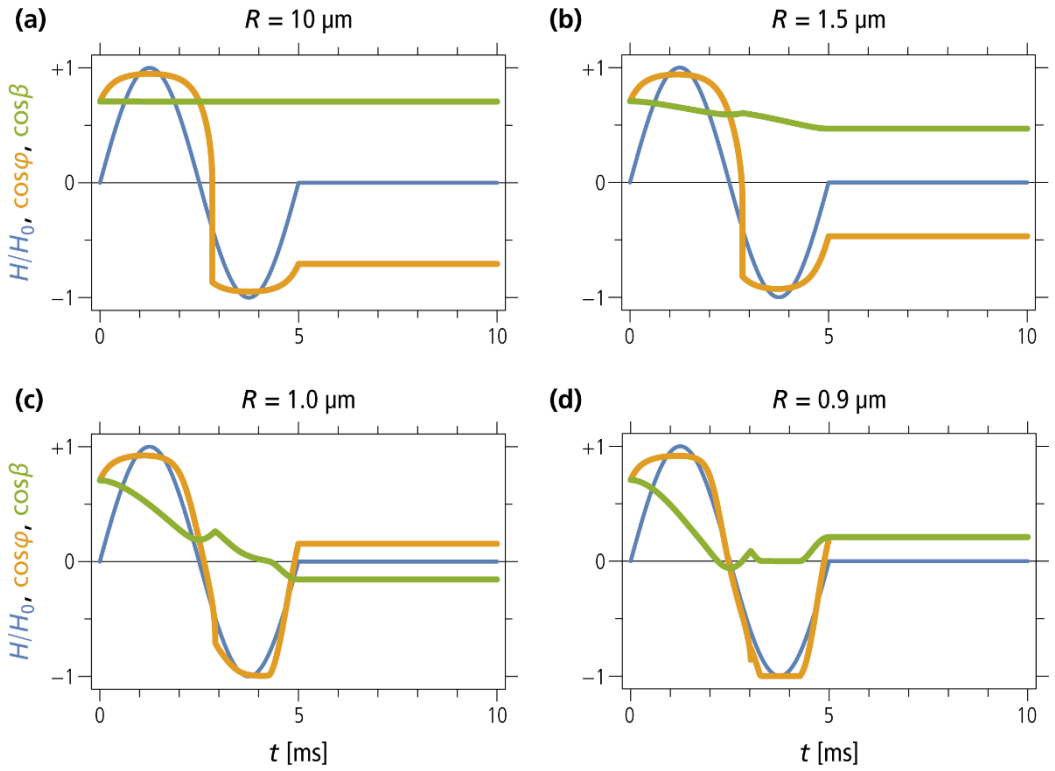

Figure 2-11 Effects of alternating field on rotation of flocs. Calculated effects of a single period of the alternating field $H = H_0\sin(2\pi\nu t)$ with $\mu_0 H_0 = 0.1$ T and $n = 200$ Hz on a floc with radius R that behaves as a uniaxial SD particle with microcoercivity $H_K = 0.08$ T. Plotted curves represent the normalized field H/H_0 and the cosine of the angle β between H_0 and the magnetic easy axis, and the angle φ between H_0 and the magnetic moment. Other model parameters are the initial particle orientation $\beta(0) = 45$ °, and the magnetic moment $m = 2 \times 10^{-16}$ Am^2. Magnetic moment and microcoercivity are representative for a single chain of 12 magnetosomes with a diameter of 40 nm each. (a) The viscous drag prevents any significant floc rotation, as seen from the constant value of cosβ, and the magnetic moment is switched during the second half of the AF cycle, as seen from the opposed signs of cosβ and cosφ. (b-c) The viscous drag is sufficient to prevent full particle rotation, and the magnetic moment is switched. (d) Magnetic moment switching is prevented by particle rotation, so that cosβ = cosφ at the end of the AF cycle, as it was at the beginning.

Overall, magnetic pre-treatments did not affect PDRM acquisition significantly (Figure 2-12). In particular, PDRM intensity is not consistently related to the magnetic moment increase expected from the magnetic pre-treatment, since $PDRM_0 \approx PDRM_{IRM} < PDRM_{AF} < PDRM_{ARM}$. Therefore, the observed PDRM intensity variations, which do not exceed 20% of $PDRM_0$, must be attributed to other factors. According to Table 2-3, only flocs which behave as individual SD particles are insensitive to magnetic pre-treatments, and therefore compatible with the results shown in Figure 2-12 and the fact the AF demagnetization curves of PDRM are identical to the AF demagnetization of ARM (Figure 2-10). For magnetofossil bearing sediments, this means that PDRM remanence carriers consist of fossil magnetosome chains that are individually attached to sediment particles. As seen in section 2.2.2 such remanent magnetization carriers contribute to ~30% of M_{rs}. On the other hand, the remaining carriers (PSD and interacting SD particles), whose

magnetic moments can be heavily affected by magnetic pre-treatments (Table 2-3), do not appear to contribute significantly to PDRM acquisition. This means that PDRM acquisition must be affected by non-magnetic parameters (such as floc size), which are systematically related to the type of magnetic carriers, i.e. intact magnetosome chains with high PDRM efficiency on one hand, and PSD, as well as interacting SD particles, on the other hand.

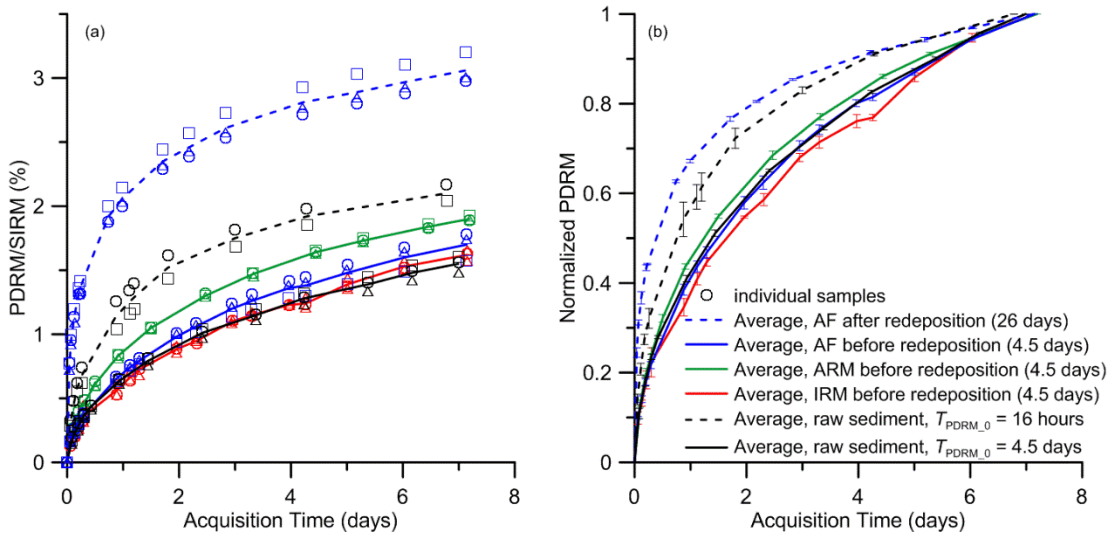

Figure 2-12 Results of PDRM acquisition after pre-treatments.(a) Minor difference in PDRM acquisition are produced by pre-treatment before redeposition (solid lines). AF demagnetization after redeposition but before acquisition results in great enhancement (blue dashed line), which is even higher than PDRM acquisition with T_{PDRM_0} = 16 hours (black dashed line). (b) The normalized curves with pretreatments before redeposition follow the same trend as PDRM acquisition of the untreated sediment. Much higher acquisition efficiencies are obtained with AF demagnetization after deposition. Numbers in the legend indicates T_{PDRM_0} for each group.

Finally, the role of AF demagnetization at different stages of PDRM acquisition experiments has been investigated. For this purpose, AF demagnetization was applied on redeposited, untreated sediment shortly before PDRM acquisition. In this case, PDRM acquisition efficiency almost doubled (Figure 2-12). Because AF demagnetization did not change PDRM acquisition results when performed before redeposition, the observed effect cannot be attributed to a systematic change of the magnetic moments. On the other hand, the AF field introduces strong magnetic torques that "vibrate" magnetic flocs, loosing inter-particle forces that prevent full magnetic alignment during and after redeposition. Reduced inter-particle forces can explain the observed increase in PDRM acquisition efficiency, which is very similar to the increase obtained by reducing the time interval between redeposition and beginning of PDRM acquisition, i.e. T_{PDRM_0} (Figure 2-12).

2.3.4 Significance of randomizing torques in sediments

PDRM acquisition results discussed in previous sections can be summarized as follows. Experiments with crushed sediment, which mimic the usual procedure used for redeposition, are characterized by a very inefficient PDRM acquisition, which attains only a fraction of the DRM

acquired under similar conditions. These results are fully compatible with previous redeposition experiments with unstirred sediment [Tauxe and Kent, 1984], and with what is expected from passive alignment of magnetic grains in the sediment matrix [Shcherbakov and Shcherbakova, 1987]. On the other hand, same experiments with fresh, untreated sediment hosting living bacteria populations are characterized by the acquisition of a PDRM that reaches a significant fraction (>30%) of the DRM and is not affected by inclination shallowing. This PDRM is similar to the magnetization acquired in stirred sediments [Kent, 1973]. Because the only difference between the two types of redeposition experiments is the degree of sediment alteration, and in particular the presence of living organisms, we must conclude that mechanical disturbances – introduced either artificially by stirring or naturally by living organisms – are essential for promoting PDRM acquisition. The mechanical disturbance of sediment by living organisms is known as bioturbation.

Bioturbation is the phenomenon by which sediment is mixed by benthic organisms within the so-called benthic mixed layer, which generally comprises the topmost 2-20 cm of the sedimentary column (Figure 2-13). A consequence of this activity is that the age of the mixed layer is continuously reset, as seen from depth-invariant concentrations of age-dependent tracers (e.g., radionuclides) [Boudreau, 1994; Trauth et al., 1997]. While the influence of bioturbation on vertical sediment transport has been widely studied, possible effects on the orientation of magnetic carriers are mostly unknown, so that opposite points of view exist on DRM preservation through the mixed layer, ranging from full preservation [e.g. Katari et al., 2000] to full destruction [e.g. Mao et al., 2014b]. Bioturbation models are usually divided into two main categories according to the invoked transport mechanism, i.e., non-local (advection-like) and local (diffusion-like). These two mechanisms affect the orientation of magnetic carriers in a specific manner which have different impacts on sedimentary NRM.

The paradigm example of so-called non-local sediment mixing is represented by the activity of burrowing organisms, in particular polychaete worms (Figure 2-13). These worms transport sediment ingested at a certain depth by egesting it near the sediment surface [Shull, 2001]. This activity produces a conveyor belt-like vertical mixing of solid material. A new DRM is acquired during redeposition of the egested sediment, so that the mixed layer is subjected to a continuous DRM renewal with no PDRM overprint [Katari et al., 2000]. Some other non-local sediment mixing mechanisms, such as crawling of crustaceans [e.g. Solan et al., 2004], are expected to work in a similar manner through sediment resuspension. On the other hand, burrowing activities unavoidably produce some small-scale (local) mixing: for example, polychaete worms release part of the ingested sediment in-situ, without transporting it to the surface [Shull, 2001].

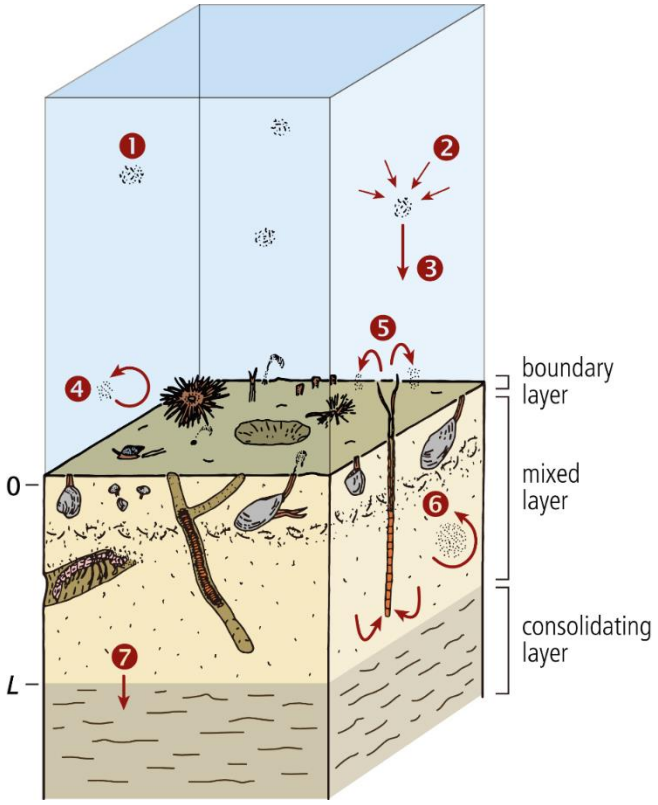

Figure 2-13 Schematic representation of processes that contribute to acquisition of sedimentary magnetizations. 1: Marine snow. 2: Flocculation (first step of DRM acquisition). 3: Settling. 4: Sediment resuspension (DRM renewal). 5: Non-local sediment mixing by polychaete worms. 6: Local (diffusive) sediment mixing (DRM randomization, PDRM acquisition). 7: Transition to the consolidating layer (DRM and PDRM locking).

Local mixing models represent sediment fluxes in terms of a solid diffusion process that depends on a single parameter: the self-diffusion or biodiffusion constant D_b, in units of length^2/time [Boudreau, 1986a; Meysman et al., 2003]. The random nature of solid diffusion at the level of individual sediment particles implies that any remanent magnetization becomes progressively overprinted. In most cases, radioactive tracer profiles can be fitted by assuming a depth-independent value of D_b over a layer of thickness L, which is identified with the surface mixed layer [Reed et al., 2006]. Local mixing models are widespread, because they provide simple estimates of the bioturbation depth L and the bioturbation intensity D_b. Values of D_b from 0.01 to 200 cm^2/yr in combination with mixing depths between 2 and 20 cm have been reported for various coastal, shelf, slope, and deep-sea sediments [e.g. Boudreau, 1994; Teal et al., 2008].

Diffusive material transport is described macroscopically by the translational Fick's law $\partial C/\partial t = D_b \Delta C$, where C is the concentration of a given substance. At the scale of individual sediment particles – defined here as elemental units that behave as individual elastic bodies – Fick's diffusion is equivalent to a random walk with net displacement $\langle r^2 \rangle = 6 D_b t$ over time t [Berg, 1983]. By analogy, the orientation of individual particles subjected to random perturbations is equivalent to an angular random walk $\langle \theta^2 \rangle = 2 D_r t$, where θ is the angle to an initial orientation, and D_r is the rotational diffusion coefficient in units of angle^2/time. The

statistical orientation of a large number of particles subjected to rotational diffusion is governed by the rotational counterpart of Fick's law, i.e.:

$$\frac{\partial p}{\partial t} = D_r \Delta p \,, \tag{2-1}$$

where $p = p(t,\theta,\varphi)$ is the probability density function of orientation vectors (e.g., magnetic moments) in spherical coordinates [Perrin, 1934]. While several studies exist on translational and rotational diffusion of colloidal suspensions, D_r has never been measured in sediment. Nevertheless, order-of-magnitude estimates of D_r can be obtained from translational diffusion. In the case of Brownian motion (i.e., particle movement caused by molecular collisions), rotational and translational diffusion are related by the Stokes-Einstein-Debye law:

$$\frac{D_r}{D_b} = \frac{\Gamma_b}{\Gamma_r} \,, \tag{2-2}$$

where Γ_b and Γ_r are the translational and rotational viscous drag coefficients, respectively, which depend on particle shape and size. For the Brownian motion of spherical and disk-like particles of radius a,

$$\left[\frac{D_r}{D_b}\right]_{spheres} = 2\left[\frac{D_r}{D_b}\right]_{disks} = \frac{3}{4a^2} \tag{2-3}$$

[Koenderink et al., 2003]. The relation between translational and rotational diffusion of dense particle aggregates, such as sediments, is more complex and less well known.

Generally, the orientation of isolated particles subjected to random perturbations in zero field is governed by eq. (2-1) with a given initial distribution of magnetic moment directions. If the initial distribution is a function of the angle θ to a reference direction (i.e., an initially applied magnetic field) and the diffusion process is isotropic, the solution of eq. (2-1) obtained from full initial alignment at $t = 0$ is given by:

$$p(\theta,t) = \frac{1}{4\pi}\sum_{l=0}^{\infty}(2l+1)\,e^{-D_r l(l+1)t}P_l(\cos\theta) \tag{2-4}$$

where P_l are Legendre polynomials of order l (Appendix A1. Rotational diffusion). The progressive magnetization loss during sediment mixing follows directly from eq. (2-4) as

$$\frac{M}{M(t=0)} = \langle\cos\theta\rangle = e^{-2D_r t} \tag{2-5}$$

[Perrin, 1934]. This expression yields the half-life $t_{1/2} = \ln 2/(2D_r)$ of any mixed layer magnetization in zero field.

As seen above, bioturbation can be modeled as rotational diffusive process that affect the orientation of magnetic flocs. Accordingly, any existing magnetization is subjected to an exponential decay in zero field, whose rate is controlled by the rotational diffusion coefficient D_r. Decay experiments have been performed by transferring the sediment to a shielded room with <500 nT residual field after acquisition of a (P)DRM. Control experiments have been performed with crushed sediment and with dried sediment, the latter for excluding possible contributions from magnetic viscosity. Results are summarized in Figure 2-14. Both DRM and PDRM acquired in fresh sediment are subjected to an exponential-like decay which is much more rapid than the

decay observed in crushed and in dried sediments. Therefore, magnetic viscosity does not contribute significantly to the observed decay and appears to be an exclusive feature of sediment that is not subjected to treatments that destroy living organisms. This provides, along with the experiments described in Chapter 3, a proof for the role of bioturbation in PDRM acquisition.

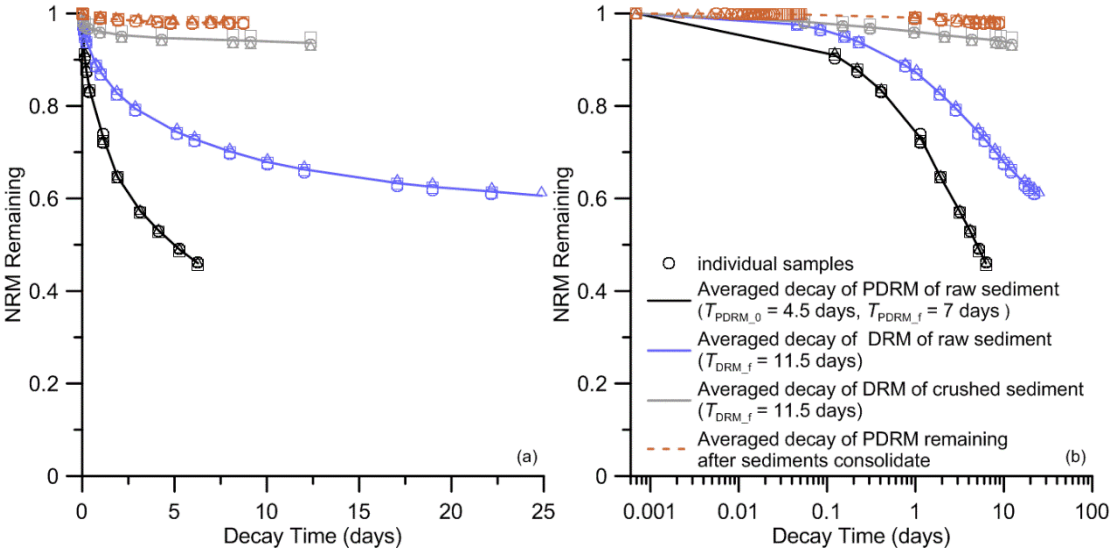

Figure 2-14 NRM decays of raw sediments in zero field on a linear scale (a) and a logarithmic scale (b). Open symbols represent measurements of individual samples and lines are averages of 3 independent samples for each group.

Though DRM and PDRM are characterized by identical total redeposition times (11.5 days), before zero field conditions are applied, PDRM decays more rapidly than DRM. The half-life time estimated from linear extrapolation of Figure 2-14b is ~5 days for the PDRM and ~90 days for the DRM. This difference cannot be attributed neither to sediment aging, since DRM and PDRM acquisition experiments shown here share the same total acquisition time, nor to differences in bioturbation rates, since identical sediment have been used. Therefore, decay times of DRM and PDRM must be controlled by specific characteristics of the corresponding remanence carriers. Floc size is a potential factor controlling the decay time through the Einstein-Debye relation between translational and rotational diffusion (eq. 2-3): inside a sediment subjected to the same translational diffusion process, D_r is inversely proportional to the square of floc size. Accordingly, PDRM acquisition could depend on the alignment of flocs that are smaller on average than those that become immediately blocked during DRM acquisition.

Decay of laboratory (P)DRM in zero field was occasionally reported in previous studies. Tauxe and Kent [1984] found that the initially acquired PDRM of river sediments, which was 10% of DRM acquired in the same field, decreased by ~ 30% in zero field in a period equivalent to the acquisition time. The loss in PDRM was considered as viscous decay. Katari et al. [2000] also discovered PDRM decay in zero fields which follows a pattern that can be fitted to a combination of exponential decay. This pattern is very similar to our results, and might be the result of bioturbation, since their experiments have been performed with untreated sediment.

2.3.5 Field dependence of NRM

In order to test the field dependence of (P)DRM, redeposition experiments have been performed in field intensities ranging from 20 μT to 150 μT with an inclination of 50 °. As seen in sections 2.3.1-2, (P)DRM intensities depend on the acquisition time. DRM is a nearly instantaneous process occurring during initial deposition. As discussed in Chapter 4, the slight DRM intensity decrease with time can be attributed to its progressive replacement with a weaker PDRM. Therefore, DRM after 16 hours acquisition time is identified here with the initial DRM. On the other hand, normalized PDRM acquisition approaches asymptotically a final equilibrium with decreasing rates almost independent of the applied field (Figure 2-15b). Therefore, PDRM intensity is identified with the PDRM acquired during 7 days after 4.5 days deposition in zero field.

Both DRM and PDRM depend non-linearly on the applied field intensity (Figure 2-15, and are well fitted by a Langevin function, i.e.

$$M = M_0 \boldsymbol{L}\left(\frac{B}{B_{\text{crit}}}\right) = f_{\text{m}} M_{\text{rs}} \boldsymbol{L}\left(\frac{B}{B_{\text{crit}}}\right), \tag{2-6}$$

where M_0 is the saturation (P)DRM obtained in $B \rightarrow \infty$, f_{m} is the ratio of M_0 to M_{rs}, $\boldsymbol{L}(x) = \coth x - 1/x$ is the Langevin function and B_{crit} is the critical field below which M increases approximately linearly with the applied field B. Best-fit B_{crit} for PDRM is higher than that for DRM (Figure 2-15a). Consistently, as seen in Figure 2-15c and d, PDRM has an expected linear response to the field up to ~ 60 μT while the dependence of DRM becomes appreciably non-linear above 40 μT. The theoretical background for the use of $\boldsymbol{L}$ is given in Chapter 4.

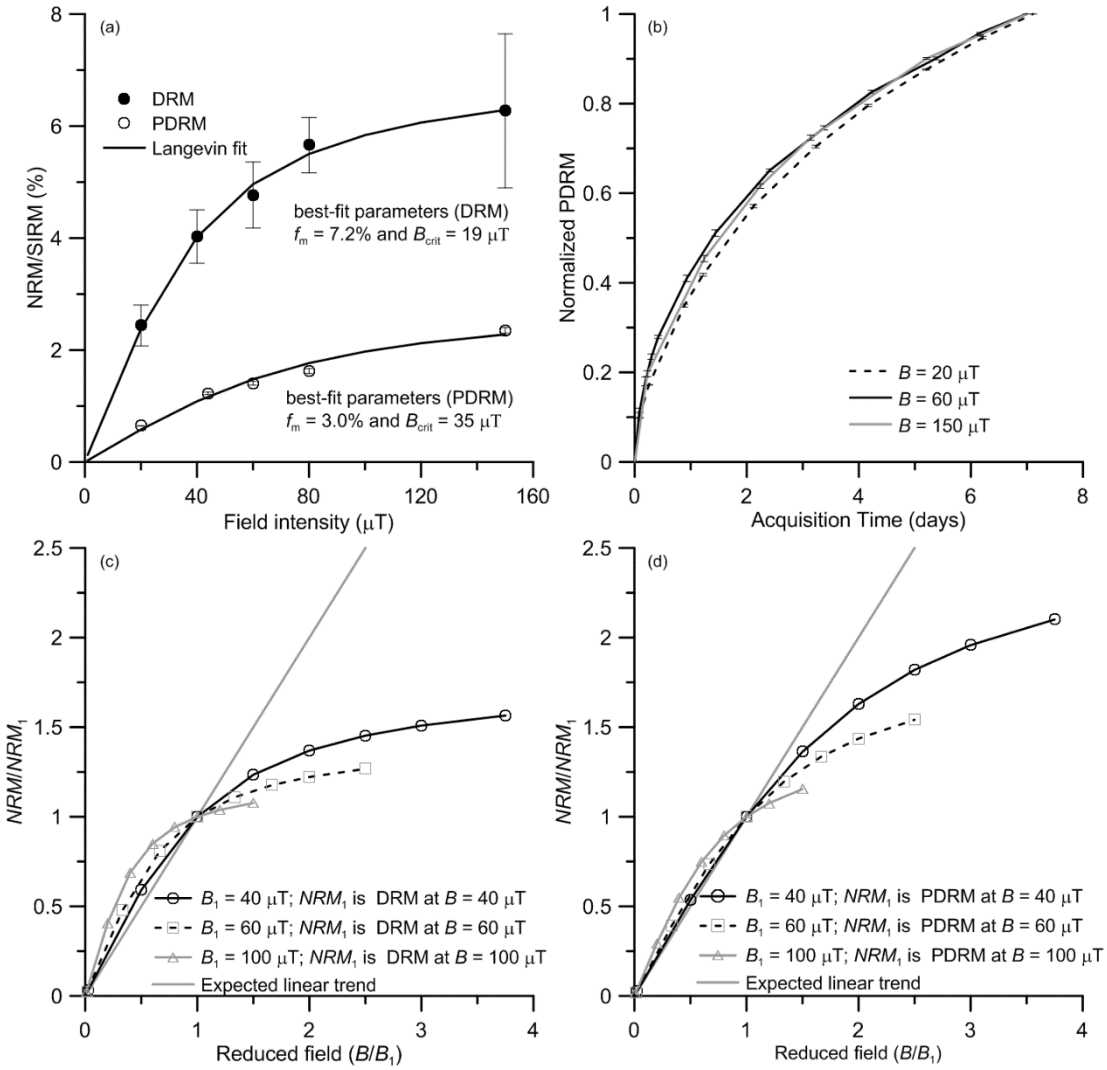

Figure 2-15 Field dependence of NRM acquired by raw sediments. (a) DRM and PDRM are acquired in different fields (B) with 50 °inclination. The acquisition time is 16 hours for DRM and 7 days for PDRM, after 4.5 days of redeposition in zero field. Experiments have been performed on triplicates, and error bars represent the standard deviation. Lines represent least-squares fits with a Langevin law. Numbers indicates the values of the critical field, B_{crit}, of eq. 2-6. (b) Normalized PDRM as a function of acquisition time. The dependence of PDRM on acquisition time is nearly independent of field intensity. (c) Nonlinearity of DRM, as seen on normalized plots. The straight line indicates the expected linear trend. When the normalizer (B_1) is much larger than B_{crit} = 20 μT, curves clearly deviate from the linear trend in the range of $0 < B/B_1 < 1$. (d) Nonlinearity of PDRM. The curves are practically linear in the range of $0 < B/B_1 < 1$ for moderate B_1 relative to B_{crit} (40μT).

2.4 Conclusions

In order to improve our understanding of the PDRM acquisition mechanism, we improved classic redeposition experiments using fresh sediment containing natural populations of living microorganisms. In this manner, natural bioturbation was not suppressed by usual treatments such as drying, grinding, and redispersion, which are often used simulate the flocculation process.

Results from these redeposition experiments were similar to previous experiments as far as DRM acquisition is concerned. On the other hand, we could demonstrate that a significant PDRM is acquired at various times after deposition, similarly to experiments with stirred sediment and unlike all redeposition experiments without stirring. The PDRM acquired after 7 days in a magnetic field reaches ~30% of the DRM, and higher PDRM intensities can be expected for longer acquisition times. Therefore, it appears, as proposed by Kent [1973], that bioturbation is an essential mechanism required for PDRM acquisition. Unlike original experiments with stirred sediments, we attained the same conclusion using a natural sediment without artificial simulations of the bioturbation process and avoiding magnetic measurements on dried sediment, which might be falsified by an additional remanent magnetization acquired during the drying process. The role of bioturbation is proved and explained in Chapter 3 and 5.

We have also demonstrated that any initial sediment magnetization, such as a DRM, decays in zero field. This decay is due to the progressive randomization of particle orientation, rather than magnetic viscosity. Randomization can be described in terms of a rotational diffusion process, which is likely promoted by microbial activity. This process is absent in sediment subjected to treatments that destroy the original microbial community (i.e. drying and crushing), where a significant PDRM acquisition is also absent. Therefore it appears that rotational diffusion of magnetic carriers inside the sediment, which is a possible manifestation of bioturbation, is the essential mechanism responsible for PDRM acquisition.

The nature of magnetic particles (flocs) involved in PDRM acquisition was investigated by performing redeposition experiments with sediment subjected to magnetic treatments (AF, ARM, IRM) expected to modify the original magnetic moments. The lack of appreciable differences with respect to the PDRM obtained with untreated sediment indicate that the magnetic moments of flocs behave as if they originate from individual SD particles. For instance, AF demagnetization did not reduce PDRM intensity and application of a saturating field did not enhance PDRM intensity, as one would expect from magnetic moments arising from non-SD magnetic carriers or flocs containing unaligned SD particles. Given the magnetofossil-bearing nature of the sediment used for the experiments, flocs involved in PDRM acquisition likely consist of single magnetosome chains adhering to one or more sediment particles. This conclusion is also supported by the identical shape of AF demagnetization curves of PDRM and ARM, where ARM is strongly selective to non-interacting SD particles and isolated magnetosome chains. Rock magnetic analyses indicate that this type of flocs contributes to ~30% of M_{rs}. The apparent lack of PDRM contributions from other types of remanence carriers (specifically PSD and interacting SD particles) must depend on their intrinsic low acquisition efficiency, due for instance to a grain size effect.

Table 2-1 Quantities used in the redeposition experiments

T_{DRM_f}	DRM acquisition time
T_{PDRM_0}	Residence time in zero field since the start of redeposition before PDRM acquisition
T_{PDRM_f}	PDRM acquisition time
DRM_{16hrs}	DRM acquired in 16 hours, i.e. T_{DRM_f} = 16 hours
$PDRM_{16hrs}$	PDRM acquired with T_{PDRM_0} = 16 hours
$PDRM_{4.5days}$	PDRM acquired with T_{PDRM_0} = 4.5 days

Table 2-2 Relative contributions of three remanence carrier categoriesidentified with FORC analysis (i.e. PSD, non-interacting SD and interacting SD particles) to the saturation remanence M_{rs} and the ARM, respectivles. Contributions to M_{rs} have been deduced from FORC magnetization, and ARM contributions from the corresponding M_{rs} values through χ_{ARM}/M_{rs} estimates.

Remanence carriers	Relative contributions to M_{rs}	Expected χ_{ARM}/M_{rs} (mm/A)	Relative contributions to ARM
PSD	16.6%	~0.3[1]	4.7%
Non-interacting SD	24.7%	~3.5[1]	81.5%
Interacting SD	58.6%	~0.25[2]	13.8%

[1] From Egli and Lowrie [2002].[2] From Chen et al. [2007]

Table 2-3 Predicted effect of different magnetic pre-treatments on the magnetic moment of flocs (none = untreated sediment, AF = AF demagnetization, ARM = AF demagnetization with a small bias field H_{arm}, IRM = application of a saturating field). The expected floc magnetic moment is given for each combination of magnetic treatment (rows) and floc structure (columns). Furthermore, m_s is the saturation moment of a floc, i.e. the magnetic moment in a saturating field, H is the geomagnetic field, χ_{arm} is the ARM susceptibility, and M_{rs}/M_s is the remanence ratio.

Structure of floc (column) Treatment(row)	1 SD or 1 chain per floc	Several unaligned SD particles (or chains) per floc	SD clusters (or collapsed chains) per floc	1 multiple magneto-some chain per floc	1 or more PSD or MD per floc
None	m_s	Small	Small	m_s	Small
AF	m_s	~0	~0	~0	~0
ARM	m_s	Small	Small	Small	$m_s\,\chi_{arm}\,H_{arm}$
IRM	m_s	~0.5 m_s	0.2-0.5 m_s	m_s	$m_s\,M_{rs}/M_s$

Chapter 3 Microbial bioturbation affects the acquisition of a natural remanent magnetization in sediment

3.1 Introduction

The ocean floor is mostly covered by sediments and about 65% of the Earth's continents is covered by sedimentary rocks [Amiotte Suchet et al., 2003]. Sediments and sedimentary rocks represent the most important archives of the Earth's history, providing continuous records of its past climate and its magnetic field [e.g. Kent, 1982; Valet and Meynadier, 1993]. The resolution of paleoclimatic and paleomagnetic records, and their lag with respect to the time of deposition, are strongly influenced by benthic organisms, in particular through their mechanical action known as bioturbation [Richter, 1952; Boudreau, 1986b, a]. Bioturbation is responsible for thorough mixing of the uppermost sediment layer, as deduced from the vertical distribution of radioactive isotopes [Aller, 1982; Boudreau, 1994]. The mixing action of bioturbation is also expected to affect the orientation of remanent magnetization carrriers through rotational diffusion, and thus the acquisition of a natural remanent magnetization (NRM) in the geomagnetic field. The resulting delay of paleomagnetic records has been modeled by a so-called lock-in function [Bleil and von Dobeneck, 1999; Roberts and Winklhofer, 2004] which describes the fraction of locked remanence carriers as a function of depth, generally below the mixed layer. On the other hand, as shown in Chapter 2, bioturbation seems to promote the acquisition of a post-depositional remanent magnetization (PDRM) inside the mixed layer, which would progressively replace a depositional remanent magnetization (DRM). Here, we provide a proof for the role of microbial biourbation for DRM replacement and PDRM acquisition by performing redeposition experiments using sediment containing different concentrations of bacteria. These results will be used to construct a general theory of (P)DRM acquisition in bioturbated sediments (Chapters 4 and 5).

3.2 Materials and methods

3.2.1 Redeposition experiments

Sediments used in this study were sampled from the same pond in Niederlippach, Bavaria, Germany. But the sediments are divided into 3 groups by the storage time in the laboratory or by the treatment prior to the redeposition experiments. Group A , B and C consist of sediments that had been stored in the aquariums in the laboratory for 1 week, 3 months and 1 year, respectively, before experiments. Group D had been separated from group C 3 months before experiments and had been sealed in vials since then. Group E had been divided from group C shortly before experiments. After being loaded into vials, specimens of group E was introduced to 4 types of

antibiotics combined as a broad-spectrum bactericide. Antibiotics used are chloromycetin (30 mg/ml), ampicillin (100 mg/ml), streptomycin (50 mg/ml) and kanamycin (50 mg/ml). Each specimen received 20 μL of each antibiotic, i.e. a total of 80 μL of antibiotics. For redeposition experiments, each specimen consists of ca. 5 ml of slurry and 10 ml of tap water which are loaded in vials (22 mm in diameters and ca. 5 cm in height). Specimens were then sealed off so that they can be randomized by shaking before NRM acquisition. The protocol of NRM acquisition follows the description in Chapter 2. Specifically, the initializing redeposition time in zero field before PDRM acquisition (T_{PDRM_0}) is fixed to be 4.5 days, and the acquisition time (T_{PDRM_f}) is 7 days for PDRM acquisition. The DRM acquisition time (T_{DRM_f}) is 11 days or 16 hours. The inclination (I_f) of the magnetizing fields is always ~ 50 °and the intensity (B) is 60 μT. Decay of (P)DRM in zero field are also monitored for some specimens right after maximum T_{PDRM_f} and T_{DRM_f} are reached.

3.2.2 Bacteria enumeration

The spread plate method [Buck and Cleverdon, 1960] was used for the enumeration of viable bacteria that can grow on agar medium. We used Lysogeny broth (LB) agar plates as culture media, which consist of 1% w/v tryptone, 0.5% w/v yeast extract, 1% w/v NaCl and H_2O [Bertani, 1951], where % w/v represents the mass concentration (ratio of weight to volume, 1% m/v = 1g/ 100ml), e.g. 10g NaCl in 1000 ml solution makes 1% w/v. LB agar media are rich in nutrition and have been standard media for the cultivation of *Escherichia coli* (*E. coli*) which is a widely studied type of microorganism. Specimens for enumeration were first loaded in vials in the same way as in the redepositional experiments. Antibiotics were introduced to specimens from Group E afterwards. All specimens were then sealed off, randomized, i.e., redeposited. They were kept undisturbed for > 10 days so that the states of compaction or porosity of sediments are similar to that of specimens in the PDRM acquisition experiments. Later, 100 μL of slurry was extracted from below the sediment/water interface with pipet and diluted with 3.9 mL of sterilized water. After sufficient homogenization by vibration, 10 μL of dilution was extracted, mixed with 80 μL of sterilized water and evenly spread on a plate. Each group of sediments has at least 3 such specimens for enumeration. The specimens were then incubated at 37 ℃ for 16 hours, after which visible colony forming units are present and counted.

3.2.3 Grain size distribution

Grain size distribution is measured for all groups of specimens on a particle size analyzer using laser diffraction technique (Beckman Coutler LS230 at the Section for Mineralogy, Petrology and Geochemistry, Munich University). The instrument is dedicated for measuring the grain size distribution of wet sample, which greatly keeps the in-situ information of sediment particles. The measuring range of the instrument is from 400 nm to 2 mm. Each specimen is measured three times.

3.3 Results and discussions

Figure 3-1a shows the PDRM acquisition results of all groups, with the average of each group being illustrated as lines. Among sediments with 1 year of storage, untreated sediments (group C) has the highest PDRM intensity, which is > 2% of its SIRM after 7 days of acquisition (Figure 3-1a). Group D presents intermediate PDRM intensity and group E has the lowest intensity of PDRM which finally reaches only < 1% of their SIRMs. Despite the difference in intensities, all groups of specimens record similar inclination of PDRM (Figure 3-1b) that is slightly larger than the inclination of the magnetizing field (indicated by the dashed line in Figure 3-1b). Except for group A, the acquisition curves of PDRM clusters after the normalization by their own maximum PDRM (Figure 3-1c), suggesting the acquisition of these specimens proceeds towards their equilibriums at very similar rates. Group A presents an evident higher acquisition rate in the first 2 days of acquisition than others, though its final intensity is not the highest.

When transferred to zero fields, previously acquired PDRM of all specimens starts to decay with different rates (Figure 3-1d). The decay rate is slowing down with time. As shown in Chapter 2, this decay is not caused by magnetic viscosity. The decay rate is conveniently described by the half-life time (T_{half}) of PDRM which is the time when half of the acquired PDRM is lost in zero fields. Among groups A-C, T_{half} increases for specimens with shorter storage time in laboratory. Among groups C-D which have identical storage time, T_{half} clearly depends on the treatments that supposedly affect the microbial activities.

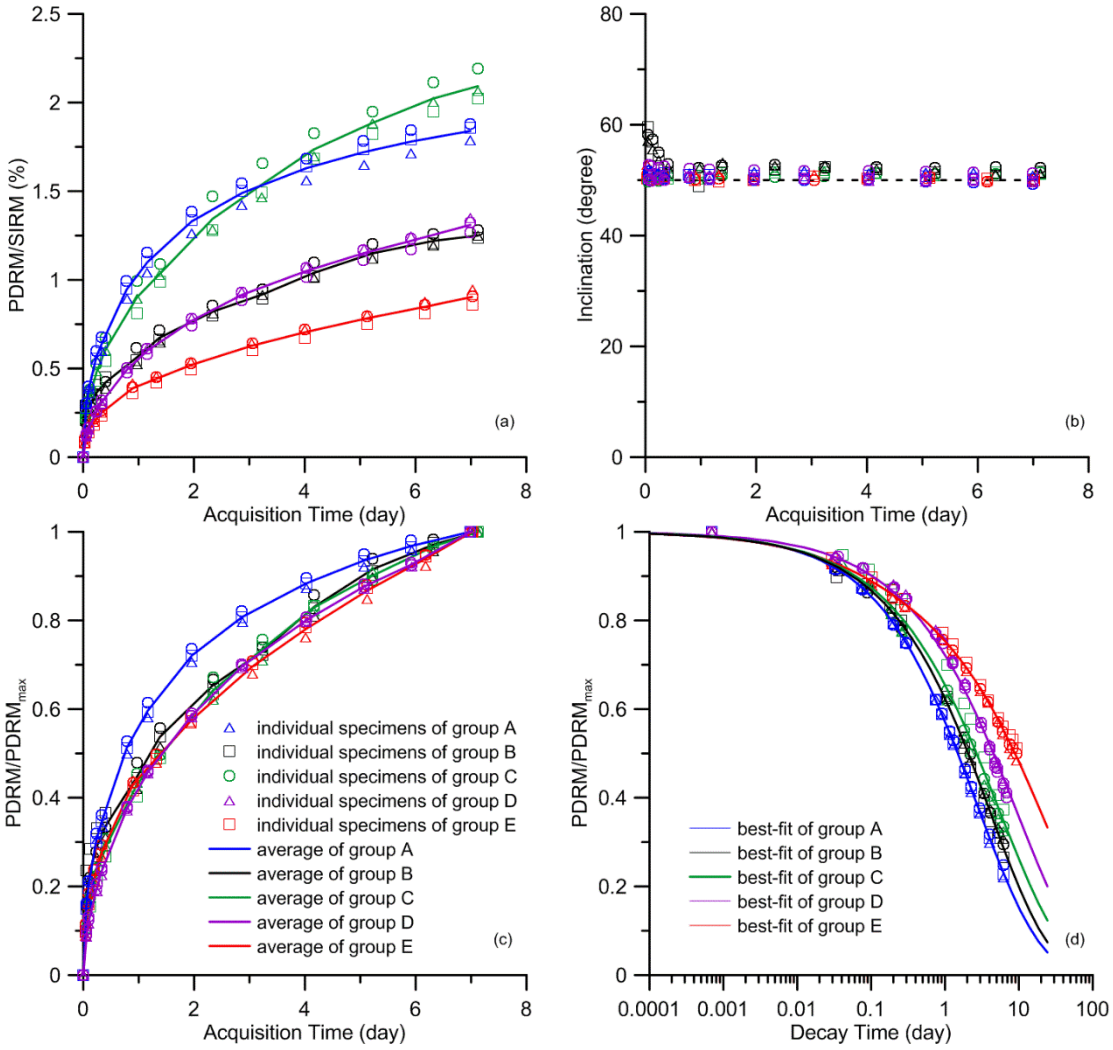

Figure 3-1 PDRM acquisition and decay. Five groups of sediments are subjected to PDRM acquisition in the field (60 μT) with 50° inclination. (a) PDRM acquisition in 7 days. T_{PDRM_0} is identically 4.5 days for all specimens. Each group has 3 parallel specimens, which are represented by symbols. The average is illustrated by solid lines. (b) Inclination of PDRM with time. The field inclination is indicated by the dashed line. PDRM is characterized by negligible inclination error. (c) Normalized PDRM by respective maximum value obtained in 7 days. Group A, which is the most fresh sediments in terms of the in-laboratory storage time, shows a different acquisition rate than other groups. (d) PDRM decay in zero fields at different rates. The experimental results can be fitted by $f_d(t) = ae^{-b\sqrt{t}} + (1-a)e^{-c\sqrt{t}}$, the best-fits are shown as solid lines. Best-fit parameters are listed in Table 3-1.

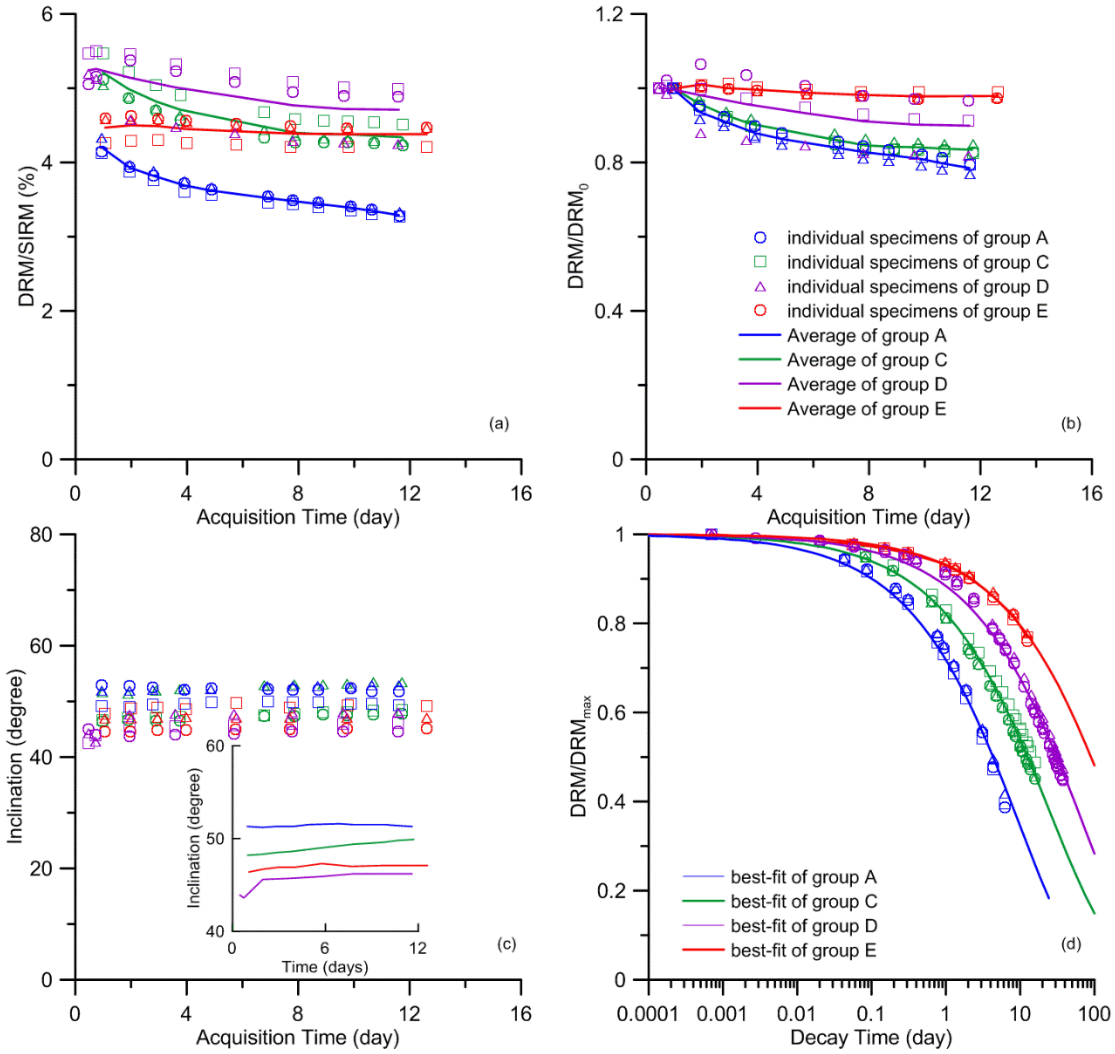

Figure 3-2 DRM acquisition and decay in zero fields of 4 groups of sediments. The magnetic field is the same as for PDRM acquisition shown in Figure 3-1. After the initial randomization, specimens were kept in the field to acquire remanence except for measurements. After each measurement specimens were immediately put back to field without randomization. (a) Evolution of DRM of 4 groups of sediments was monitored for > 11 days. Each group has 3 parallel specimens (symbols), the average is illustrated by solid lines. Group E shows negligible changes upon time, whereas DRMs of other groups consistently decline in field. The scatters within groups are larger than that of PDRM in Figure 3-1a. (b) Normalization by respective initial DRMs decreases the scatter in general. It shows the relative pattern over time is consistent and suggests the poorer reproducibility of DRM is introduced in the very early stage (<12 hours) when the mechanical state of specimens are most unstable. (c) Inclination shallowing occurs to most specimens with different extents. The average inclination of each group is shown in the inset, which shows that the inclination of all groups gets closer to the field inclination (50 °) over time. (d) When transferred to zero fields, DRMs begin to decrease and the data can be fitted by the same function that fits PDRM decay.

Figure 3-2a shows the evolution of DRM in ~11 days for above mentioned sediments except group B. The relatively large scatter of DRM intensities within the same groups is probably caused by slight differences in the rapidly changing sediment properties during the initial stages

of deposition. In fact, if DRMs are normalized by their initial values, results within the same groups become less scattered except for group D (Figure 3-2b). All groups show decline in the intensity of DRM with different extents. Unlike PDRM, most DRM consistently present inclination shallowing (Figure 3-2c). The averages of inclination of DRM are shown in the inset of Figure 3-2c for clarity. It is interesting to notice that the inclination of group C is getting closer to 50 °as acquisition time increases. There is also such a tendency for other groups, though tiny. The hypothesis that compaction results in the decline in DRM seems less satisfactory because (1) compaction can hardly lead to the improvement in inclination and (2) the change in heights of different specimens are very similar while the amount of loss in DRM are different. A better explanation is therefore in demand.

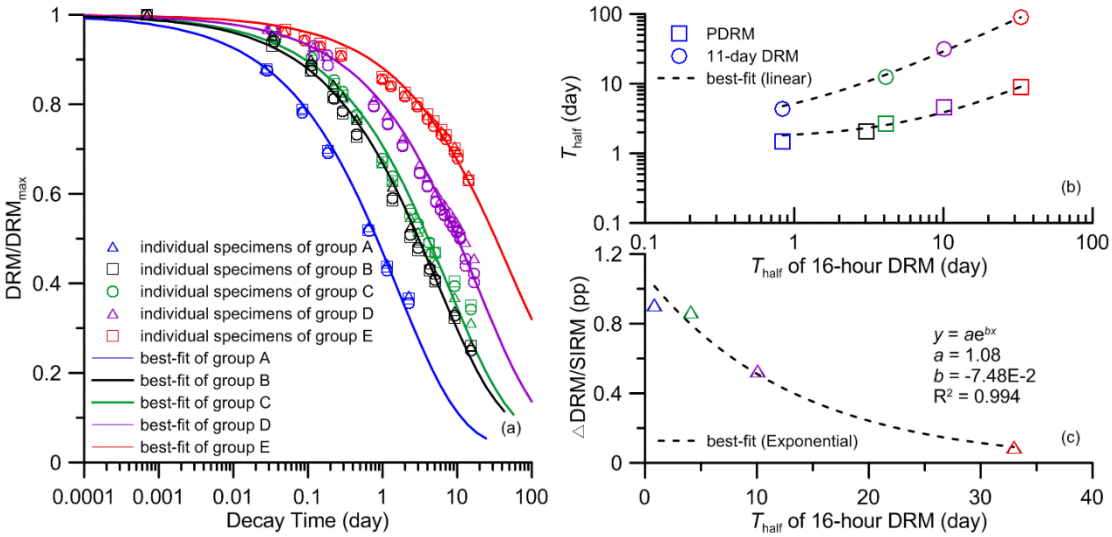

Figure 3-3 Decay of DRM acquired in 16 hours. (a) All samples had received 16 hours of DRM acquisition in a field of 60 μT before the decay test. The decay were observed in zero fields. Solid lines are best-fits by the same function as for PDRM. The half decay time (T_{half}) of each group is estimated from best-fits. (b) T_{half} of 16-hour DRM is linearly proportional to T_{half}'s of 11-day DRM (circles) and PDRM (squares). (c) The amount of lost in DRM during 11 days of acquisition is inversely correlated with T_{half} by the exponential law, which indicates the correlation between DRM lost in field and DRM decay in zero fields. Concentration of viable bacteria and T_{half}'s of (P)DRM are listed in Table 3-2.

We noticed that the specimens can be ranked as A > C > D > E by the relative amount of loss in DRM (average value) during 11 days of acquisition (Figure 3-2b), which is consistent with the ascending orders of T_{half} of PDRM (Figure 3-1d) and T_{half} of DRM (Figure 3-2d). Question is whether the loss of remanence in and off field have common origin, i.e., are the randomizing forces responsible for (P)DRM decay (happening 11 days after initializing redeposition) also affecting the acquisition of DRM within the 11 days since redeposition? To answer this question, first we need to verify the existence of randomizing effect in the first 11 days of acquisition. To this end, we can monitor the change of DRM in zero fields after 16 hours of acquisition (DRM_{16hrs}). The mechanical conditions of the sediments in this case is identical to that during 11 days of DRM acquisition. As Figure 3-3a shows, DRM_{16hrs} of all groups of specimens start to

decay in the similar pattern to that shown in Figure 3-2d, which confirms that randomizing forces are present since the early stage of redeposition. It turns out that T_{half} of DRM_{16hrs} can also be ranked in the identical order, i.e. A < B < C < D < E, which allows us to conclude that the randomizing forces in the early stage do not result from compaction, because compaction should be proceeding identically among specimens whose settling velocities are identical. Alternatively, the randomizing forces should have common origin with those responsible for the decays of PDRM and of 11-day DRM, as indicated by the good correlations among the T_{half}'s of 16-hour and 11-day DRMs and T_{half}'s of PDRMs (Figure 3-3b). Moreover, the DRM loss in 11 days varies among groups, and the values are inversely proportional to the T_{half} of DRM_{16hrs} (Figure 3-3c). Altogether, it implies that all the interesting phenomena discovered so far in this study, from DRM loss in fields to (P)DRM decay in zero fields, can be possibly accounted for by a common reason which is randomization of remanence carriers. In this scenario, some DRM carriers are broken down under the randomizing forces upon time. Such dissembled carriers probably have larger size because their floc strength tends to be weaker [Jarvis et al., 2005]. Meanwhile a fraction of the affected particles should be able to adjust their orientation after breakage, which in fact becomes a process of PDRM acquisition. The overall effect is therefore expected to result in decline in net amplitude but slight improvement in the inclination.

The next question is what causes the randomization if it is not compaction. Notice that the addition of antibiotics simultaneously results in a series of significant changes in the acquisition behaviors, i.e. lowest PDRM intensity, smallest DRM loss in field and slowest rates of (P)DRM decay in zero fields, making the antibiotics the candidate for the prominent difference of group E from the others. The volume of antibiotics is negligible to the volume of water and sediments of each specimen (< 0.6% vol), it should not cause any dramatic changes in the mechanical conditions such as dynamic viscosity and flocculation. For example, the grain size distribution of group E is similar to those of other groups (Figure 3-4). Therefore, antibiotics affected PDRM acquisition only through changing the number of living microbes (Table 3-2), and thus the intensity of bioturbation.

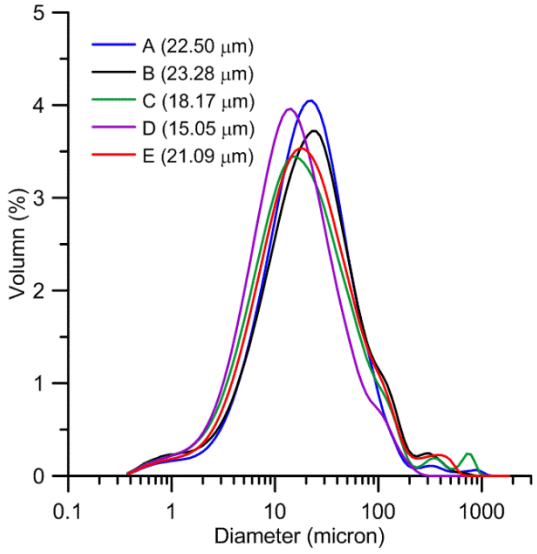

Figure 3-4 Grain size distributions of sediments of all groups. Numbers in the brackets are the median grain size of each group. No systematic difference is observed.

3.4 Conclusions

In this chapter, we control the microbial population in sediments investigated for redeposition experiments, creating five groups of samples with decreasing bacteria concentrations. The PDRM acquisition rates, as well as the (P)DRM decay rates, appear to be controlled by bacteria concentration, with fastest acquisition/decay occurring in sediment with the largest concentrations. Because the addition of antibiotics is not expected to affect other sediment properties except for the concentration of microorganisms, our experiments demonstrate the role of microbes – and therefore bioturbation – in post-depositional processes involving the orientation of remanent magnetization carriers.

Tables of Chapter 3

Table 3-1 Best-fit parameters for PDRM decay curves

Group	*a*	D_1	D_2
A	1.06E+00	9.40E-02	3.83E+00
B	1.26E+00	8.15E-02	2.89E-01
C	1.00E+00	4.49E-02	/
D	1.00E+00	2.65E-02	/
E	9.24E-01	1.06E-02	3.50E+00

Best-fit parameters for 16-hour DRM decay curves

Group	a	D_1	D_2
A	9.65E-01	1.59E-01	1.88E-13
B	9.41E-01	4.72E-02	4.00E-15
C	9.53E-01	3.36E-02	1.52E-14
D	9.57E-01	1.35E-02	9.79E-17
E	8.97E-01	5.03E-03	4.27E-16

Table 3-2 Viable bacteria counts and half-life times of PDRM and DRM(16 hours)

Group	Bacteria count (10^3 cells/mL)	T_{half} of PDRM (day)	T_{half} of DRM (day)
A	279.25 ± 10.24	1.54	0.73
B	246.67 ± 9.24	2.03	2.58
C	213.50 ± 15.77	2.63	3.58
D	206.63 ± 7.76	4.37	11.00
E	126.00 ± 8.71	8.88	26.51

Chapter 4 General theory on the acquisition of natural remanent magnetization in bioturbated sediment

The content in this chapter was published in Geochemistry, Geophysics, Geosystems. in 2015.

Abstract

We present a general theory for the acquisition of natural remanent magnetizations (NRM) in sediment under the influence of (a) magnetic torques, (b) randomizing torques, and (c) torques resulting from interaction forces. Dynamic equilibrium between (a) and (b) in the water column and at the sediment-water interface generates a detrital remanent magnetization (DRM), while much stronger randomizing torques may be provided by bioturbation inside the mixed layer. These generate a so-called mixed remanent magnetization (MRM), which is stabilized by mechanical interaction forces. During the time required to cross the surface mixed layer, DRM is lost and MRM is acquired at a rate that depends on bioturbation intensity. Both processes are governed by a MRM lock-in function. The final NRM intensity is controlled mainly by a single parameter γ that is defined as the product of rotational diffusion and mixed layer thickness, divided by sedimentation rate. This parameter defines three regimes: (1) slow mixing ($\gamma < 0.2$) leading to DRM preservation and insignificant MRM acquisition, (2) fast mixing ($\gamma > 10$) with MRM acquisition and full DRM randomization, and (3) intermediate mixing. Because the acquisition efficiency of DRM is larger than that of MRM, NRM intensity is particularly sensitive to γ in case of mixed regimes, generating variable NRM acquisition efficiencies. This model explains (1) lock-in delays that can be matched with empirical reconstructions from paleomagnetic records, (2) the existence of small lock-in depths that lead to DRM preservation, (3) specific NRM acquisition efficiencies of magnetofossil-rich sediments, and (4) some relative paleointensity artifacts.

4.1 Introduction

Understanding the acquisition of a natural remanent magnetization (NRM) by sediment settling in the Earth's magnetic field is a long-standing problem in paleomagnetism that has been subjected to detailed experimental and theoretical investigations for over 60 years [e.g. Roberts et al., 2013]. The two main NRM acquisition processes considered by these investigations are the depositional remanent magnetization (DRM), which is acquired during and shortly after deposition, and a delayed, so-called post-depositional remanent magnetization (PDRM). DRM acquisition models focus on flocculation of settling particles in the water column, particle rolling at the point of deposition [Griffiths et al., 1960; Jezek et al., 2012; Bilardello et al., 2013], and

resuspension/reflocculation near the sediment-water interface [van Vreumingen, 1993; Katari and Tauxe, 2000; Tauxe et al., 2006; Heslop, 2007; Shcherbakov and Sycheva, 2010]. On the other hand, PDRM is defined as a remanent magnetization that is acquired upon magnetic particle rotation against the yield strength of sediment until it is fully locked inside the consolidating layer [Shcherbakov and Shcherbakova, 1987; Roberts et al., 2013]. Delayed PDRM acquisition has been modeled by a so-called lock-in function, which represents the fraction of blocked PDRM as a function of depth below the surface mixed layer [Bleil and von Dobeneck, 1999; Channell and Guyodo, 2004; Roberts and Winklhofer, 2004; Suganuma et al., 2011].

The role of bioturbation as a possible PDRM acquisition mechanism was first considered by Kent [1973] and Tucker [1980], who assumed that remanence carriers could be realigned during sediment disturbance by benthic organisms. This type of PDRM originates inside the surface mixed layer, where benthic organisms are active, rather than below. Lock-in functions with non-zero contributions from the surface mixed layer have been proposed by Channell and Guyodo [2004]. Although the role of sediment mixing during PDRM acquisition has been recognized, the exact mechanism remains unclear. Mao et al. [2014b] explained laboratory PDRM acquisition in sediment containing living magnetotactic bacteria in terms of a dynamic equilibrium between aligning magnetic torques on the one hand, and randomizing forces due to sediment mixing on the other hand. With explicit reference to the physical alignment of magnetofossils, this type of PDRM has been referred to as ‘biogenic remanent magnetization’ [Heslop et al., 2013], in order to distinguish it from the more general concept of biogeochemical remanent magnetizations acquired within a chemical lock-in zone [Tarduno and Wilkison, 1996; Tarduno et al., 1998; Larrasoaña et al., 2014]. Because bioturbation can affect a wide range of remanence carriers, including those with non-biogenic origins, we use the term ‘mixing remanent magnetization’ (MRM) for all types of remanent magnetizations acquired in sediment through internally driven mixing. As far as laboratory experiments are concerned, MRM is not necessarily identifiable with the PDRM acquired by sediment stirring [e.g. Kent, 1973], because, as we will discuss in section 4.2, bioturbation is characterized by specific mixing signatures.

The role of MRM as a source of NRM is unknown, given the existence of contradictory conclusions about DRM preservation inside the surface mixed layer. For example, Katari et al. [2000] reported substantial NRM preservation in marine sediments exposed to the burrowing activity of polychaete worms in a reversed polarity field for 3 weeks. On the other hand, simple calculations based on solid diffusion constants associated with bioturbation support the opposite conclusion that any original magnetic orientation will be randomized before magnetic particles reach the consolidating layer [Mao et al., 2014b]. The scope of the present paper is to provide a general model for remanent magnetization acquisition inside the surface mixed layer using a minimum set of physical parameters to characterize bioturbation and mechanical sediment properties. This model is used to explain important known aspects of NRM acquisition, namely (1) lock-in delays through a lock-in function that can be matched with empirical reconstructions based on paleomagnetic records, in particular those of Channell and Guyodo [2004], (2) the occurrence of DRM preservation and small lock-in depths for specific sedimentary settings [Tauxe et al., 2006], (3) the specific NRM acquisition efficiency of magnetofossil-rich sediments

[e.g. McNeill and Kirschvink, 1993], and (4) variable NRM acquisition efficiency that can explain relative paleointensity artifacts [Yamazaki et al., 2013; Ouyang et al., 2014].

4.2 Sediment mixing models

Bioturbation is the phenomenon by which sediment is mixed by benthic organisms within the so-called benthic mixed layer, which generally comprises the topmost 2-20 cm of the sedimentary column (see Figure 2-13). A consequence of this activity is that the age of the mixed layer is continuously reset, as seen from depth-invariant concentrations of age-dependent tracers (e.g., radionuclides) [Boudreau, 1994; Trauth et al., 1997]. While the influence of bioturbation on vertical sediment transport has been widely studied, possible effects on the orientation of magnetic carriers are mostly unknown, so that opposite points of view exist on DRM preservation through the mixed layer, ranging from full preservation [e.g. Katari et al., 2000] to full destruction [e.g. Mao et al., 2014b]. Bioturbation models are usually divided into two main categories according to the invoked transport mechanism, i.e., local (diffusion-like) and non-local (advection-like). These two mechanisms affect the orientation of magnetic carriers in a specific manner, leading to different DRM preservation and MRM acquisition capabilities, as discussed in the following.

4.2.1 Non-local mixing models

The paradigm example of so-called non-local sediment mixing is represented by the activity of burrowing organisms, in particular polychaete worms (see Figure 2-13). These worms transport sediment ingested at a certain depth by egesting it near the sediment surface [Shull, 2001]. This activity produces a conveyor belt-like vertical mixing of solid material: upward transport occurs inside the worms, while the surrounding sediment is slowly buried by the resuspended and redeposited material egested near the sediment surface. A new DRM is acquired during redeposition, so that the mixed layer is subjected to a continuous DRM renewal with no PDRM overprint [Katari et al., 2000]. Some other non-local sediment mixing mechanisms, such as crawling of crustaceans [e.g. Solan et al., 2004], are expected to work in a similar manner through sediment resuspension. On the other hand, burrowing activities unavoidably produce some small-scale (local) mixing: for example, polychaete worms release part of the ingested sediment in-situ, without transporting it to the surface [Shull, 2001].

Non-local sediment transport is modeled through a so-called exchange function $K(z_1, z_2)$, which expresses the velocity of sediment transport from depth z_1 to depth z_2 [Boudreau, 1986b; Meysman et al., 2003] (see Appendix A0 for a list of symbols and mathematical notations used in this Chapter). Only exchange functions of the type $K(z_1, 0)$ can be expected to preserve magnetizations inside the mixed layer, because randomized sediment is supplied just at the sediment-water interface (i.e., $z_2 = 0$). However, more realistic models, based for instance on exponential exchange functions of the type $K(z_1, z_2) \propto e^{-|z_1 - z_2|/\lambda}$ [e.g. Solan et al., 2004], assume that sediment transport takes place between any pair of depths with consequent DRM loss.

Non-local transport models cannot be solved uniquely with respect to tracer concentration profiles, so that arbitrary assumptions need to be made about the exchange function and the fraction of transported material subjected to DRM losses.

4.2.2 Local mixing models

Local mixing models represent sediment fluxes in terms of a solid diffusion process that depends on a single parameter: the self-diffusion or biodiffusion constant D_b, in units of length^2/time [Boudreau, 1986a; Meysman et al., 2003]. The random nature of solid diffusion at the level of individual sediment particles implies that any remanent magnetization becomes progressively overprinted. In most cases, radioactive tracer profiles can be fitted by assuming a depth-independent value of D_b over a layer of thickness L, which is identified with the surface mixed layer [Reed et al., 2006]. Local mixing models are widespread, because they provide simple estimates of the bioturbation depth L and the bioturbation intensity D_b. Values of D_b from 0.01 to 200 cm^2/yr in combination with mixing depths between 2 and 20 cm have been reported for various coastal, shelf, slope, and deep-sea sediments [e.g. Boudreau, 1994; Teal et al., 2008]. In reality, mixing depth estimates depend on tracer half-lives, as expected in the case of smoothly declining bioturbation rates at the bottom of the mixed layer. Some organisms are capable of burrowing to depths of 2 m [e.g. Pemberton et al., 1976]; however, such deep mixing is probably rare. D_b is proportional to sediment biomass, and thus to available nutrients [Reed et al., 2006]. A positive correlation with the organic carbon flux is also found for L, with an upper limit of ~20 cm imposed by biological constraints [Trauth et al., 1997; Boudreau, 1998]. Finally, a weak positive correlation exists between D_b and the sedimentation rate ω, because nutrients are more abundant in coastal environments, where sediment accumulates more rapidly [Boudreau, 1994].

Diffusive material transport is described macroscopically by the translational Fick's law $\partial C/\partial t = D_b \Delta C$, where C is the concentration of a given substance. At the scale of individual sediment particles – defined here as elemental units that behave as individual elastic bodies – Fick's diffusion is equivalent to a random walk with net displacement $\langle r^2 \rangle = 6D_b t$ over time t [Berg, 1983]. By analogy, the orientation of individual particles subjected to random perturbations is equivalent to an angular random walk $\langle \theta^2 \rangle = 2D_r t$, where θ is the angle to an initial orientation, and D_r is the rotational diffusion coefficient in units of angle^2/time. The statistical orientation of a large number of particles subjected to rotational diffusion is governed by the rotational counterpart of Fick's law, i.e.:

$$\frac{\partial p}{\partial t} = D_r \Delta p \,, \tag{4-1}$$

where $p = p(t,\theta,\varphi)$ is the probability density function of orientation vectors (e.g., magnetic moments) in spherical coordinates [Perrin, 1934]. While several studies exist on translational and rotational diffusion of colloidal suspensions, D_r has never been measured in sediment. Nevertheless, order-of-magnitude estimates of D_r can be obtained from translational diffusion. In the case of Brownian motion (i.e., particle movement caused by molecular collisions), rotational and translational diffusion are related by the Stokes-Einstein-Debye law:

$$\frac{D_r}{D_b} = \frac{\Gamma_b}{\Gamma_r}, \tag{4-2}$$

where Γ_b and Γ_r are the translational and rotational viscous drag coefficients, respectively, which depend on particle shape and size. For the Brownian motion of spherical and disk-like particles of radius a,

$$\left[\frac{D_r}{D_b}\right]_{spheres} = 2\left[\frac{D_r}{D_b}\right]_{disks} = \frac{3}{4a^2} \tag{4-3}$$

[Koenderink et al., 2003]. The relation between translational and rotational diffusion of dense particle aggregates, such as sediments, is more complex and less well known. Significant deviations from the Stokes-Einstein-Debye relation have been reported for colloidal suspensions [Koenderink et al., 2003] and colloidal clay gels [Jabbari-Farouji et al., 2012], which means that translational and rotational diffusion can be decoupled by strong inter-particle interactions. For example, the so-called cage effect, by which particles are confined inside void spaces, suppress particle translation but not rotation. Of particular interest for sediments is the case of colloidal clay gels, where D_r/D_b is lowered by up to two orders of magnitudes with respect to eq. (4-3) [Kim et al., 2011]. Bioturbation could have a similar effect through non-local transport mechanisms (section 4.2.1).

Generally, the orientation of isolated particles subjected to random perturbations in zero field is governed by eq. (4-1) with a given initial distribution of magnetic moment directions. If the initial distribution is a function of the angle θ to a reference direction (i.e., an initially applied magnetic field) and the diffusion process is isotropic, the solution of eq. (4-1) obtained from full initial alignment at $t = 0$ is given by:

$$p(\theta,t) = \frac{1}{4\pi}\sum_{l=0}^{\infty}(2l+1)e^{-D_r l(l+1)t}P_l(\cos\theta), \tag{4-4}$$

where P_l are Legendre polynomials of order l (Appendix A1. Rotational diffusion). The progressive magnetization loss during sediment mixing follows directly from eq. (4-4) as

$$\frac{M}{M(t=0)} = \langle\cos\theta\rangle = e^{-2D_r t} \tag{4-5}$$

[Perrin, 1934]. This expression yields the half-life $t_{1/2} = \ln 2/(2D_r)$ of any mixed layer magnetization in zero field. The fraction of DRM surviving the transit of sediment through the mixed layer is obtained from eq. (4-5) if t is identified with the mean residence time L/ω. In this case, we obtain $\langle\cos\theta\rangle = e^{-\gamma}$, where $\gamma = 2D_rL/\omega$ is what we shall call the (average) rotational diffusivity parameter of the surface mixed layer. We can now try to evaluate the fate of a DRM inside the mixed layer on the basis of D_r-estimates obtained from eq. (4-3). Using $a < 100$ μm for the typical size of sediment particles [Sverdrup et al., 1942] together with D_b-estimates corresponding to various sedimentary settings listed in Table 4-1, we obtain $D_r > 150$ rad^2/yr and unrealistically small DRM half-lives of < 20 hours. On the other hand, luminophore imaging of ongoing macroscopic bioturbation are characterized by $a \approx 1$ mm [Solan et al., 2004], in which case $D_r > 1.5$ rad^2/yr and $t_{1/2} < 84$ days. Even smaller diffusion values can be obtained on the basis

of sub-Fickian rotational diffusion processes. In such cases, DRM might survive its journey through the mixed layer.

The problem with DRM survival estimates based on D_b is that an unknown fraction of the biodiffusion rate originates from the non-local transport processes discussed in section 4.2.1, whose efficiency in terms of rotational diffusion is unknown. In the following, we discuss a different strategy for obtaining a lower limit of D_r, which is based on bioturbation caused by microorganisms. Because the size of many microorganisms is comparable with that of sediment particles, the associated mixing action is of local nature by definition, greatly reducing uncertainties of D_r/ D_b. On the other hand, direct measures of microscopic bioturbation rates are not available, except for some key observations related to magnetotactic bacteria living in sediment. Their poor (~1%) alignment with the Earth's magnetic field contrasts with observations of the same bacteria in water, which demonstrates the existence of mechanical interactions between motile microorganisms and sediment particles [Mao et al., 2014a].

The displacement of motile microorganisms is governed by a biased random walk (chemotaxis) with self-diffusion coefficient D_B [Berg, 1983]. Collisions with non-motile particles transmit part of this diffusion to the whole sediment, proportionally to the volume fraction ε of motile organisms [Wilson et al., 2011] and to the probability of mechanical interactions with sediment, which we assume to be proportional to the ratio between microorganism and sediment particle cross-sections. Therefore, we set $D_b = \varepsilon (a_b/a)^2 D_B$ for microorganism-driven solid diffusion in sediment, where a_b and a are the radii of microorganisms and sediment particles, respectively. Furthermore, $\varepsilon = \varepsilon_{mob} N v$ is deduced from benthic microbial abundances N in cells/cm^3 [Kallmeyer et al., 2012], mean cell volumes $v \approx 0.03$ μm^3 [e.g. Cole et al., 1993; Šestanović et al., 2005], and fraction $\varepsilon_{mob} > 0.2$ of motile microbes [Fenchel, 2001; Mitchell and Kogure, 2006]. Finally, microscopy of cultured bacteria suspensions yields $D_B \approx 0.1$ cm^2/yr [Wilson et al., 2011; Martinez et al., 2012], while $D_B \approx 1$ cm^2/yr can be deduced from the displacement of magnetotactic bacteria in sediment shielded from magnetic fields (i.e., $\langle r^2 \rangle = 0.2$ cm over 14 days, Mao et al. [2014b]).

Using the most conservative estimates of D_B in combination with $a \approx$ 10 - 100 μm and $a_b \approx 0.2$ μm, we obtain D_r values comprised between 6×10^{-9} and 0.02 rad^2/yr (Table 4-1), which, being based only on part of the whole benthic community, should be considered as a lower limit of rotational biodiffusion. Accordingly, upper limits for the DRM fraction that survives bioturbation are comprised between ~0 and ~100%, depending on the sedimentary setting (Table 4-1). The best chances of DRM survival occur in nutrient-poor (i.e., small D_rL) and rapidly accumulating sediment (i.e., large ω), where $\gamma < 1$. Even if our estimates are affected by order-of-magnitude uncertainties, they provide strong evidence for the possibility that significant fractions of the total NRM can be acquired inside the surface mixed layer. Furthermore, cases with partial DRM preservation listed in Table 4-1 are of particular interest for relative paleointensity reconstructions, because, as we will see later, different DRM and PDRM acquisition efficiencies can lead to NRM fluctuations driven by the rotational diffusivity γ of the surface mixed layer.

4.3 Equilibrium solutions for particle orientations in water and sediment

The orientation of sediment particles is controlled by the simultaneous action of (a) driving forces (i.e., bioturbation and Brownian motion), (b) viscous forces, (c) many-body interaction forces (e.g., hard contacts, electrostatic, Van der Waals) and (d) external forces (gravity, magnetic torques). The nature of most forces is extremely complex and unknown in detail; therefore, we approach the problem in a statistical manner. Torques are conveniently defined as the gradient $-\nabla V$ of a so-called torque potential $V(\theta,\varphi)$ expressed in spherical coordinates (θ,φ), where θ is the angle to the applied field. In this case, magnetic torques are generated by $V=-mB\cos\theta$, where *B* is the ambient field and *m* the magnetic moment of individual sediment particles or flocs. On the other hand, the random nature of interactions with neighbor particles is best described by an appropriately defined random potential, as shown later in section 4.3.2.

The probability density function $p=p(t,\theta,\varphi)$ of particle orientations subjected to rotational diffusion in a torque potential *V* is governed by the so-called Smoluchowski-Debye equation:

$$\frac{\partial p}{\partial t}=D_{\mathrm{r}}\Delta p+\frac{1}{\Gamma_{\mathrm{r}}}\nabla\left(p\nabla V\right), \tag{4-6}$$

where Γ_{r} is the rotational viscous drag coefficient. This coefficient depends on the size and shape of the diffusing particles: for example, $\Gamma_{\mathrm{r}}=8\pi\eta a^3$ for spheres with radius *a* immersed in a fluid with dynamic viscosity η. Under stationary conditions, *p* reaches a dynamic equilibrium with the ambient field, fulfilling eq. (4-6) with $\partial p/\partial t=0$. The general solution of the Smoluchowski-Debye equation at equilibrium is the Boltzmann distribution:

$$p(\theta,\varphi)=p_0\exp\left(\frac{-V(\theta,\varphi)}{D_{\mathrm{r}}\Gamma_{\mathrm{r}}}\right), \tag{4-7}$$

where p_0 is a constant ensuring that the total probability associated with *p* is 1 (Appendix A). The expected magnetization *M* resulting from magnetic moment orientations with distribution *p* is obtained by integrating the *z*-components of the moment vectors over the unit sphere, i.e.,

$$\frac{M}{M_0}=\int_{\varphi=0}^{2\pi}\int_{\theta=0}^{\pi}p(\theta,\varphi)\cos\theta\sin\theta\,\mathrm{d}\theta\,\mathrm{d}\varphi, \tag{4-8}$$

where M_0 is the maximum magnetization obtained from full alignment in the external field.

In the following, we discuss specific solutions of the Smoluchowski-Debye equation representing limit cases of particles or flocs with negligible interactions, as typically encountered in the water column and near the sediment-water interface, and with strong interacting forces, as expected in the mixed layer, and more so in the consolidating layer.

4.3.1 Isolated particles in a perturbed medium

We assume magnetic particles to be suspended in a viscous medium, with rotational diffusion originating from Brownian motion or from turbulence. The sole potential acting on the particles originates from magnetic torques, i.e., $V=-mB\cos\theta$. In this case, eq. (4-7) yields the well-known Fisher-Von Mises distribution [Fisher, 1953]:

$$p(\theta) = \frac{\kappa}{4\pi \sinh \kappa} e^{\kappa \cos \theta}, \tag{4-9}$$

with $\kappa = mB/(D_r\Gamma_r)$. The associated magnetization obeys a Langevin law with:

$$\frac{M_{eq}}{M_0} = \boldsymbol{L}\left(\frac{mB}{D_r\Gamma_r}\right) \tag{4-10}$$

where $\boldsymbol{L}(x) = \coth x - 1/x$ is the Langevin function. The fluctuation-dissipation theorem gives $D_r = k_B T/\Gamma_r$ for the case of Brownian motion, where k_B is the Boltzmann constant and T the absolute temperature, so that

$$\frac{M_{eq}}{M_0} = \boldsymbol{L}\left(\frac{mB}{k_B T}\right) \tag{4-11}$$

describes the alignment of magnetic particles in undisturbed fluids. This solution has been used to quantify the statistical alignment of magnetic bacteria in water [Frankel and Blakemore, 1980; Mao et al., 2014b]. An important generalization of eq. (4-11) is obtained if $k_B T$, which is the mean torque of perturbations arising from molecular collisions, is replaced by the mean torque τ_p of unspecified random perturbations, i.e.,

$$\frac{M_{eq}}{M_0} = \boldsymbol{L}\left(\frac{mB}{\tau_p}\right) \tag{4-12}$$

(Figure 4-1). An essential condition for the validity of eq. (4-12) is that flocs behave as discrete bodies with negligible reciprocal interaction forces. For example, τ_p can be identified with the amplitude of hydrodynamic torques from small vortices created by magnetic flocs sinking in the water column [Heslop, 2007]. In this case, eq. (4-12), along with an appropriate description of flocculation dynamics [Shcherbakov and Sycheva, 2010], governs DRM acquisition. Using the calculations of Heslop [2007], eq. (4-12) yields $M_{eq}/M_0 = 0.88$ for 8 μm flocs with an aspect ratio of 1.1 sinking in a 50 μT field, and $M_{eq}/M_0 = 0.09$ for 12 μm flocs. This example illustrates the well-known problem of non-linear DRM acquisition by smaller flocs [Tauxe et al., 2006].

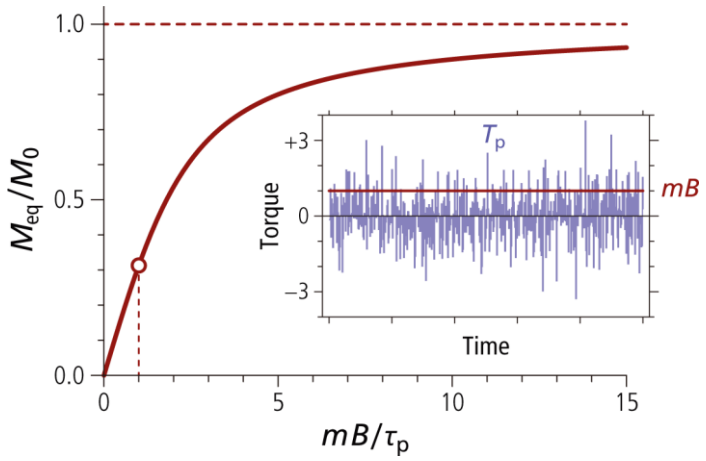

Figure 4-1 Normalized equilibrium magnetization, M_{eq}/M_0, of particles with magnetic moment m in a magnetic field B, when subjected to random perturbing torques T_p with zero mean and standard deviation τ_p. The magnetization corresponding to $mB/\tau_p = 1$ is marked by a dot, with a sequence of 500 perturbations shown in the inset.

4.3.2 Equilibrium magnetization in mixed sediment

Mao et al. [2014b] used eq. (4-12) to explain PDRM acquisition experiments in sediments with 68-88% porosity, identifying τ_p with the typical energy of microscopic bioturbation events. A serious limit of this approach is represented by the fact that individual sediment particles (defined as the smallest units with elastic body behavior) are not independent from each other, as required by eq. (4-12). Instead, a dense network of inter-particle forces grows rapidly below the sediment-water interface, as seen in colloidal suspensions upon reaching a critical packing fraction [Weitz, 2011]. This network holds individual particles in place against random perturbations, and is responsible for the rheological response of sediment to mechanical stresses. As with the case of random perturbations, we are interested in particle rotation, and represent holding forces in terms of torques derived from a so-called "holding" potential $U(\theta,\varphi)$. Each particle is characterized by its own holding potential, which depends on the relative position of neighbor particles, and the type of interaction forces (e.g., hard contacts, electrostatic, Van der Waals). Given the disordered nature of sediment, this potential possesses local minima corresponding to a certain number of random, or almost random orientations at equilibrium.

Small perturbations produce reversible particle rotation within the potential wells of U, which determine the elastic response of sediment. Larger perturbations, on the other hand, might be sufficient to overcome the potential barriers between local minima, in which case irreversible particle rotation will occur, yielding plastic deformations. Especially for irreversible rotations, holding potentials change in response to relative particle displacement/rotation, so that a rigorous formulation of $U(\theta,\varphi)$ must take the time evolution of particle interactions into account. Because details about such interactions are largely unknown, we proceed with a simplified approach based on static random potentials. These potentials can reproduce the fundamental difference between sediment and diluted suspensions, i.e., the existence of forces that must be overcome in order to irreversibly change particle orientations. Holding potentials are ultimately responsible for blocking remanence carriers against changes of the ambient field and, in the laboratory, against applied fields, for instance during alternating field (AF) demagnetization.

As seen in section 4.3.1, solutions of the Smoluchowski-Debye equation for the statistical distribution $p(\theta,\varphi)$ of particle orientations at equilibrium are governed by the total potential of each particle, which is now given by $V_i = -m_i B\cos\theta + U_i(\theta,\varphi)$ for particle i. Because each particle is subjected to its own holding potential, $p(\theta,\varphi)$ is the ensemble average of single particle solutions, i.e.,

$$p(\theta,\varphi) = \left\langle c_i \exp\left(\frac{m_i B\cos\theta - U_i(\theta,\varphi)}{D_r \Gamma_r} \right) \right\rangle, \tag{4-13}$$

where $\langle \ldots \rangle$ is used to indicate an ensemble average. $D_r\Gamma_r$ is conveniently replaced by the amplitude τ_p of randomizing torques. In order to evaluate eq. (4-13), we need an explicit formulation of U_i as a random potential with an appropriate number of local minima representing stable orientations in the force field caused by neighbor particles. For this purpose, we follow the general solution approach of Alexiewicz [2000] and represent U_i as a series of spherical harmonic functions, i.e.,

$$U_i(\theta,\varphi) = \sum_{l,m} u_l(\xi_{i,m}\cos m\varphi + \zeta_{i,m}\sin m\varphi)P_l^m(\cos\theta)\,, \tag{4-14}$$

where P_l^m are the associated Legendre polynomials with Schmidt quasi-normalization [Winch et al., 2005], u_l are coefficients expressing the expected spectral amplitude of terms with order l, and $\xi_{i,m}$, $\zeta_{i,m}$ are random realizations of a statistical variable with zero expectation, unit variance, and a given probability density function, e.g., the normal distribution $\boldsymbol{N}(0,1)$. The spectral amplitudes u_l should be chosen so that the number of local minima is comprised between 2 (i.e. uniaxial holding potentials) and the maximum number (~10, Torquato [1995]) of nearest random packing neighbors. Furthermore, the associated torques $\mathbf{T}_i = -\nabla U_i$ shall be characterized by a white spherical harmonic spectrum. These conditions can be satisfied only if the sum in eq. (4-14) is truncated to a certain maximum harmonic degree n. In this case,

$$U_i(\theta,\varphi) = \left[\sum_{l=1}^{n}\frac{l}{2l+1}\right]^{-1/2}\sum_{l=1}^{n}\frac{1}{\sqrt{(l+1)(2l+1)}}\sum_{m=0}^{l}(\xi_{i,m}\cos m\varphi + \zeta_{i,m}\sin m\varphi)P_l^m(\cos\theta) \tag{4-15}$$

yields unit root mean square torques, i.e., $\langle T_i^2\rangle = 1$ (see Appendix A3. Construction of random holding potentials for a proof based on Constable and Parker [1988]). Some realizations of U_i with n = 4,6,9 are shown in Figure 4-2.

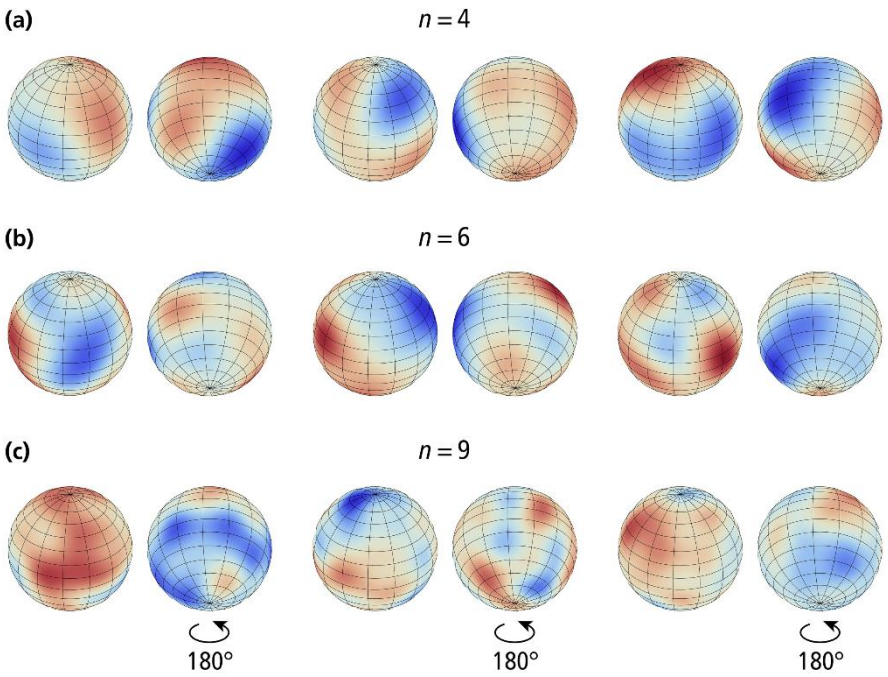

Figure 4-2 Examples of random holding potentials $U(\theta,\varphi)$ generated with eq. (15) using spherical harmonic functions with maximum degree n = 4 (a), n = 6 (b), and n = 9 (c). Three examples are given for each n, with the right-hand image showing the same potential as the left-hand one after 180 ° rotation. Stable particle orientations are defined by local minima of $U(\theta,\varphi)$ (blue).

The ensemble average of eq. (4-13) with U_i given by eq. (4-15) yields the mean equilibrium magnetization:

$$\frac{M_{\mathrm{eq}}}{M_0}=\left\langle \frac{1}{p_{0,i}}\iint_{\Omega}\exp\left(\frac{m_i B}{\tau_{\mathrm{p}}}\cos\theta-\frac{\tau_{\mathrm{h}}}{\tau_{\mathrm{p}}}U_i(\theta,\varphi)\right)\sin\theta\cos\theta\,\mathrm{d}\theta\,\mathrm{d}\varphi\right\rangle, \tag{4-16}$$

where Ω denotes integration over the unit sphere, and τ_{p}, τ_{h} are the root mean square amplitudes of perturbing and holding torques acting on individual particles, respectively.

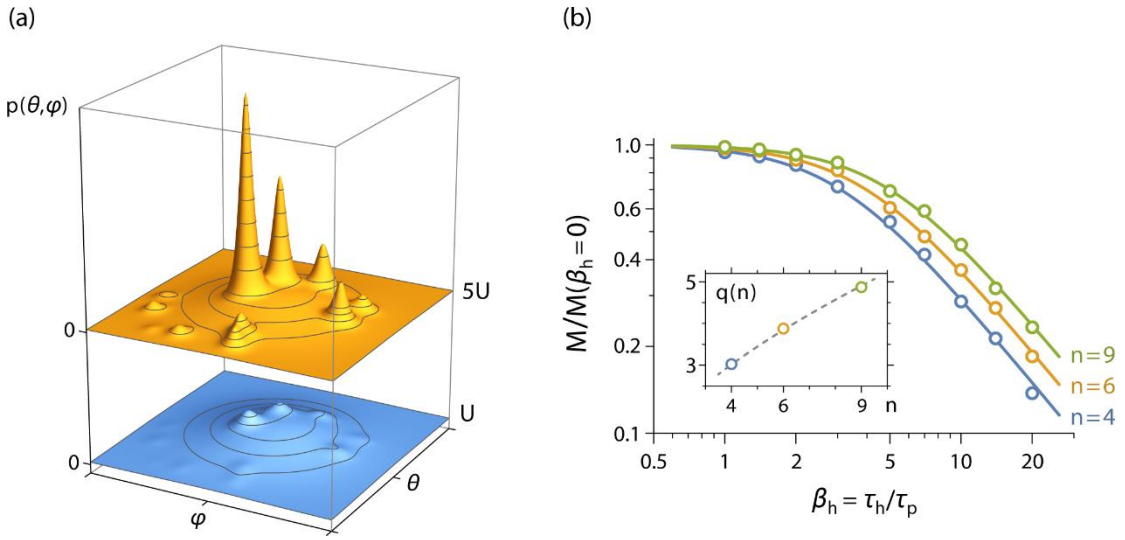

Figure 4-3 Effects of holding poentials on particle alignment. (a) Probability density function $p(\theta,\varphi)$ of particle orientation in a total potential $-mB+U$ (blue surface) and $-mB+5U$ (orange surface), where U is a random holding potential. Local minima of U produce probability maxima at random orientations (peaks) that do generally not coincide with the direction (θ_0,φ_0) of B. This effect is particularly pronounced for large amplitudes of U (orange surface), resulting in smaller mean particle alignments and equilibrium magnetizations. (b) Decrease of the equilibrium magnetization M in random holding potentials of the type shown in Figure 4-2, with respect to the case of no holding potential (i.e., β_{h} = 0). Each dot corresponds to the ensemble average of up to 3×10^5 random potential realizations with maximum spherical harmonic order n = 4,6,9. Lines are least-squares fits of the numerical results according to eq. (4-18). The dependence of the fitting parameter q on n is shown in the inset.

Eq. (4-16) cannot be evaluated analytically; however, the main characteristics of the equilibrium magnetization can be understood by considering two limit cases. The first limit case is that of a weak holding potential, i.e., $\tau_{\mathrm{h}} \ll \tau_{\mathrm{p}}$, which means that particles are practically free to rotate under the influence of perturbing torques, yielding the Langevin law in eq. (4-12). For strong holding forces, i.e., $\tau_{\mathrm{h}} \gg \tau_{\mathrm{p}}$, the orientation of individual particles is dictated by local, randomly positioned minima of U_i. Such orientations deviate from the equilibrium resulting from the interplay between magnetic and perturbing forces, thereby reducing the overall alignment with the applied field (Figure 4-3a). In practice, the Langevin approximation obtained by neglecting the holding potential is valid for $\tau_{\mathrm{h}}/\tau_{\mathrm{p}}<1$ (Figure 4-3b). Above this limit, M_{eq}/M_0 starts to decrease with increasing τ_{h}, i.e.,

$$\frac{M_{\mathrm{eq}}}{M_0}\approx \boldsymbol{L}\left(q\frac{mB}{\tau_{\mathrm{h}}}\right) \tag{4-17}$$

where q is a constant that depends weakly on the maximum order n of the spherical harmonics used to construct the random holding potentials (i.e., $q \approx 3.0, 3.9, 4.9$ for $n = 4, 6, 9$, respectively). Finally, a general analytical approximation of eq. (4-16) that holds for both limit cases as well as intermediate solutions is given by

$$\frac{M_{\mathrm{eq}}}{M_0} \approx \boldsymbol{L}\left(\frac{mB}{\sqrt{\tau_{\mathrm{p}}^2 + (\tau_{\mathrm{h}}/q)^2}}\right) \tag{4-18}$$

(Figure 4-3b). In this case, $q \approx 1.31n^{0.6}$ is the value of the "Boltzmann factor" $\beta_{\mathrm{h}} = \tau_{\mathrm{h}} / \tau_{\mathrm{p}}$ for which the equilibrium MRM attained in small fields is $2^{-1/2} \approx 71\%$ of the value predicted by the Langevin law in absence of holding forces. If $mB \ll \tau_{\mathrm{p}}$, as expected inside the mixed layer (see section 4.4), a linear approximation of eq. (4-18) based on $\boldsymbol{L}(x) \approx x/3$ yields

$$\frac{M_{\mathrm{eq}}}{M_0} \approx \frac{mB}{3\sqrt{\tau_{\mathrm{p}}^2 + (\tau_{\mathrm{h}}/q)^2}}\,. \tag{4-19}$$

An important effect of the holding potential, beside that of lowering the equilibrium MRM, consists in slowing down the rate at which this equilibrium is approached: as τ_{h} becomes larger than τ_{p}, fewer perturbations are able to overcome the energy barriers of U_i to produce irreversible magnetic moment rotations, until the system becomes entirely fixed for $\tau_{\mathrm{h}} \gg \tau_{\mathrm{p}}$. This effect plays a fundamental role in locking the acquired MRM at the bottom of the mixed layer, as explained in section 4.4.

4.3.3 Inclination shallowing

Sediment NRM is often affected by inclination shallowing, due to rotation of elongated magnetic grains toward horizontal directions [Griffiths et al., 1960; Mitra and Tauxe, 2009; Jezek et al., 2012] and to sediment compaction [Arason and Levi, 1990]. While compaction-shallowing occurs at depths of several tens of meters below the mixed layer and is not relevant for initial NRM acquisition, a possible MRM shallowing source is represented by sediment texture. Sediment texture is typically produced by the preferred horizontal layering of platy particles (e.g., clay). Although texture buildup inside the mixed layer is counteracted by mixing, a certain degree of mechanical anisotropy can be expected in clay-rich sediment. Direct measurements of mechanical strength anisotropies are not available for the mixed layer; however, an upper limit can be deduced from data for pure clays, where the relative shear strength anisotropy is usually comprised between 20 and 60% with an average of ~40% [Won, 2013].

On a microscopic scale, mechanical strength anisotropies are caused by interaction forces with direction-dependent mean amplitudes, which introduce preferred directions for the orientation of non-equidimensional sediment particles. The direction of magnetic moments is affected by this phenomenon only if the following conditions are met simultaneously: (1) magnetic sediment particles are not equidimensional, and (2) the corresponding net magnetic moment direction is systematically related to particle shape. Magnetite-clay aggregates [Galindo-Gonzalez et al., 2009] fulfill these conditions if the magnetic moment of adhering magnetite crystals is parallel to large faces of clay platelets, as is expected for magnetosome chains. Magnetic textures created by this mechanism can be modeled by adding a systematic term A to

the random holding potentials, with preferred directions defined by local minima of *A*. The simplest form for such a potential is given by an uniaxial anisotropy contribution $A = \tau_a \cos(2\theta)/2$, where θ is the angle to the vertical and τ_a is the maximum torque amplitude produced by *A*. In case of MRM acquisition in inclined fields, the total potential acting on magnetic particles is then given by:

$$V(\theta,\varphi) = -mB(\mathbf{n}\cdot\mathbf{b}) + \frac{\tau_a}{2}\cos(2\theta) + U_i(\theta,\varphi) \tag{4-20}$$

where $\mathbf{n} = (\sin\theta\cos\varphi, \sin\theta\sin\varphi, \cos\theta)$ is the unit vector representing the direction of magnetic moments in a field $\boldsymbol{B}$ parallel to the unit vector $\mathbf{b} = (\sin\psi, 0, \cos\psi)$. As seen in section 4.3.2, random potentials U_i have the effect of dispersing magnetic moments orientations without changing their mean direction. Therefore, U_i can be neglected in inclination shallowing calculations and the mean direction of the acquired MRM is obtained by integration of the Boltzmann distribution associated with eq. (4-20) after setting $U_i = 0$, i.e.,

$$\langle\mathbf{n}\rangle \propto \int_0^{2\pi}\int_0^{\pi} e^{\beta_m(\mathbf{n}\cdot\mathbf{b}) - \beta_a\cos(2\theta)/2}\,\mathbf{n}\sin\theta\,\mathrm{d}\theta\,\mathrm{d}\varphi, \tag{4-21}$$

where $\beta_m = mB/\tau_p$. Furthermore, $\beta_a = \tau_a/\tau_p$ is a new "Boltzmann factor" representing the ratio between anisotropy and perturbing torques. Because $\beta_m \ll 1$ inside the mixed layer, eq. (4-21) can be linearized with respect to β_m and solved analytically (Appendix A4. Inclination shallowing), obtaining the classical inclination shallowing equation

$$\tan I = f_a \tan I_B \tag{4-22}$$

of King [1955], where $I = 90° - \theta$ and $I_B = 90° - \psi$ are the magnetization and field inclinations, respectively, and

$$f_a = \frac{1 - \sqrt{\frac{\beta_a}{\pi}}\,\frac{2e^{-\beta_a}}{\operatorname{erf}\sqrt{\beta_a}}}{\beta_a - \frac{1}{2} + \sqrt{\frac{\beta_a}{\pi}}\,\frac{e^{-\beta_a}}{\operatorname{erf}\sqrt{\beta_a}}} \tag{4-23}$$

is the inclination shallowing factor associated with the anisotropy potential *A* (Figure 4-4a). Maximum inclination shallowing effects observed in nature correspond to $f_a \approx 0.4$ [Tauxe and Kent, 2004], which, if associated with a MRM, would require $\beta_a \approx 2.5$ (Figure 4-4b). On the other hand, if MRM blocking occurs at $\tau_h/\tau_p \approx 1$, as discussed in section 4.4, β_a is identifiable with the relative anisotropy τ_a/τ_h of holding forces. This anisotropy can be expected to coincide with the relative anisotropy derived from mechanical strength parameters. Assuming $\tau_a/\tau_h \le 20\%$ for sediments containing up to 50% clay, the maximum MRM inclination shallowing does not exceed 2.3 °. Much smaller effects are expected for sediment particles lacking strong shape anisotropies, such as in carbonaceous sediments, where MRM inclination shallowing should be negligible.

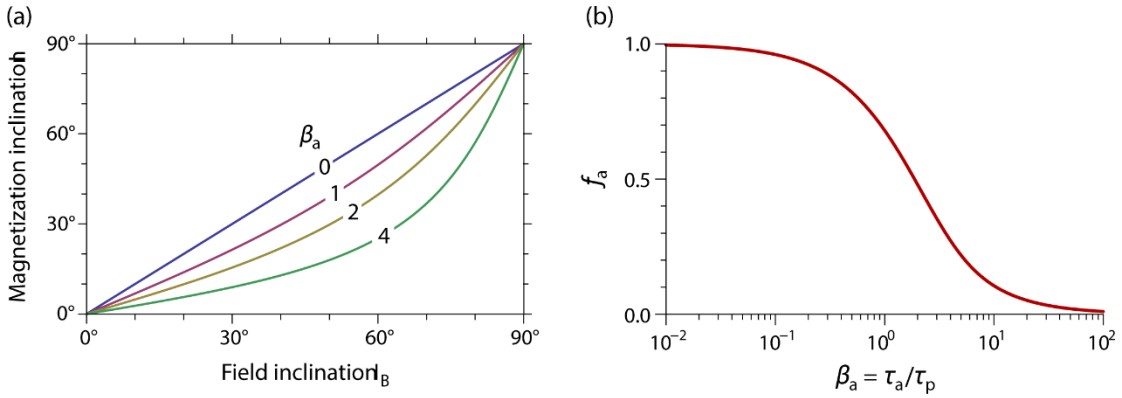

Figure 4-4 Effects of anisotropic holding potential on inclination shallowing. (a) Inclination shallowing of the equilibrium MRM, calculated with eq. (4-22 and 23) for given values of $\beta_a = \tau_a/\tau_p$, which represent increasing amplitudes of the anisotropy term $A = \tau_a \cos(2\theta)/2$ of the holding potential. (b) Inclination shallowing parameter f_a as a function of β_a according to eq. (4-23).

4.4 MRM acquisition and the lock-in function

As seen in section 4.3, a dynamic equilibrium between ordering forces (i.e., magnetic torques) and randomizing forces (i.e., bioturbation and mechanical interactions) is established inside the surface mixed layer if stationary conditions are maintained for sufficiently long times. The equilibration time depends on the mixing rate of sediment, which decreases with increasing depth, especially near the boundary between mixed and consolidating layers, up to the point where the MRM equilibrium becomes fixed. In the framework of PDRM models, the amount of blocked magnetization is expressed as a function of depth through a so-called lock-in function [Roberts and Winklhofer, 2004]. In this section, we model MRM acquisition and its lock-in by following the journey of sediment flocs from the water column to the consolidating layer. For this purpose, we use a coordinate system that moves with the mean sinking (in water) or burial (in the sediment column) velocity $\omega = \mathrm{d}z/\mathrm{d}t$. A thin horizontal layer anchored within this coordinate system will not always contain the same material because of different sinking velocities (in water) and diffusion (in water and sediment). As seen in section 4.3, rotational diffusion in the presence of magnetic torques and mechanical particle interactions is governed by the Smoluchowski-Debye equation, so that the statistical distribution $p(t,\theta,\varphi)$ of particle orientations inside our layer at any time t is given by:

$$\frac{1}{D_r(z'(t))}\frac{\partial p}{\partial t} = \Delta p + \frac{1}{\tau_p(z'(t))}\nabla\left[\, p\nabla\left(-mB\cos\theta + \tau_h(z'(t))U\right)\right], \tag{4-24}$$

where $\tau_h U$ is a random potential generating torques with root mean square amplitude τ_h, and τ_p is the root mean square amplitude of random perturbing torques (e.g., turbulence in water and bioturbation in sediment). Furthermore,

$$z'(t) = \frac{z(t)}{L} = \frac{1}{L}\int_0^t \omega(z')\,\mathrm{d}t \tag{4-25}$$

is the reduced depth of our layer as a function of time, and D_r, ω, τ_p, and τ_h are assumed to be steady-state sediment properties that depend only on the reduced depth $z' = z/L$, where L is the thickness of the mixed layer.

A general analytical expression for the time-dependent solution of eq. (4-24 and 25) is not known; therefore, we proceed with some simplifications. The first simplification consists in assuming ω to be a constant, in which case eq. (4-25) reduces to $z' = \omega t/L$. Next, we neglect all potentials and look for a general solution of the (time-dependent) diffusion equation:

$$\frac{\partial p}{\partial t} = D_r(\omega t/L)\Delta p, \tag{4-26}$$

which describes the fate of a given magnetization in zero field over time. As far as the effect of potentials on the preservation of remanent magnetizations is concerned, the reduced probability for successful irreversible rotations against strong holding torques (section 4.3.2) is equivalent to a decrease of D_r, as we will be shown below. Before proceeding to solve eq. (4-26), we need to specify the dependence of the rotational diffusion constant D_r on depth, assuming that it is entirely caused by bioturbation. Available estimates of the biodiffusion constant (D_b) are generally given as bulk averages over the mixed layer. As discussed by Reed et al. [2006], reconstructions of $D_b(z')$ from tracer dynamics require assumptions about the bioturbation mechanism, with possible solutions ranging from nearly depth-independent functions to a Gaussian-like decrease of $D_b(z')$ when moving down from the sediment-water interface. The latter model is considered more realistic, because D_b is expected to depend on the concentration of benthic organisms, and therefore on nutrient concentration profiles dictated by organic matter consumption [Rabouille and Gaillard, 1991; Boudreau, 1998; Reed et al., 2006].

Generally, organic carbon concentrations decrease exponentially within the mixed layer, down to levels that no longer support the energetic costs of deep burrowing [Berner, 1980; Rabouille and Gaillard, 1991; Roberts and Winklhofer, 2004]. Therefore, we assume that the concentration of motile benthic organisms responsible for bioturbation is proportional to the exponential decrease of organic carbon content with depth. Accordingly, the simplest bioturbation model assumes D_b and D_r to be proportional to exponential-like organic carbon profiles, i.e., $D_r = D_{r,0}c_b(z')$ where $D_{r,0}$ is the maximum value of D_r (typically at the top z = 0 of the sedimentary column) and $c_b(z')$ is an exponential profile with $c_b(0) = 1$, e.g., $c_b(z') = e^{-3z'}$ (Figure 4-5b). Additional factors that affect D_r are (1) species-dependent biological limits, for example, burrowing depths, and (2) the reduced probability of irreversible particle rotation as the mechanical strength of sediment (i.e., τ_h) increases. These two factors are somewhat connected because motile organisms will not thrive where their activity is severely limited by the mechanical strength of sediment.

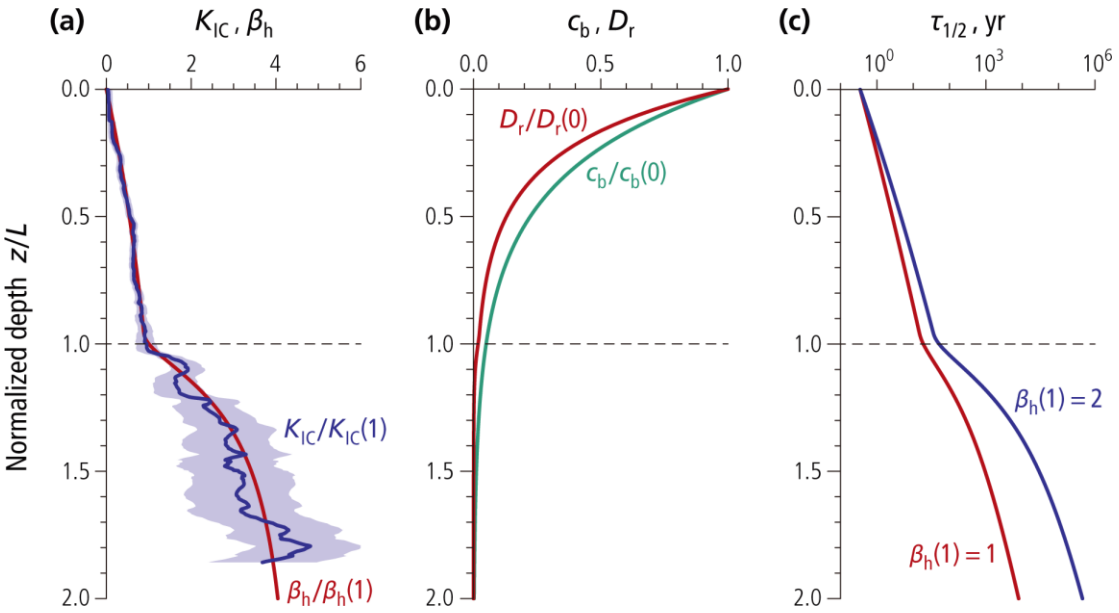

Figure 4-5 Typical sediment property profiles relevant for DRM preservation and MRM acquisition. (a) Sediment strength, expressed as the ratio $\beta_h = \tau_h/\tau_p$ between root mean square amplitudes of holding torques, τ_h, and perturbing torques, τ_p (red line). Perturbing torque amplitudes are assumed to be independent of sediment depth, while τ_h is assumed to be proportional to tensile fracture toughness (K_{IC}) profiles measured in marine sediment (from data in Johnson et al. [2012]). The average (blue line) of three K_{IC} profiles with double standard deviation confidence band (shaded) is shown after normalization with respect to sediment depth and amplitude in order to obtain a unit value at the bottom of the mixed layer (dashed line), so that $\beta_0 = \beta_h(L) = 1$. (b) Normalized profiles of benthic organism concentration c_b and rotational diffusion D_r according to eq. (4-27). (c) Equilibration half-time $\tau_{1/2}$ of mixed layer magnetizations, calculated on the basis of properties shown in (a) and (b). Two β_h-profiles proportional to (a) have been chosen. Note the logarithmic time axis in (c).

Limitation of D_r by sediment resistance is quantified by the probability for random perturbations (i.e., torques with amplitude τ_p) to overcome the energy barriers of the holding potential $\tau_h U$. This situation is equivalent to that of thermal activations, where the probability of thermal perturbations with energy $k_B T$ to overcome a given energy barrier ΔE is expressed by the Arrhenius law $e^{-\Delta E/k_B T}$. Mean energy barriers of the holding potential are dictated by the typical excursions of $\tau_h U(\theta,\varphi)$ over the unit sphere, which coincide with τ_h. In this case, the probability of irreversible particle rotations is given by $e^{-\tau_h/\tau_p}$ and our model for the rotational diffusion constant becomes

$$D_r = D_{r,0} c_b(z') e^{-\beta_h(z')}, \tag{4-27}$$

with $\beta_h(z') = \tau_h/\tau_p$. Lacking specific information on bioturbation forces, we assume that τ_p (i.e., the driving "force" of bioturbation) is a constant, while τ_h increases with depth because of sediment compaction. As a last step of our model construction, we need a reasonable estimate of $\tau_h(z')$. Since displacement of benthic organisms is attributed to crack propagation [Dorgan et al., 2005], we assume τ_h to be proportional to the tensile fracture toughness K_{IC} of sediment, and we use profiles of this parameter measured by Johnson et al. [2012] to construct the depth dependence of β_h. These profiles are characterized by a continuous increase of $K_{IC}(z)$ with a

kink and at the bottom $z = L$ of the mixed layer that marks the onset of consolidation (Figure 4-5a). The nearly linear dependence of K_{IC} on depth within the mixed layer can be attributed mainly to compaction. Similar profiles are also seen with shear strength measurements [Locat et al., 2002].

From a rheological point of view, continuous shear associated with bioturbation is expected to reduce the shear strength (a phenomenon known as shear thinning, e.g., Barnes [1997]). On the other hand, benthic organisms can excrete gelation substances that produce the opposite effect. Indeed, mixed results have been found upon adding selected species of burrowing organisms [Meadows and Tait, 1989]. Therefore, we avoid explicit links between β_h and the concentration c_b of benthic organisms, and define $\beta_h(z')$ as proportional to the K_{IC}-profiles of Johnson et al. [2012], with absolute values determined by $\beta_0 = \beta(1)$ (Figure 4-5a). In the absence of direct β_h-estimates, we assume that the bottom of the mixed layer corresponds to places where bioturbation becomes increasingly difficult because of holding forces that exceed the driving forces of bioturbation. This criterion is equivalent to setting $\beta_0 \geq 1$. Our model for $D_r(z)$ uses a minimum set of reasonable assumptions about bioturbation and mechanical sediment properties, yielding a pseudo-exponential profile of D_r through the mixed layer (Figure 4-5b), which is similar to D_b-profiles assumed elsewhere [e.g. Bentley et al., 2006].

The time evolution of the remanent magnetization of a sediment layer initially located at a depth z_0 below the sediment-water interface is obtained from eq. (4-26) with the initial condition $p(\theta, t = 0)$ corresponding to a given value M_{ini} of M. Any initial distribution p of the form given by eq. (4-4) yields the same normalized solution $M(t)/M_{ini}$. Because the layer moves down with respect to the sediment-water interface, this solution can be converted into a depth profile through $z = z_0 + \omega t$, obtaining

$$\frac{M(z, z_0)}{M_{ini}} = \exp\left[-2\frac{L}{\omega}\int_{z_0/L}^{z/L} D_r(u)\,\mathrm{d}u \right] \tag{4-28}$$

(Appendix A5. Lock-in model). If D_r from eq. (4-27) is substituted into this solution, initial magnetizations decay more or less rapidly to zero or to a constant value, depending on the starting depth z_0 (Figure 4-6a). Magnetization decays are more rapid near the top of the sediment column, where D_r is maximal, and slow down as the consolidating layer is approached. A common characteristic of all solutions is that $M(z, z_0)$ becomes constant below a certain "full blocking" depth $z_B > L$ inside the consolidating layer. Magnetizations $M(z_B, z_0)$ at this depth represent fractions of the initial magnetizations acquired at z_0 that survived the journey though the mixed layer. These fractions yield, by definition, the MRM lock-in function

$$\Lambda(z') = \exp\left[-2\frac{L}{\omega}\int_{z'}^{z'_B} D_r(u)\,\mathrm{d}u \right], \tag{4-29}$$

where $z'_B = z_B/L$ (Figure 4-6b). Unlike most definitions of the lock-in function commonly used in PDRM models, $\Lambda(z')$ does not start inside the consolidating layer. Instead, it is defined for all depths below the sediment-water interface, as proposed by Channell and Guyodo [2004]. The reason for such a wide lock-in function is that magnetizations acquired inside the mixed layer can be preserved. Moreover, it is possible for a DRM, which in our model is equivalent to $M(0, z_0 = 0)$, to be partially preserved (i.e., $M(z_B, z_0 = 0) > 0$) for some combinations of D_r, L, and ω (Figure 4-6a), in accordance with our preliminary estimates in section 4.2. In this

case, the lock-in function is characterized by $\Lambda > 0$ at the sediment-water interface, and small lock-in depths can result in combination with the minimal mixing depths (e.g., $L \approx 2$ cm) encountered in some pelagic sediments [Tauxe et al., 2006].

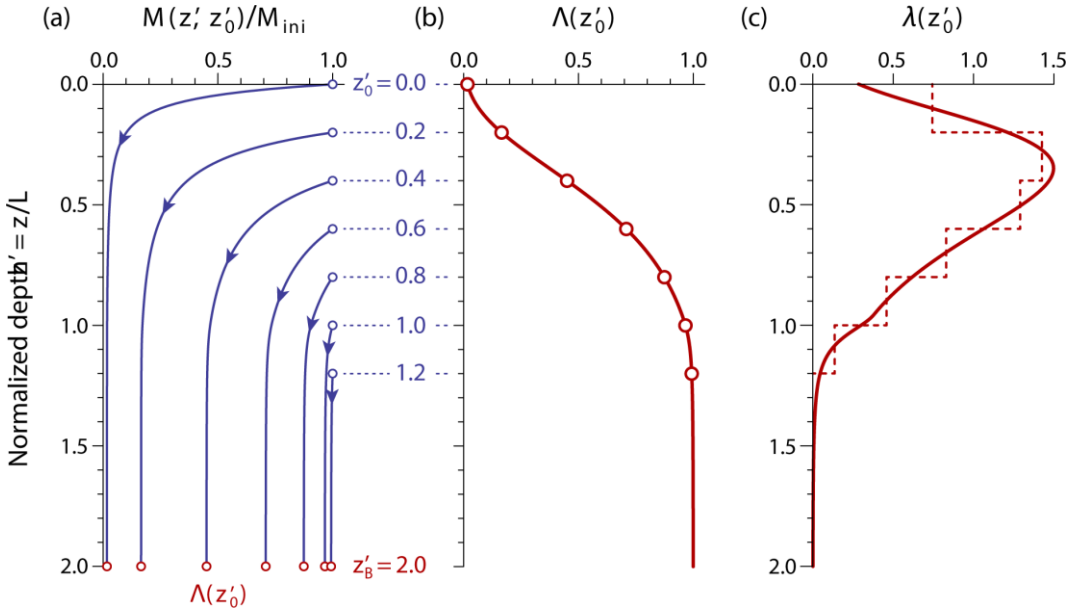

Figure 4-6 Illustration of the MRM lock-in process. (a) Evolution of normalized initial magnetizations acquired at different depths z'_0 (blue dots), as the corresponding sediment layer gets buried (lines). All magnetizations converge to constant values at depths $z' > z'_B = 2$ (red dots). These values define the lock-in function $\Lambda(z'_0) = M(z'_B, z'_0)$ shown in (b). The particular case $M(z'_B, z'_0 = 0)$ corresponds to the DRM fraction that survives its journey through the mixed layer. (b) Lock-in function deduced from (a). (c) First derivative $\lambda(z'_0)$ of the lock-in function (solid line), which defines the relative contribution of each depth to the final magnetization. The dashed line represents magnetizations corresponding to differences between curves in (a).

The last element of our MRM acquisition model provides an estimate of the MRM intensity that is ultimately locked inside the consolidating layer, as discussed in the following. For this purpose, we define the lock-in probability density $\lambda(z')$ as the derivative of $\Lambda(z')$ with respect to z' (Figure 4-6c). Accordingly, $\lambda(z')M_{eq}(z')$ represents the relative contribution to the locked MRM that is delivered by the equilibrium remanence, $M_{eq}(z')$, acquired inside a layer of thickness dz at depth z, as specified by eq. (4-18). The total NRM is therefore obtained by integration of $\lambda(z')M_{eq}(z')$ over z', i.e.,

$$\frac{M_{NRM}}{M_0} = \Lambda(0)\frac{M_{DRM}}{M_0} + \int_0^{z'_B} \lambda(z')\frac{M_{eq}(z')}{M_0}\,dz', \tag{4-30}$$

where $\Lambda(0)M_{DRM}$ is the DRM fraction that survives burial through the mixed layer. Using the result derived in section 4.3 for the equilibrium MRM we finally obtain the chief result of this paper, i.e.:

$$\frac{M_{NRM}}{M_0} = \Lambda(0)\frac{M_{DRM}}{M_0} + \frac{M_{MRM}}{M_0}, \tag{4-31}$$

where the MRM lock-in function is given by

$$\Lambda(z') = \exp\left[-\gamma \int_{z'}^{z'_B} c_b(u)\, e^{-\beta_h(u)} \mathrm{d}u\right], \tag{4-32}$$

(Figure 4-7a), and the acquired MRM is given by

$$\frac{M_{MRM}}{M_0} = \gamma \int_0^{z'_B} \Lambda\, c_b\, e^{-\beta_h} \boldsymbol{L}\left(\frac{mB}{\tau_p} \frac{1}{\sqrt{1+(\beta_h/q)^2}}\right) \mathrm{d}z', \tag{4-33}$$

where $\gamma = 2D_0 L/\omega$ is the rotational diffusivity parameter of the mixed layer introduced in section 4.2. The first and second term on the right-hand side of eq. (4-31) are the DRM and MRM contributions to the acquired NRM, respectively. Both terms are functions of γ, whose unit is rad^2. This parameter represents the mean squared angle of a random walk produced by rotational diffusion during the typical residence time of sediment particles within the mixed layer. DRM preservation is only possible with $\gamma < 1$, while full MRM acquisition with complete DRM obliteration is obtained with $\gamma \gg 1$.

Numerical evaluations of eq. (4-31-33) reveal that a transition from a DRM-dominated to a MRM-dominated NRM occurs between $\gamma = 0.2$ and $\gamma = 10$ (Figure 4-7). Accordingly, we define three regimes of sedimentary NRM acquisition: (1) a slow mixing regime for $\gamma \leq 0.2$, where the preserved magnetization is essentially a DRM, (2) a fast mixing regime for $\gamma \geq 10$, where DRM is fully randomized and replaced by a MRM, and (3) an intermediate mixing regime with $0.2 < \gamma < 10$, where DRM and MRM coexist, both contributing to a total NRM. Faster sediment mixing regimes push the MRM lock-in function below the mixed layer (Figure 4-7a), where the biodiffusion rate declines rapidly, producing large lock-in depths that are compatible with some paleomagnetic records [e.g. Sagnotti et al., 2005; Suganuma et al., 2011].

Because DRM and MRM are characterized by different acquisition efficiencies, total NRM intensities can be particularly sensitive to γ in case of intermediate mixing regimes, due to varying DRM and MRM proportions. On the other hand, MRM intensity is relatively insensitive to mechanical sediment properties (i.e., β_h in Figure 4-8a,b) and bioturbation parameters (i.e., c_b in Figure 4-8c,d), especially for fast mixing regimes. Moreover, the total magnetization is governed only by the ratio between magnetic and perturbing torques for mixing regimes characterized by $20 < \gamma < 500$, according to the limit case of eq. (4-19) with $\tau_h \to 0$.

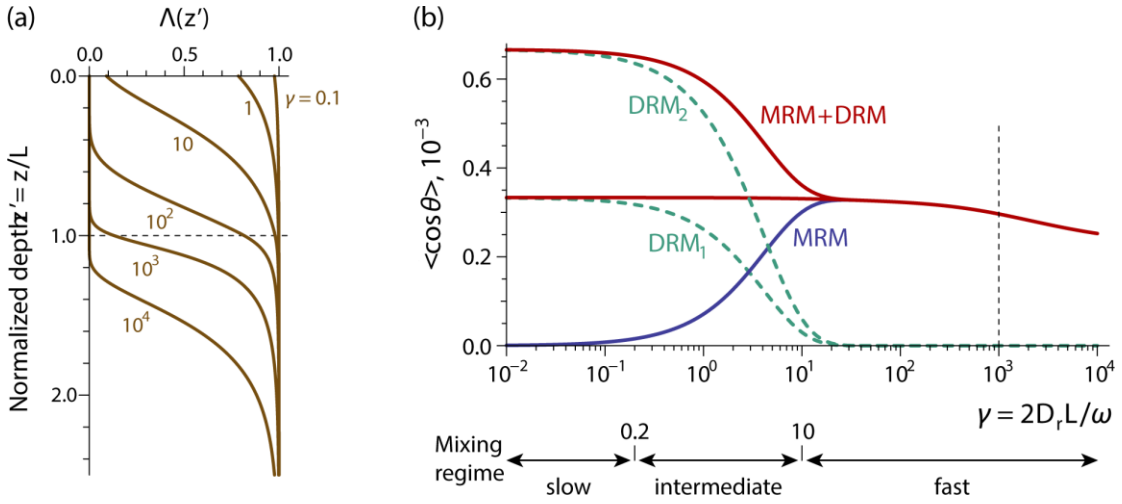

Figure 4-7 Lock-in functions and remanent magnetizations acquired in a sediment with properties shown in Figure 4-5 and $\beta_m = 10^{-3}$ (i.e., acquisition in a 50 μT field when the mean amplitude τ_h of holding and perturbing torques at the bottom of the mixed layer is equal to the torque exerted by a 50 mT field). (a) Lock-in functions $\Lambda(z')$ for selected values of the rotational diffusivity parameter $\gamma = 2D_r L/\omega$. The value $\Lambda(0)$ of the lock-in function at the sediment-water interface yields the fraction of locked-in DRM. The bottom of the mixed layer is marked by the dashed line. (b) Finally locked DRM and MRM as a function of γ for two DRM settings, i.e., DRM_1 acquired with same perturbation strength as MRM (i.e., $\tau_{p,DRM} = \tau_{p,MRM}$) and the more realistic DRM_2 acquired in a less perturbed environment (i.e., $\tau_{p,DRM} = 0.5\tau_{p,MRM}$). Three mixing regimes yielding full, intermediate, and no DRM preservation, respectively, are shown below. The vertical dashed line marks the limit above which lock-in starts below the mixed layer.

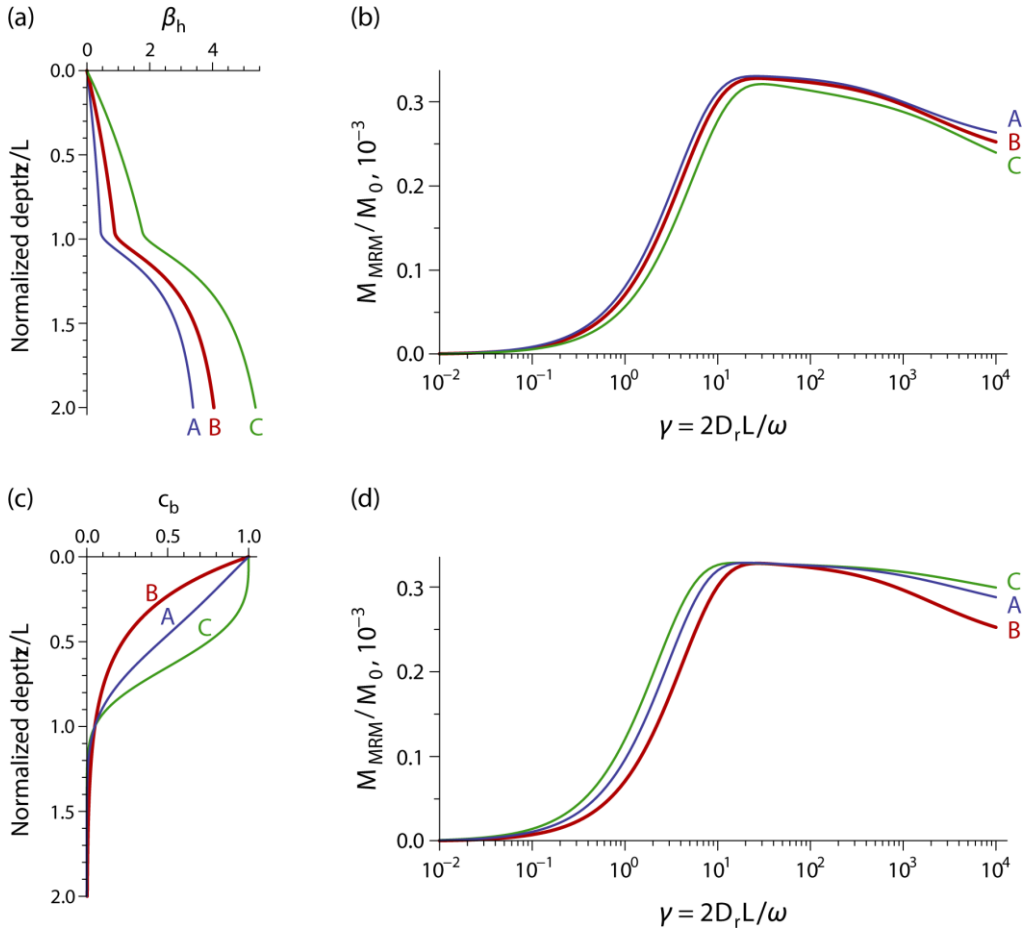

Figure 4-8 Sensitivity of MRM acquisition to variations of the model profiles shown in Figure 4-5. (a) Sediment strength variations, expressed by proportional β_h-profiles with $\beta_h(1) = 0.5$ (case A), $\beta_h(1) = 1$ (case B as in Figure 4-5a), and $\beta_h(1) = 2$ (case C). (b) MRM intensities that correspond to the cases shown in (a). (c) Variations of normalized concentration profiles c_b of benthic organisms according to an exponential model (case B as in Figure 4-5b), a more box-shaped function (case C), and an intermediate case (case A). (d) MRM intensities that correspond to the cases in (c). MRM intensities depends only weakly on variations of the profiles shown in (a) and (c), especially in case of fast mixing regimes with $20 \le \gamma \le 500$.

4.5 Discussions

In sections 4.3 and 4.4 we derived equations that describe the mean alignment of magnetic particles subjected to the simultaneous action of aligning torques (i.e., magnetic and texture) and randomizing torques (i.e., turbulence, bioturbation, and inter-particle mechanical interactions). DRM and MRM acquisition depend on the mean intensity of such torques and on the frequency of "successful" perturbations inside the corresponding environments (i.e., water column, sediment-water interface, and mixed layer). Dynamic equilibrium between the abovementioned torques is described by a Langevin law of the type $M_{eq} = M_0 \boldsymbol{L}(\beta_m)$, where M_0 is the magnetization of fully aligned magnetic moments, and the "Boltzmann factor" $\beta_m = \tau_m/\tau_p$ is the ratio between the amplitudes of magnetic torques, $\tau_m = mB$, and perturbing torques, τ_p. Two main cases can be distinguished according to the nature of perturbing torques. In the first case,

magnetic moments are carried by discrete units (i.e., flocs) with few reciprocal interactions. While falling inside the water column, magnetic flocs are subjected to Brownian perturbations, as well as hydrodynamic disturbances produced by turbulence [Heslop, 2007]. The typical intensity of such disturbances yields relatively large values of β_m, which produce the well-known problem of non-linear DRM field dependencies [e.g. Tauxe et al., 2006]. This problem is mitigated by accretion of large (>20 μm) flocs through random aggregation of smaller units.

Floc density increases dramatically at the sediment-water interface, where a network of interaction forces begins to form. The physics of DRM acquisition remains the same as long as individual flocs behave as independent units with few interactions. Perturbing forces are presumably larger than in the water column, due to sediment resuspension by benthic organisms and continuous floc reorientation in a turbulent hydrodynamic regime (Figure 4-1). In most cases, sediment mixing is expected to be fast enough to expose all materials inside the mixed layer to repeated resuspension events and DRM renewal. Under these conditions, new magnetic carriers formed inside the mixed layer, such as magnetosome chains, acquire the same type of NRM as older carriers, and are subjected to the same lock-in delay. This is confirmed by results of Ouyang et al. [2014], who did not find a systematic time lag between detrital and biogenic NRM components in paleointensity records from the South China Sea.

Interaction forces between sediment particles grow rapidly below the sediment-water interface, as soon as a sufficient number of contact points is reached. In this case, individual magnetic flocs are no longer independent units, and, in the absence of perturbations, the orientation of magnetic moments becomes locked, yielding a stable remanent magnetization. Bioturbation, however, produces irreversible particle rotations by overcoming the holding forces. Flocs are expected to break into smaller units whose internal binding forces exceed those produced by bioturbation. Such units might be identified with the “fundamental flocs” assumed in some DRM models [e.g. Tauxe et al., 2006]. As far as magnetofossils are concerned, fundamental flocs might consist of magnetosome chains adhering to clay particles, as postulated by Mao et al. [2014a]. We have modeled bioturbation by the action of perturbing torques, τ_p, against so-called holding potentials. The amplitude of τ_p depends on a detailed representation of bioturbation mechanisms [e.g. Dorgan et al., 2005]; nevertheless, opposing torques, τ_h, caused by inter-particle forces must be overcome for successful displacement of living organisms. Therefore, $\beta_h = \tau_h/\tau_p \approx 1$can be reasonably assumed at the bottom of the mixed layer, where τ_h is also responsible for preservation of a remanent magnetization against the torques resulting from the application of (large) magnetic fields. A crude estimate of torques produced by bioturbation can be derived from $\tau_h/\tau_p \approx 1$ and critical fields B_h required to produce irreversible magnetic moment rotation in fresh sediment samples taken from the bottom of the surface mixed layer. In this case, the “Boltzmann factor” $\beta_m = mB/\tau_p$ is simply given by B/B_h, where B is the field in which NRM was acquired. Using $B_h > 20$ mT as a representative value for the mixed layer [Mao et al., 2014a], one obtains $\beta_m < 2.5\times10^{-3}$ for typical geomagnetic field intensities. In this case, we expect the intensity of magnetizations acquired inside the mixed layer to be proportional to the geomagnetic field.

The time required for any magnetization to reach full equilibrium with the ambient field inside the mixed layer is inversely proportional to the rotational diffusion constant D_r associated with bioturbation. Direct measurements of D_r are not available, and estimates based on total diffusion are extremely difficult to obtain, due to the unknown efficiency of benthic organisms in inducing irreversible particle rotations. We attempted crude lower limit estimates of D_r on the basis of microbial abundances [Kallmeyer et al., 2012], relying on the assumption that the translational and rotational diffusion of microbes is of the same type as for the well-known case of Brownian motion (Table 4-1). With such estimates, equilibration times are comprised between 30 yr and 30 kyr, depending on the sedimentary setting. The fate of a DRM is dictated by D_r and by the typical residence time L/ω of sediment particles inside a mixed layer of thickness L, which are collectively summarized by the so-called mixed layer diffusivity parameter $\gamma = D_r L/\omega$, where ω is the sedimentation rate. Three mixing regimes can be distinguished on the basis of γ, i.e., (1) slow mixing ($\gamma \leq 0.2$) that leads to full DRM preservation, (2) fast mixing ($\gamma > 10$) during which DRM is completely replaced by a MRM, and (3) intermediate mixing where NRM is a mixture of DRM and MRM (Figure 4-7b). According to our calculations, inclination shallowing is not expected for MRMs acquired in the fast mixing regime.

Since MRM is essentially a particular type of PDRM, its conversion to a stable NRM depends on a so-called lock-in function, which represents the relative contribution of each depth below the sediment-water interface to the final magnetization. The value of the lock-in function at the sediment-water interface represents the DRM fraction that survives sediment mixing. Lock-in functions associated with slow mixing regimes (e.g., Figure 4-7a with $\gamma < 10$) are representative of pelagic environments with low nutrient inputs, shallow mixed layers ($L \approx 2$ cm), and small lock-in depths of the order of 1 cm, as postulated by Tauxe et al. [2006]. On the other hand, non-zero values of the lock-in function are confined below the mixed layer in case of rapid mixing regimes, yielding typical lock-in depths of $\sim 2L \approx 20$ cm (e.g., Figure 4-7a with $\gamma > 1000$). These lock-in depths are compatible with estimates obtained from paleomagnetic records by Suganuma et al. [2011]. Because of the strong sensitivity of the lock-in function to mixing regimes, acquired MRM intensities depend mainly on γ, increasing from 0 for slow mixing to the equilibrium magnetization $M_0 \boldsymbol{L}(\beta_m)$ for rapid mixing. Numerical MRM intensity estimates can be compared with the NRM of magnetofossil-bearing sediments characterized by rapid mixing regimes. Because of the excellent dispersion of intact magnetofossil chains, with estimated mean distances >9 times the chain length [Ludwig et al., 2013], magnetic flocs probably contain a single magnetosome chain or chain bundle with maximum magnetic moment [Hanzlik et al., 2002], as inherited from living cells. In this case $M_0 \approx M_s$ can be assumed, and using $M_{rs}/M_s \approx 0.4$ [e.g. Ludwig et al., 2013; Mao et al., 2014a], we deduce $\mathrm{MRM}/M_{rs} \approx (7\text{-}9) \times 10^{-4}$ for $20 \leq \gamma \leq 1000$ (Figure 4-7b). This estimate agrees well with representative NRM values of magnetofossil-bearing platform carbonates [McNeill and Kirschvink, 1993].

Our analysis of DRM and MRM acquisition enables a first discussion of the sensitivity of relative paleointensity records to fluctuations of the NRM acquisition efficiency. With few exceptions associated with extremely rapid accumulation of nutrient-poor sediment material (e.g., ice rafting), bioturbation is sufficiently active to expose the whole mixed layer to repeated

resuspension and redeposition events, so that DRM and MRM can be assumed to be carried by the same kind of magnetic particles. Fluctuations of NRM acquisition efficiency in terms of (non-measurable) magnetic moment alignments are, therefore, entirely due to the acquisition mechanism. As discussed above, equilibrium DRM and MRM intensities are mainly controlled by β_m, with major differences being related to the intensity τ_p of random perturbations. In both cases, τ_p is mainly controlled by the action of benthic organisms, but not by their concentrations. This means that major changes in the type of benthic fauna are required to introduce significant modifications of resuspension (for DRM) and bioturbation (for MRM) mechanisms. On the other hand, the concentration of benthic organisms is directly proportional to D_r and controls the timing of DRM randomization and MRM acquisition inside the mixed layer. Therefore, moderate fluctuations of the sedimentary environment are expected to change γ through variations of benthic biomass and sedimentation rate. As long as these variations occur around a slow ($\gamma \leq 0.2$) or fast ($\gamma > 10$) mean mixing regime, NRM is controlled either by a DRM or a MRM with nearly constant acquisition efficiency, and can be expected to support reliable paleointensity reconstructions. On the other hand, fluctuations of intermediate mixing regimes produce variations in the relative contributions of DRM and MRM. DRM is more efficient than MRM; therefore, the net result is that NRM acquisition efficiency changes in a way that could be erroneously attributed to geomagnetic field variations.

4.6 Conclusions

A general model has been developed for initial NRM acquisition near the sediment-water interface and inside the surface mixed layer. This model considers individual particles – defined as the smallest sediment units with elastic body behavior – under the influence of (1) magnetic torques, τ_m, which tend to align magnetic moments with the Earth's field, (2) holding torques, τ_h, which arise from inter-particle interactions (e.g. hard contacts, Van der Waals, electrostatic), and (3) random perturbing torques, τ_p, associated with Brownian motion, turbulence (in the water column), and bioturbation (in sediment). The sum of magnetic and holding torques is described by properly constructed random potentials with a given number of local minima. In the absence of perturbations (i.e., $\tau_p = 0$), stable particle orientations coincide with these minima. Irreversible particle rotation is produced by perturbing torques upon overcoming the energy barriers between local minima of the random potential. A sequence of such irreversible events is equivalent to a rotational diffusion process with diffusion coefficient D_r. This process is formally described by a Smoluchowski-Debye equation (eq. 4-6), whose stationary solution is a Boltzmann distribution of magnetic moments (eq. 4-7). The Boltzmann distribution defines the remanent magnetization resulting from a dynamic equilibrium between the long-term action of aligning torques (τ_m) on the one hand, and the average effect of random torques (τ_p and τ_h) on the other hand (eq. 4-18). Dynamic equilibrium is reached within a typical time that is inversely proportional to D_r (eq. 4-5).

The magnitudes of D_r, τ_p, and τ_h evolve during different stages of NRM acquisition (Figure 2-13). Holding torques are completely absent inside the water column (i.e., $\tau_h = 0$), and relatively weak perturbations allow the growth of loose particle aggregates (i.e., flocs). The concentration of flocs increases sharply across the sediment-water interface, where mechanical interactions, and thus τ_h , start to build up. The DRM acquired in this region is still unstable, due to the small holding forces. DRM intensities are governed by a Langevin law (eq. 4-12), whereby relatively large acquisition efficiencies and non-linear field dependencies are obtained if $\tau_p \leq \tau_m$. As flocs become buried inside the surface mixed layer, τ_h increases proportionally to the mechanical strength of sediment. Bioturbation produces irreversible magnetic moment reorientations in all cases where $\tau_p \geq \tau_h$ so that DRM is progressively replaced by a new, so-called mixing remanent magnetization (MRM). Because perturbing torques produced by bioturbation are presumably much stronger than those encountered in the water column, MRM intensity is expected to be smaller than DRM intensity (eq. 4-18).

The amounts of surviving DRM and acquired MRM at each depth below the sediment-water interface are controlled by a lock-in function (eq. 4-29), whose shape is mainly determined by the so-called rotation diffusivity parameter $\gamma = D_r L/\omega$, where L is the thickness of the surface mixed layer, and ω is the sedimentation rate. DRM is preserved as the only NRM contribution if $\gamma < 0.2$ (slow mixing regimes), and is completely replaced by a MRM for $\gamma > 10$ (fast mixing regimes). The strongest changes in NRM acquisition efficiency are thus expected for intermediate mixing regimes characterized by $0.2 < \gamma < 10$. Estimates of γ depend critically on D_r, for which direct measurements are not available. Lower D_r limits, obtained from minimum bioturbation rates expected from motile microorganisms, suggest that slow, fast, and intermediate mixing regimes exist for different sedimentary settings (Table 4-1).

The abovementioned DRM and MRM acquisition processes can introduce relative paleointensity artifacts in addition to those generated by normalization with laboratory magnetizations [Roberts et al., 2012]. Accordingly, we distinguish two main categories: (1) artifacts introduced by NRM acquisition efficiency variations in terms of remanence carrier alignment (e.g., DRM and MRM fractions), and (2) artifacts introduced by magnetic components with different intrinsic ratios between their NRM contributions and a normalizer magnetization (e.g., IRM, ARM). For example, intact magnetofossils have saturated magnetic moments that yield larger NRM/IRM and NRM/ARM values compared to other remanence carriers with the same degree of alignment. Variable combinations of the two artifact sources can generate contradictory or ambiguous results. For example, Ouyang et al. [2014] reported NRM/ARM ratios that are 2-4 times higher for biogenic magnetite with respect to a detrital component, while Channell et al. [2013] did not report significant differences between the two components.

Ambiguities associated with paleointensity artifacts are clearly illustrated with the example of the eastern equatorial Pacific sediment cores described by Yamazaki et al. [2013], where an inverse correlation has been observed between NRM acquisition efficiency (i.e., NRM/IRM) and a proxy for magnetizations due to magnetofossils (i.e., ARM/IRM). This correlation can be explained as an artifact of category 1 or 2, or both. In the first case, increased ARM/IRM values can be associated with faster bioturbation, assuming that magnetotactic bacteria represent a

certain fraction of the benthic biomass. Faster bioturbation is characterized by higher D_r- and L-values, and is driven by larger nutrient supplies. Nutrient supply is in turn supported by primary production and/or increased mineral fluxes [Sarmiento and Gruber, 2006], the latter being directly related to the sedimentation rate ω. The net effect of these changes on pelagic sediment mixing depends on the coupled parameters D_r, L, and ω: the combined increase of D_r and L likely exceeds corresponding variations of ω. In this case, γ is expected to co-vary with magnetofossil concentrations. The slow-to-intermediate mixing regime deducible from Table 4-1 for the locations analyzed by Yamazaki et al. [2013] would react to increased γ with a decrease of the overall NRM acquisition efficiency (i.e., NRM/IRM), due to DRM randomization (Figure 4-7). This mechanism can explain the inverse correlation between NRM/IRM and ARM/IRM observed by Yamazaki et al. [2013], with the lowest NRM/IRM values being typical of magnetofossil MRM acquisition, as well as the weak correlation with sedimentation rate. On the other hand, two magnetic components with the same NRM acquisition efficiency (e.g., in terms of NRM/IRM) but different ARM/IRM values (as is the case for detrital and magnetofossil components, see Egli [2004]) will generate an inverse correlation between NRM/IRM and ARM/IRM.

Our analytical models provide testable predictions about possible effects of sedimentary environments on NRM acquisition. Dedicated experiments are needed to obtain reliable estimates of bioturbation rates and mechanical sediment properties. A better knowledge of these parameters could lead to successful correction of variable NRM acquisition efficiencies in relative paleointensity records and to selection of the most reliable records on the basis of favorable sedimentary settings rather than limited variations of rock magnetic properties.

Acknowledgements

All results in this paper have been generated numerically using equations and methods explained in the text. X. Zhao is supported by the German Research Foundation (Grant Nr. EG294/2-1) and by the Ludwig-Maximilians University. We are grateful to Andrew Roberts, Lisa Tauxe, an anonymous reviewer, and the Associated Editor, David Heslop, for constructive comments that helped to improve this paper.

Table 4-1 Summary of surface mixed layer properties for selected sedimentary settings.

Location	ω cm/kyr	L cm	$D_{b,tr}$ cm^2/yr	$D_{b,bac}$ (10 μm) cm^2/yr	D_r (10 μm) rad^2/yr	γ (10 μm)	DRM %
N Pacific gyre	0.2 [1]	3.3 (2-6) [3]	0.02-0.3 [2]	8×10^{-11}	6×10^{-5}	2	14-100
S Pacific gyre	0.2 [1]	3.3 (2-6) [3]	0.02-0.3 [2]	3×10^{-11}	2×10^{-5}	0.8	52-100
Eq. Pacific	0.5 [1, 3]	7 (5-8) [3]	0.2-0.3 [2]	3×10^{-8}	0.02	600	0-94
Southern Ocean	0.31 [4]	6 (5-7) [3]	0.1-0.7 [2]	2.4×10^{-8}	0.02	700	0-93
NW Atlantic	5 [5]	10 (9-12) [3]	0.65 [6]	2.4×10^{-8}	0.02	70	0-99

Explanations. ω is the sedimentation rate; L is the thickness of the mixed layer; $D_{b,tr}$ is the translational diffusion constant deduced from tracers. $D_{b,bac}$ is the estimated minimum translational diffusion constant associated with benthic microorganisms, based on $D_b = \varepsilon_{mob}(a_b/a)^2 N v D_B$ with $\varepsilon_{mob} = 0.2$, $v \approx 0.03\ \mu m^3$, $a_b = (3v/4\pi)^{1/3} \approx 0.2\ \mu m$, $a = 10\mu m$, $D_B = 0.1\ cm^2/yr$ and N from Kallmeyer et al. [2012]. Values for $a = 100\mu m$ are 100 times smaller. D_r is the minimum rotational diffusion constant deduced from $D_{b,bac}$ and eq. (4-3) with $a = 10\mu m$. Values for $a = 100\mu m$ are 10^4 times smaller. $\gamma = 2D_r L/\omega$ is an estimate of the minimum rotational diffusivity parameter of the mixed layer, based on D_r and $a = 10\mu m$. The last column is the maximum relative fraction $e^{-\gamma}$ of DRM that survives bioturbation, based on $a = 10 - 100\mu m$. [1] Hammond et al. [1996]. [2] Smith and Rabouille [2002]. [3] Pisias et al. [1995]. [4] Geibert et al. [2005]. [5] Anderson et al. [1988]. [6] Computed with eq. (2) of Boudreau [1994].

Chapter 5 Microbially-assisted recording of the Earth's magnetic field in sediment

Abstract

Sediments continuously record variations of the Earth's magnetic field and thus provide one of the few seamless archives for studying the geodynamo [Opdyke and Channell, 1996]. The recording process occurs via the magnetization acquired by the alignment of magnetic grains during and after sediment deposition, known as depositional (DRM) and post-depositional (PDRM) remanent magnetization, respectively [Tauxe, 1993]. (P)DRM acquisition mechanisms have been investigated for over 50 years, yet many aspects remain unclear. A key issue concerns the controversial role of bioturbation, i.e. the mechanical disturbance of sediment by benthic organisms, during PDRM acquisition [Kent, 1973; Katari et al., 2000; Roberts et al., 2013]. A recent theory on bioturbation-driven PDRM appears to solve many inconsistencies between laboratory experiments and paleomagnetic records [Egli and Zhao, 2015], yet it lacks experimental proof. Here we fill this gap by documenting, for the first time, the generation of a bioturbation-controlled PDRM in laboratory redeposition experiments.

5.1 Introduction

(P)DRM acquisition can be understood by following the path of settling particles in the water column and inside the surface mixed layer, until their orientation becomes fixed during consolidation (Figure 5-1a). A net magnetization is generated by particles with a magnetic moment *m* when they rotate towards the local Earth's field *B* under the action of the magnetic torque $\tau_m = mB$. In the water column and at the sediment-water interface, complete alignment is prevented by particle aggregation [Tauxe et al., 2006], hydrodynamic forces [Heslop, 2007], and rolling [Bilardello et al., 2013], so that DRM intensity depends on the strength of *B*. A PDRM can be acquired after deposition inside the sediment column. Two main acquisition mechanisms have been proposed. In the first case, PDRM is acquired without disturbance from irreversible rotation of particles for which τ_m exceeds the torques generated by inter-particle forces [Shcherbakov and Shcherbakova, 1987]. Since these torques are generally much stronger than τ_m, only few magnetic carriers will be affected, and most of the original DRM remains intact [Katari et al., 2000]. The second acquisition mechanism relies on particle realignment by random torques associated with bioturbation. Bioturbation was simulated in the laboratory by stirring water-saturated sediment in the presence of an ambient field, where a relatively strong magnetization was acquired proportional to the applied field [Kent, 1973]. A major problem with these experiments is that the samples were dried before the magnetization was measured, so one cannot exclude that the magnetic remanence originated from the drying process itself [Henshaw and Merrill, 1979].

Regardless of the acquisition mechanism, most PDRM models assume that lock-in of magnetization only begins once substantial surface mixing has ceased, i.e. below the mixed layer [Roberts and Winklhofer, 2004; Roberts et al., 2013], so that DRM and PDRM are mutually exclusive. A different viewpoint arose from a statistical model of PDRM acquisition in the surface mixed layer (Chapter 4). This model considers bioturbation as a rotational diffusion process similar to that of Brownian motion, which occurs in the presence of random inter-particle forces. In this case, particle orientations are governed by the Smoluchowski-Debye equation, whose solution under stationary conditions yields the equilibrium magnetization

$$M_{\mathrm{eq}} = M_0 \left\langle \boldsymbol{L}\left(\frac{m_i B}{\tau_{\mathrm{p}}} \right) \right\rangle \tag{5-1}$$

where $\langle\rangle$ denotes the ensemble average over particles with magnetic moments m_i, subjected to randomizing torques of mean amplitude τ_{p}; M_0 is the magnetization corresponding to full alignment, and L is the Langevin function. DRM acquisition is also described by eq. (5-1) with appropriate values of τ_{p} representing disturbances at the sediment-water interface. In weak fields (i.e., $m_i B \ll \tau_{\mathrm{p}}$), M_{eq} is approached exponentially, i.e. $M - M_{\mathrm{eq}} = \Delta M e^{-2Dt}$, where M is the remanent magnetization, ΔM the initial value of M - M_{eq}, and D the rotational diffusion coefficient associated with bioturbation (Appendix B). The degree of DRM replacement by a bioturbation-driven PDRM depends on the diffusivity parameter $\gamma = DL/\omega$, where L is the thickness of the mixed layer and ω the sedimentation rate. This parameter defines three mixing regimes: (1) a slow ($\gamma < 0.2$) regime where DRM is preserved, (2) a fast ($\gamma > 10$) regime where DRM is completely replaced by PDRM, and (3) intermediate regimes with partial DRM preservation. Within this framework, DRM and PDRM are products of similar processes under different conditions: DRM coincides with M_{eq} during the initial stages of sediment deposition in the absence of strong perturbing forces, while PDRM represents the evolution of M_{eq} over a much longer time in an environment with strong perturbations.

This Chapter quantifies the data from redeposition experiments of Chapter 2 and 3 using abovementioned theory (Chapter 4). A short summary of the experiments is listed as follows.

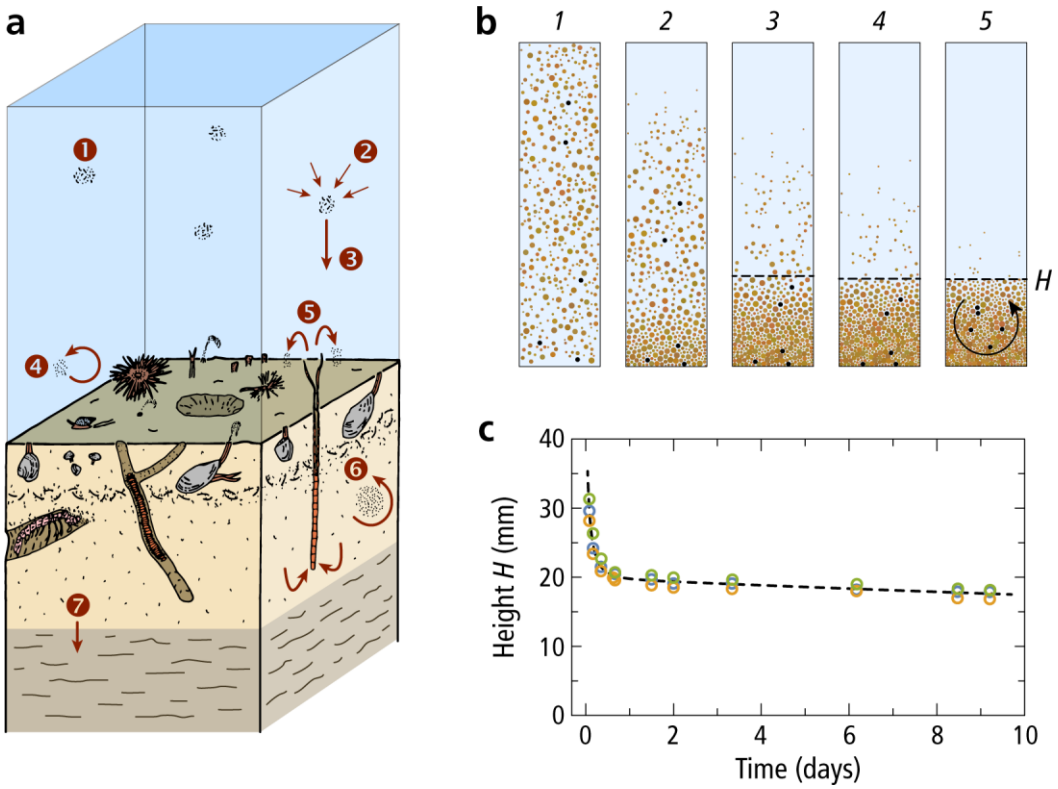

Figure 5-1 Acquisition of sedimentary NRM in nature and in the laboratory. **a**, 1: marine snow, 2: flocculation, 3: settling, 4: sediment resuspension, 5: non-local mixing, e.g. by polychaete worms, 6: local (diffusive) sediment mixing leading to particle reorientation, 7: burial to the consolidating layer. **b**, Schematic representation of sediment redeposition in five time frames. A homogeneous sediment suspension settles in a magnetic field, forming a clear sediment-water interface (dashed) after some time. The same five particles are highlighted by black dots in each frame. A DRM is acquired by alignment of magnetized particles in the ambient field during deposition (frames 1-4). This magnetization is stabilized by inter-particle forces developing at contact points (frames 3-4). Sediment mixing (arrow in frame 5) is responsible for particle realignment after deposition and generates a PDRM. **c**, Height *H* of the sediment-water interface (dots), for three redeposition experiments. The dashed line is a guide for the eye. A nearly stable interface is obtained within the first day.

5.2 Materials and methods

The particularity of these experiments is that we used fresh sediment containing abundant living microorganisms, including magnetotactic bacteria [Jogler et al., 2010; Mao et al., 2014a; Mao et al., 2014b]. We also avoided treatments commonly employed to disaggregate sediments and modify the aqueous solutions, which reduce or eliminate the original microorganism communities. As a short summary, Organic-rich clay/silt sediment material used for this study comes from a small pond situated next to our paleomagnetic laboratory in Niederlippach (Germany, 48°35'15" N, 12°04'43" E). The sediment was collected from the uppermost ~10 cm and transferred to glass aquaria at ambient temperature, where a new stably stratified oxygen gradient was re-established within one week [Mao et al., 2014b]. Magnetotactic bacteria populations live in the topmost 10 cm of sediment, where up to 300 motile cells/µl have been counted in fresh sediment [Jogler et al., 2010]. Cell counts declined by a factor ~10 after one year of storage in aquaria [Mao et al., 2014a]. A similar decline is also seen on total bacteria concentrations estimated with the spread plate method.

Sediment with different microorganism concentrations has been obtained after laboratory storage in glass aquaria during 1 week (group A: 280 cells/µl), 3 months (group B: 247 cells/µl) and 1 year (group C: 213 cells/µl). Aliquots of group C sediment have been subjected to treatments aimed at further reducing the microorganism concentration, i.e. sealed storage for 3 months, which removes the natural oxygen gradient [Mao et al., 2014a] (group D: 207 cells/µl), and addition of broad-spectrum antibiotics as described in Chapter 3 (group E: 126 cells/µl).

Redeposition experiments were performed in glass vials using sediment material from groups A-E. Remanent magnetizations were measured with a vertical bore superconducting rock magnetometer [Wack and Gilder, 2012]. Each vial was prepared by diluting 5 ml of sediment slurry in 10 ml tap water, sealed, and then vigorously shaken in order to create a homogeneous suspension as a starting condition for all experiments (Figure 5-1b). For DRM acquisition experiments, the vials were placed in controlled fields of various intensities and inclinations generated by Helmholtz coils. A clear sediment-water interface formed within 22 hours (Figure 5-1c). Magnetizations were measured periodically during the experiments by carefully transferring the vials to the magnetometer to avoid mechanical disturbances. A measurement series lasted ~10 minutes, when the vials lay in residual shielded room fields of <500 nT, before being returned to the controlled field environment. Each DRM (and PDRM) experiment was performed in triplicate (e.g., with three independent vials). For the PDRM acquisition experiments, sediment suspensions were allowed to settle in a null field for five days, which is a sufficient time to obtain a stable sediment column. A controlled field was subsequently applied for ~7 days (PDRM acquisition), followed again by zero-field conditions for the remaining time to monitor the decay of the PDRM.

5.3 Results and discussions

PDRM acquisition (Figure 5-2a), is due exclusively to mechanical alignment of magnetic particles, as confirmed by the lack of acquired PDRM and zero-field decay in control samples where particle rotation was hindered by full drying. Acquisition and decay curves were modeled assuming a statistical distribution of rotational diffusion coefficients D rather than a single coefficient, as smaller particles reorient faster than large ones by virtue of the Stokes-Einstein-Debye relation between rotational and translational diffusion [Jabbari-Farouji et al., 2012; Egli and Zhao, 2015]. The same type of distribution, $p_r(D/\bar{D})$, where $\bar{D}$ is the median, controls the shape of all PDRM acquisition/decay curves (Appendix B) within experimental errors (Figure 5-2b). Differences between median rotational diffusion coefficients $\bar{D}$ deduced from acquisition and decay curves are mostly limited to a factor of two (Figure 5-2c), being therefore small in comparison to the four orders of magnitude span of p_r (Figure 5-2d). This means that measured acquisition/decay curves reflect equilibration with the ambient field under nearly stationary conditions. Typical values of $\bar{D}$ for groups A-E, on the other hand, vary in proportion to the measured bacteria concentrations (Figure 5-2c-d). This can only be expected if a diffusion process governs PDRM acquisition at a rate ($\bar{D}$) that is in turn controlled by bioturbation. Sediment ageing effects can be excluded because groups C-E are approximately of same age yet follow the same trend defined by groups A-C. The shape of p_r is reproduced by the grain size distribution of sediment (Figure 5-2d) upon substituting the grain diameter a with the Stokes-Einstein-Debye relation $D \propto a^{-2}$ (see Appendix B).

DRM acquisition and its progressive replacement by PDRM was investigated through similar experiments where a magnetic field was applied from the beginning of deposition and maintained for ~11 days, before measuring its decay in zero field over a period of time (Figure 5-3a). Contrary to redeposition experiments performed with sediment material containing no living microorganisms [Barton et al., 1980; Tauxe et al., 2006], the DRM in our experiments slowly decays with time even during continuous field exposure, rather than increasing asymptotically. DRM decay becomes rapid and similar to that of PDRM once the field is removed. As in the case of PDRM experiments, magnetic viscosity effects could be ruled out, so that magnetization changes are caused only by particle reorientation. Other aspects of these experiments, such as the recording of shallower than expected inclinations (called inclination shallowing, Figure 5-3c-d), mimic those in "classic" redeposition experiments with no living organisms.

The initial DRM intensity and the equilibrium PDRM intensity depend nonlinearly on the intensity of the applied field for fields exceeding ~30 μT, typical of surface field intensities on Earth. This dependence is well fitted by an analytical approximation of eq. (5-1) assuming a uniform distribution of mB/τ_p, which has been used with success in the past [King, 1955; Barton et al., 1980] (Figure 5-3b). Independent fits of the DRM and PDRM data predict very similar saturation values (i.e., the magnetization caused by full grain alignment), which means that no grains carrying a DRM are excluded from PDRM acquisition. Therefore, differences between the

two magnetization types arise entirely from different degrees of partial magnetic moment alignment. Such differences depend ultimately on τ_p, since the same magnetic moments from the same grains are involved in both cases (i.e., same values of mB during DRM and PDRM acquisition). In particular, τ_p deduced from the PDRM acquisition curve in Figure 5-3b is twice as large as for the DRM curve, confirming that grain alignment perturbations increase below the sediment-water interface, due to stronger inter-particle forces overcome by bioturbation. With these data in mind, DRM decay in the applied field can be explained by the fact that the DRM acquired during the initial stages of deposition is progressively replaced by a new equilibrium – the PDRM – as τ_p increases due to the buildup of inter-particle bonds. Because PDRM in weak field is 50% lower than DRM, the net effect is a decrease of the total magnetization.

5.4 Conclusions

Our experiments confirm that bioturbation is responsible for the acquisition of a PDRM inside the surface mixed layer, which eventually replaces the initial DRM if rotational diffusion is fast enough with respect to the mean residence time of particles in this layer. These experiments support the conclusion that DRM and PDRM represent two stages of a statistical equilibrium between magnetic and perturbing torques: DRM is the first stage that applies to the sediment-water interface, and PDRM is the later stage developing inside the more strongly perturbed mixed layer. The kinetics of particle reorientation, which is dictated by the rotational diffusion coefficient, determines whether DRM survives the new equilibrium or it is replaced by a PDRM. The difference between DRM and PDRM intensities might be larger in naturally deposited sediment, owing to higher shear strengths that must be overcome by τ_p. The effect of salinity on flocculation [Katari and Tauxe, 2000] is another factor that must be taken into consideration when extrapolating our (P)DRM intensities to natural sediments. This new quantitative understanding of how sediment becomes magnetized in the Earth's field will hopefully facilitate the development of better techniques for paleointensity reconstructions, especially if proxies for bioturbation activity can be used.

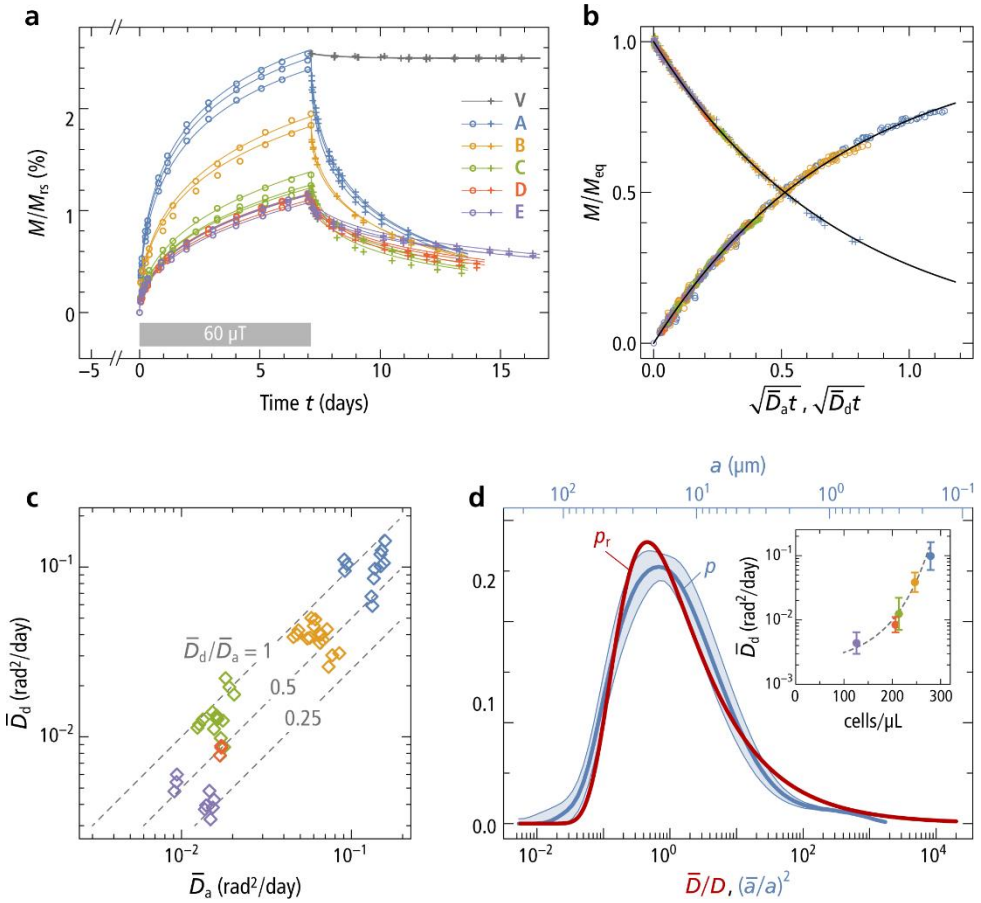

Figure 5-2 PDRM acquisition experiments. **a**, Magnetization vs. time for sediment groups A-E (circles, crosses), after normalization by the mean saturation remanence M_{rs}. Sediment was redeposited in a null field (day -5 to day 0). A 60 μT field with 50 ° inclination was applied during the next 7 days and turned off for the remaining time. Lines are model curves obtained from the distribution of D shown in (**c**). Group V designates the PDRM decay due to magnetic viscosity in three fully dried samples, where particle reorientation is no longer possible. **b**, PDRM acquisition of groups A-E in 20, 40, 60, 80, 100, and 150 μT and subsequent zero-field decay. Magnetizations are normalized by the equilibrium PDRM (M_{eq}) that would be reached after an infinite time. Acquisition/decay times are normalized by the median rotational diffusion coefficients, $\bar{D}_a$ and $\bar{D}_d$, as deduced from least-squares fits of the measured curves (Appendix B). All data collapse onto a single acquisition/decay curve (black lines), as expected in case of identical distributions of the rotational diffusion coefficient. **c**, Median rotational diffusion coefficients $\bar{D}_a$ and $\bar{D}_d$ deduced from individual acquisition/decay curves of sediment groups A-E. $\bar{D}_a$ has been corrected for the effect of field intensity (see Appendix B). Dashed lines indicate constant values of $\bar{D}_d/\bar{D}_a$, with $\bar{D}_d/\bar{D}_a = 1$ expected for stationary conditions. **d**, Probability density function p_r of the rotational diffusion coefficient D, reconstructed from the normalized acquisition/decay curves shown in (**b**), and mean distribution p of grain diameters a for sediment groups A-E (the shaded band corresponds to ± one standard deviation of 40 measurements). D and a on the lower axis are normalized by their medians. The median $\bar{D}_d$ of sediment groups A-E vs. measured bacteria concentrations is shown in the insert. The dashed line is a guide for the eye.

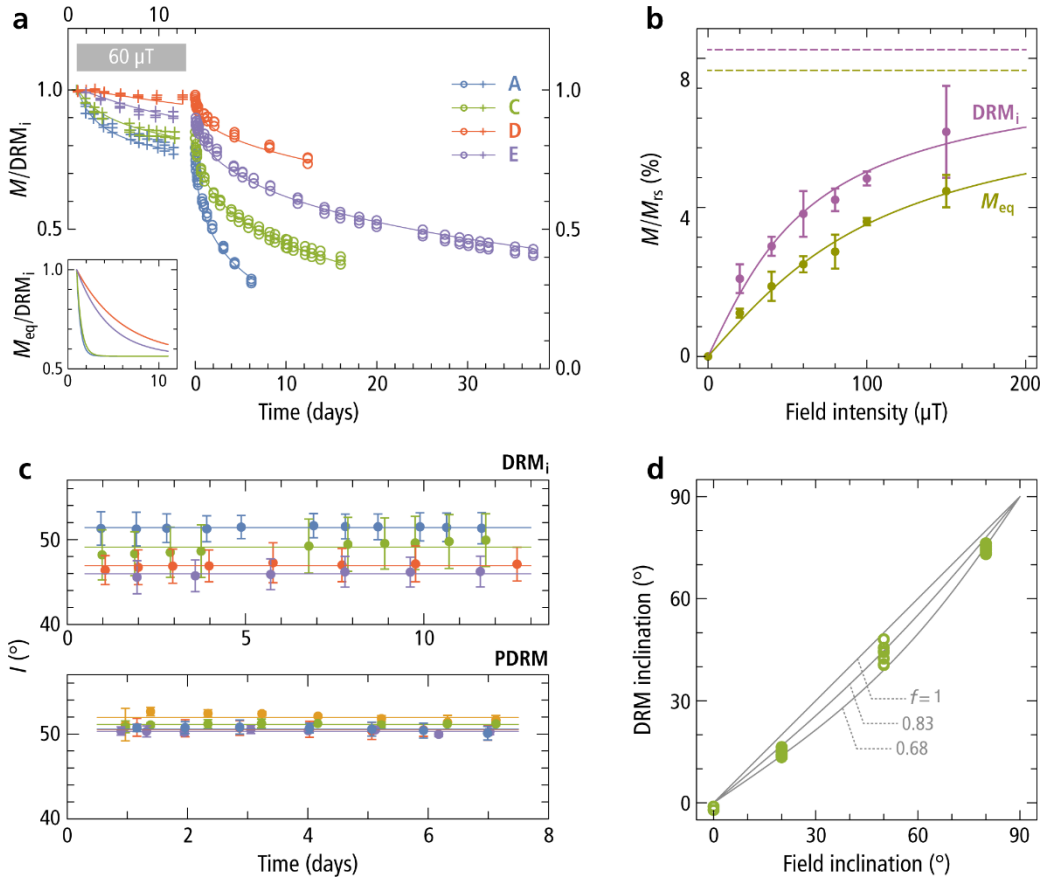

Figure 5-3 DRM experiments. **a**, DRM acquired in 60 μT by sediment groups A,C, D, and E, and subsequent decay in a null field. Lines are fits obtained by assuming that the initial DRM (DRM_i) is progressively replaced by a PDRM acquired in the applied field. A magnetization decay of the same type shown in Figure 5-2 follows after removing the applied field. Curve fits have been obtained assuming that DRM_i and equilibrium PDRM (M_{eq}) intensities are identical at the beginning of the experiments (i.e. $M_{eq}/DRM_i = 1$, see insert). The subsequent exponential decrease of M_{eq}, caused by the buildup of inter-particle forces, has been chosen so that the final M_{eq}/DRM_i matches the measurements shown in (**b**). The exponential decrease of M_{eq} needed to reproduce the observed DRM changes in time is faster for sediments containing more bacteria (i.e. groups A and C). **b**, Dependence of DRM_i and M_{eq} on field intensity. M_{eq} has been calculated from PDRM acquisition curves as shown in Figure 5-2. Solid lines are least-squares fits with $M = M_0 S(B/B_0)$, where $S(x) = x^{-1}\ln[x^{-1}\sinh(x)]$ is a suitable approximation of eq. (5-1), M_0 is the magnetization corresponding to full alignment of the magnetic moments (dashed lines), and B_0 = 15.5 μT and 26.7 μT for DRM_i and M_{eq}, respectively. **c**, Inclination of DRM_i and PDRM acquired a field with 50 °inclination. Lines are averages of all experiments with sediment groups A-E. DRM_i inclinations are slightly shallower, especially in sediments containing less bacteria, while no systematic shallowing is observed for the PDRMs. d, Inclination of DRM_i in 60 mT fields with 0, 20 °, 50 °, and 80 °inclinations (circles). Solid lines are plots of the inclination shallowing law $\tan I = f \tan I_B$, where I and I_B are the inclinations of DRM_i and the applied field, respectively, and f is an empirical factor [King, 1955]. These results confirm that DRM_i has the typical properties of a DRM, as seen with traditional redeposition experiments.

Appendix A
Supplementary materials for Chapter 4

A0. List of symbols and mathematical notations

General:

b	Unit vector parallel to the magnetic field direction
B	Magnetic field intensity (flux density)
ΔE	Energy barrier
φ,ψ	Azimuthal angles (spherical coordinates)
k_B	Boltzmann constant
M	Magnetization (generic)
M_{rs}	Saturation remanence
M_s	Saturation magnetization
m	Magnetic moment (of individual grains)
n	Unit vector parallel to a magnetic moment
t	Time
T	Absolute temperature
θ	Angle to a reference direction (e.g. to the magnetic field vector)
z	Depth below the sediment-water interface
$z'=z/L$	Normalized depth below the sediment-water interface

Sediment properties:

a	Radius of sediment particles (smallest elastic units in sediment)
K_{IC}	Tensile fracture toughness
η	Dynamic viscosity
L	Mixing depth (thickness of the mixed layer)
ω	Sedimentation rate (= sinking velocity)

Bioturbation:

a_b	Mean radius of microbes
$c_b(z')$	Magnetic field intensity (flux density)
D_b	Normalized profile of D_r
D_B	Self-diffusion coefficient of microorganisms
D_r	Rotational diffusion constant of the mixed layer
$D_{r,0}$	Maximum value of D_r (at the sediment-water interface $z' = 0$)
ε	Volume fraction of motile microorganisms inside the mixed layer
ε_{mob}	Fraction of motile microorganisms
$\gamma = 2D_rL/\omega$	Rotational diffusivity parameter of the mixed layer

Γ_b	Translational viscous drag coefficient
Γ_r	Rotational viscous drag coefficient
$K(z_1,z_2)$	Exchange function (non-local mixing)
$p(\theta,\varphi)$	Probability density function of particle orientations (spherical coordinates)
$t_{1/2}$	Half-life of remanent magnetization inside the mixed layer

NRM acquisition:

B_h	Minimum field for rotating remanence carriers against holding forces
$\beta_h = \tau_h/\tau_p$	Boltzmann factor of holding torques
$\beta_m = \tau_m/\tau_p$	Boltzmann factor of magnetic torques
$\beta_0 = \beta_h\|_{z=L}$	Boltzmann factor at the bottom of the mixed layer
DRM	Depositional remanent magnetization
L	Langevin function
MRM	Mixing remanent magnetization
M_0	Maximum remanent magnetization (full magnetic moment alignment)
M_{eq}	Equilibrium magnetization
M_{ini}	Initial magnetization
M_{NRM}	NRM intensity
M_{DRM}	DRM intensity
M_{MRM}	MRM intensity
N	Normal distribution
NRM	Natural remanent magnetization
$\lambda(z')$	Lock-in function (probability density) of the reduced depth
$\Lambda(z')$	Lock-in function (cumulative) of the reduced depth
PDRM	Post-depositional remanent magnetization
q	Value of β_h for which MRM acquisition efficiency is reduced by ~29%
$\tau_m = mB$	Maximum magnetic torque amplitude
τ_h	Root mean square of holding torques (from holding potentials)
τ_p	Root mean square of random perturbation torques
T_i ,T_i	Torque acting on particle i (vector and module)
$U(\theta,\varphi)$	Normalized holding potential
$V(\theta,\varphi)$	Total torque potential
z_0	Initial depth of a magnetized sediment layer
z_B	Full blocking depth (where lock-in process is completed)

Inclination shallowing:

$A(\theta,\varphi)$	Normalized anisotropy potential
$\beta_a = \tau_a/\tau_p$	Boltzmann factor of anisotropy torques
f_a	Inclination shallowing factor
τ_a	Maximum amplitude of anisotropy torques

A1. Rotational diffusion

Rotational diffusion is governed by the rotational counterpart of the translational Fick's law:

$$\frac{\partial p}{\partial t} = D_r \Delta p \tag{A1-1}$$

where $p = p(t,\theta,\varphi)$ is the probability density distribution of the orientation vector in spherical coordinates [Perrin, 1934]. In the following, we demonstrate that

$$p(t,\theta) = \frac{1}{4\pi}\sum_{l=0}^{\infty}(2l+1)e^{-D_r l(l+1)t}P_l(\cos\theta) \tag{A1-2}$$

is a solution of (A2-1) yielding full alignment at $t = 0$. Because p depends only on θ, eq. (A1-1) can be rewritten as:

$$\frac{\partial p}{\partial t} = D_r \frac{1}{\sin\theta}\frac{\partial}{\partial\theta}\left[\sin\theta\frac{\partial p}{\partial\theta}\right] \tag{A1-3}$$

Inserting the solution given in eq. (A1-2) we obtain

$$\frac{\partial p}{\partial t} = -D_r \frac{1}{4\pi}\sum_{l=0}^{\infty}(2l+1)l(l+1)e^{-D_r l(l+1)t}P_l(\cos\theta) \tag{A1-4}$$

for the left-hand side of eq. (A1-3), and, using the substitution $x = \cos\theta$ and the definition of Legendre polynomials

$$\begin{aligned}\Delta p(t,\theta) &= D_r \frac{1}{4\pi}\sum_{l=0}^{\infty}(2l+1)e^{-D_r l(l+1)t}\frac{1}{\sin\theta}\frac{\partial}{\partial\theta}\left[\sin\theta\frac{\partial P_l}{\partial\theta}\right]\\ &= D_r \frac{1}{4\pi}\sum_{l=0}^{\infty}(2l+1)e^{-D_r l(l+1)t}\frac{\partial}{\partial x}\left[(1-x^2)\frac{\partial P_l}{\partial x}\right]\\ &= -D_r \frac{1}{4\pi}\sum_{l=0}^{\infty}(2l+1)l(l+1)e^{-D_r l(l+1)t}P_l(\cos\theta)\end{aligned} \tag{A1-5}$$

for the right-hand side, proving the identity of the two sides. Integration of p over the unit sphere gives:

$$p(t,\theta) = \frac{1}{2}\sum_{l=0}^{\infty}(2l+1)e^{-D_r l(l+1)t}\int_0^{\pi}P_l(\cos\theta)\sin\theta d\theta = \frac{1}{2}\int_0^{\pi}P_0(\cos\theta)\sin\theta d\theta = 1 \tag{A1-6}$$

as expected for a probability density function. Finally,

$$\langle\cos\theta\rangle = 2\pi\int_0^{\pi}p(t,\theta)\cos\theta\sin\theta d\theta = \frac{3}{2}e^{-2D_r t}\int_0^{\pi}P_l(\cos\theta)\cos\theta\sin\theta d\theta = e^{-2D_r t} \tag{A1-7}$$

represents the mean magnetic moment alignment.

A2. Analytical solution of the Smoluchowski-Debye equation

The Smoluchowski equation

$$\frac{\partial p}{\partial t} = D_r \Delta p + \frac{1}{\Gamma_r} \nabla \left(p \nabla V \right) \tag{A2-1}$$

describes the probability density $p = p(t,\theta,\varphi)$ of particle orientations subjected to rotational diffusion in a torque potential $V(\theta,\varphi)$. The stationary case is given by

$$D_r \Delta p = -\frac{1}{\Gamma_r} \nabla \left(p \nabla V \right) \tag{A2-2}$$

As general solution of eq. (A2-2) we assume $p = ce^{aV}$ with coefficients c and a to be determined. Accordingly:

$$\begin{aligned} \Delta p &= \frac{1}{\sin\theta} \frac{\partial}{\partial \theta} \left[\sin\theta \frac{\partial p}{\partial \theta} \right] + \frac{1}{\sin^2\theta} \frac{\partial^2 p}{\partial \varphi^2} \\ &= \frac{1}{\sin\theta} \frac{\partial}{\partial \theta} \left[\sin\theta ace^{aV} \frac{\partial V}{\partial \theta} \right] + \frac{1}{\sin^2\theta} \frac{\partial}{\partial \varphi} ace^{aV} \frac{\partial V}{\partial \varphi} \\ &= aV \frac{1}{\sin\theta} \left[a \sin\theta \left(\frac{\partial V}{\partial \theta} \right)^2 + \cos\theta \frac{\partial V}{\partial \theta} + \sin\theta \frac{\partial^2 V}{\partial \theta^2} \right] + aV \frac{1}{\sin^2\theta} \left[a \left(\frac{\partial V}{\partial \varphi} \right)^2 + \frac{\partial^2 V}{\partial \varphi^2} \right] \end{aligned} \tag{A2-3}$$

and

$$\begin{aligned} \nabla \left(p \nabla V \right) &= \nabla \left(p \frac{\partial V}{\partial \theta} \hat{\theta} + p \frac{1}{\sin\theta} \frac{\partial V}{\partial \varphi} \hat{\varphi} \right) \\ &= \frac{1}{\sin\theta} \frac{\partial}{\partial \theta} \left[p \sin\theta \frac{\partial V}{\partial \theta} \right] + \frac{1}{\sin\theta} \frac{\partial}{\partial \varphi} \left[p \frac{1}{\sin\theta} \frac{\partial V}{\partial \varphi} \right] \\ &= \frac{1}{\sin\theta} \frac{\partial}{\partial \theta} \left[ce^{aV} \sin\theta \frac{\partial V}{\partial \theta} \right] + \frac{1}{\sin\theta} \frac{\partial}{\partial \varphi} \left[ce^{aV} \frac{1}{\sin\theta} \frac{\partial V}{\partial \varphi} \right] \\ &= V \frac{1}{\sin\theta} \left[a \sin\theta \left(\frac{\partial V}{\partial \theta} \right)^2 + \cos\theta \frac{\partial V}{\partial \theta} + \sin\theta \frac{\partial^2 V}{\partial \theta^2} \right] + V \frac{1}{\sin^2\theta} \left[a \left(\frac{\partial V}{\partial \varphi} \right)^2 + \frac{\partial^2 V}{\partial \varphi^2} \right] \end{aligned} \tag{A2-4}$$

Comparison of the two terms gives

$$a = \frac{-1}{D_r \Gamma_r} \tag{A2-5}$$

Finally, integration of the solution over the unit sphere must give a probability of 1, i.e.:

$$\int_{\varphi=0}^{2\pi} \int_{\theta=0}^{\pi} p(\theta) \sin\theta d\theta d\varphi = 1 \tag{A2-6}$$

yielding

$$c = \left[\int_{\varphi=0}^{2\pi} \int_{\theta=0}^{\pi} e^{-V/(D_r \Gamma_r)} \sin\theta d\theta d\varphi \right]^{-1} \tag{A2-7}$$

A special solution is obtained with potential $V=-mB\cos\theta$ describing the torque of a particle with magnetic moment m in a field B, where θ is the angle between m and B. In this case, the Fisher-Von Mises distribution

$$p(\theta) = \frac{x}{4\pi \sinh x} e^{x\cos\theta} \tag{A2-8}$$

with

$$x = \frac{mB}{D_{\mathrm{r}}\Gamma_{\mathrm{r}}} \tag{A2-9}$$

is obtained.

A3. Construction of random holding potentials

Random potentials yielding a "white" field spectrum on a sphere have been introduced for the purpose of representing paleosecular variations of the geomagnetic field. Using Gauss coefficients with variance

$$\left\langle h_{l,m}^2 \right\rangle = \left\langle g_{l,m}^2 \right\rangle = \frac{\sigma^2}{(l+1)(2l+1)} \tag{A3-1}$$

Constable and Parker [1988] obtained the following expression for the component B_θ of the "white spectrum" geomagnetic field at the core-mantle boundary:

$$\left\langle B_\theta^2 \right\rangle = \frac{\sigma^2}{2}\sum_{l=1}^{n}\frac{l}{2l+1} \tag{A3-2}$$

Because **B** is random and all its components are equal, the same result holds for $<B_\varphi^2>$. Eq. (A3-2) can be applied in identical form to the torque produced by the same potential used for representing the geomagnetic field. In this case:

$$\left\langle T^2 \right\rangle = \left\langle T_\theta^2 \right\rangle + \left\langle T_\varphi^2 \right\rangle = \sigma^2\sum_{l=1}^{n}\frac{l}{2l+1} \tag{A3-3}$$

A4. Inclination shallowing

Mean inclination shallowing effects are described by random perturbations of magnetic moments subjected to the potential

$$V(\theta,\varphi) = -mB(\mathbf{n}\cdot\mathbf{b}) + \frac{\tau_{\mathrm{a}}}{2}\cos(2\theta) + U_i(\theta,\varphi) \tag{A4-1}$$

where $\mathbf{n}$ =(sinθcosφ,sinθsinφ,cosθ) is the unit vector representing the direction of magnetic moments in a magnetic field $\boldsymbol{B}$ parallel to the unit vector $\mathbf{b}$=(sinφ cosφ,0,cosφ) . The probability density of magnetic moment directions at equilibrium is given by the Boltzmann distribution associated with V, i.e.

$$p(\theta,\varphi) \propto \exp\left[\beta_m \mathbf{n}\cdot\mathbf{b} - \frac{\tau_{\mathrm{a}}}{2}\cos(2\theta)\right] \tag{A4-2}$$

If $\beta_{\mathrm{m}} \ll 1$, as expected in sediment during MRM acquisition, eq. (A4-2) can be linearized, obtaining

$$\begin{aligned} p(\theta,\varphi) &\propto (1+\beta_m \mathbf{n}\cdot\mathbf{b})e^{-u\cos 2\theta} \\ &= (1+\beta_m \sin\theta\cos\varphi\sin\psi + \beta_m\cos\theta\cos\psi)e^{-u\cos 2\theta} \end{aligned} \tag{A4-3}$$

with $u = \tau_a/2$. The expectation for the horizontal component of the mean magnetic vector is obtained by integration of $p(\theta,\varphi)\mathbf{n}$ over the unit sphere, i.e.:

$$\begin{aligned} h &\propto \int_0^{2\pi}\int_0^{\pi}\left(1+\beta_m \sin\theta\cos\varphi\sin\psi+\beta_m\cos\theta\cos\psi\right)e^{-u\cos 2\theta}\sin^2\theta\cos\varphi d\theta d\varphi \\ &= \beta_m\sin\psi\int_0^{2\pi}\int_0^{\pi}e^{-u\cos 2\theta}\sin^3\theta\cos^2\varphi d\theta d\varphi \\ &= \pi\beta_m\sin\psi\int_0^{\pi}e^{-u\cos 2\theta}\sin^3\theta d\theta \end{aligned} \tag{A4-4}$$

Similarly, the expectation of the vertical component is given by:

$$\begin{aligned} v &\propto \int_0^{2\pi}\int_0^{\pi}\left(1+\beta_m \sin\theta\cos\varphi\sin\psi+\beta_m\cos\theta\cos\psi\right)e^{-u\cos 2\theta}\sin\theta\cos\theta d\theta d\varphi \\ &= 2\pi\int_0^{\pi}\left(1+\beta_m\cos\theta\cos\psi\right)e^{-u\cos 2\theta}\sin\theta\cos\theta d\theta \\ &= 2\pi\int_0^{\pi}e^{-u\cos 2\theta}\sin\theta\cos\theta d\theta+2\pi\beta_m\cos\psi\int_0^{\pi}e^{-u\cos 2\theta}\sin\theta\cos^2\theta d\theta \\ &= 2\pi\beta_m\cos\psi\int_0^{\pi}e^{-u\cos 2\theta}\sin\theta\cos^2\theta d\theta \\ &= 2\pi\beta_m\cos\psi\int_0^{\pi}e^{-u\cos 2\theta}\sin\theta d\theta-2\pi\beta_m\cos\psi\int_0^{\pi}e^{-u\cos 2\theta}\sin^3\theta d\theta \end{aligned} \tag{A4-5}$$

The ratio between these two results yields the classical inclination shallowing law

$$\tan I=\frac{v}{h}=2\left[\frac{\int_0^{\pi}e^{-u\cos 2\theta}\sin\theta d\theta}{\int_0^{\pi}e^{-u\cos 2\theta}\sin^3\theta d\theta}-1\right]\tan I_B \tag{A4-6}$$

with $I = 90°-\theta$ and $I_B = 90°-\psi$ being the magnetization and field inclinations, respectively. Analytical solution of the integrals in eq. (A4-6) finally gives:

$$\begin{aligned} f &= \frac{2g}{4u-g} \\ g &= 1-\sqrt{\frac{u}{2\pi}}\frac{4}{e^{2u}\operatorname{erf}\sqrt{2u}} \end{aligned} \tag{A4-7}$$

and thus eq. (4-23) upon back substitution of u.

A5. Lock-in model

The MRM lock-in function is derived from the time evolution of a fictive initial magnetization corresponding to full magnetic moment alignment, instantaneously acquired at a depth z_0 below the sediment-water interface. The sediment layer containing this magnetization gets progressively buried with a velocity $\omega = dz/dt$ while it is subjected to a depth-dependent rotational diffusion $D_r(z)$. In absence of an external magnetic field, the fate of this magnetization is governed by the diffusion equation

$$\frac{\partial p}{\partial t}=D_r\left(z(t)\right)\Delta p \tag{A5-1}$$

for the statistical distribution $p(\theta,\varphi)$ of magnetic moment orientations and

$$z(t) = z_0 + \int_0^t \omega\big(z(u)\big)\,du \tag{A5-2}$$

The depth dependence of D_r is conveniently expressed in normalized coordinate $z' = z/L$. Assuming ω to be a constant, in this case, eq. (A5-1) is rewritten as

$$\frac{\partial p}{\partial t} = D_r\left(\frac{z_0 + \omega t}{L}\right)\Delta p \tag{A5-3}$$

Eq (A5-3) is solved in a similar manner as the diffusion equation with constant diffusion coefficient (see Appendix A1), assuming

$$p(t,\theta) = \frac{1}{4\pi}\sum_{l=0}^{\infty}(2l+1)f_l(t)P_l(\cos\theta) \tag{A5-4}$$

where $f_l(t)$ are generic functions with $f_l(0) = 1$. The left-hand side of eq. (A5-3) becomes:

$$\frac{\partial p}{\partial t} = \frac{1}{4\pi}\sum_{l=0}^{\infty}(2l+1)f_l'(t)P_l(\cos\theta) \tag{A5-5}$$

where f_l' is the first derivative of f_l. For the right-hand side of eq. (A5-3) we obtain:

$$\begin{aligned}\Delta p(t,\theta) &= \frac{1}{4\pi}\sum_{l=0}^{\infty}(2l+1)f_l(t)\frac{1}{\sin\theta}\frac{\partial}{\partial\theta}\left[\sin\theta\frac{\partial P_l}{\partial\theta}\right]\\ &= \frac{1}{4\pi}\sum_{l=0}^{\infty}(2l+1)f_l(t)\frac{\partial}{\partial x}\left[(1-x^2)\frac{\partial P_l}{\partial x}\right]\\ &= -\frac{1}{4\pi}\sum_{l=0}^{\infty}(2l+1)l(l+1)\,f_l(t)P_l(\cos\theta)\end{aligned} \tag{A5-6}$$

Comparison of the two sides yields:

$$f_l'(t) = -l(l+1)D_r\left(\frac{z_0 + \omega t}{L}\right)f_l(t) \tag{A5-7}$$

with general solution

$$f_l(t) = \exp\left[-l(l+1)\int_0^t D_r\left(\frac{z_0 + \omega u}{L}\right)du\right] \tag{A5.8}$$

The mean magnetic moment alignment is then given by:

$$\begin{aligned}\langle\cos\theta\rangle &= \frac{3}{2}f_1(t)\int_0^{\pi}P_1(\cos\theta)\cos\theta\sin\theta\,d\theta\\ &= f_1(t) = \exp\left[-2\int_0^t D_r\left(\frac{z_0 + \omega u}{L}\right)du\right]\end{aligned} \tag{A5-9}$$

Using $t = (z-z_0)/\omega$ we finally obtain:

$$\frac{M(z_0,z)}{M_0} = \langle\cos\theta\rangle = \exp\left[-2\frac{L}{\omega}\int_{z_0'}^{z'}D_r(u)\,du\right] \tag{A5-10}$$

from which all results in Chapter 4 are obtained.

Appendix B
Supplementary materials for Chapter 5

B1. PDRM acquisition kinetics

The magnetization acquired during PDRM experiments is controlled by the statistical distribution $p(t,\theta,\varphi)$ of magnetic grain orientations at the time t , where orientations are expressed in spherical coordinates by the angle θ between magnetic moment vector and applied field direction, and the azimuthal angle φ. This distribution obeys the Smoluchowski-Debye equation:

$$\frac{\partial p}{\partial t} = D\Delta p + \frac{1}{\Gamma}\nabla\left(p\nabla V\right) \tag{B1-1}$$

where D is the rotational diffusion coefficient, Γ is the rotational viscous drag coefficient (e.g. $\Gamma = 8\pi\eta a^3$ for spheres with radius a immersed in a fluid with dynamic viscosity η), and V is a potential whose gradient defines a deterministic torque $\tau = -\nabla V$ that adds to the random torques associated with D [Egli and Zhao, 2015]. The potential V is the sum of (1) a systematic term $-m_i B\cos\theta$, which yields the magnetic torque experienced by particles with magnetic moments m_i in the applied field B, and (2) a random "holding potential" U_t that accounts for mechanical interaction forces between particles. The general solution of equation (B1-1) at equilibrium (i.e. $\partial p / \partial t = 0$) is the Boltzmann distribution

$$p_{eq}\left(\theta,\varphi\right) = p_0 \exp\left[\frac{-V\left(\theta,\varphi\right)}{D\Gamma}\right] \tag{B1-2}$$

where p_0 is a constant ensuring that the total probability associated with p_{eq} is 1.

As discussed by Egli and Zhao [2015], the overall effect of the holding potential is formally equivalent to an increase in Γ. Accordingly, $V = -mB\cos\theta$ is the effective potential acting on the particles and equation (B1-1) can be rewritten as:

$$\frac{1}{D}\frac{\partial p}{\partial t} = \frac{1}{\sin\theta}\frac{\partial}{\partial\theta}\left[\frac{\partial p}{\partial\theta}\sin\theta + \beta p\sin^2\theta\right] \tag{B1-3}$$

where $\beta = mB/(D\Gamma)$ is the so-called Boltzmann factor. Upon substituting $x = \cos\theta$ and $t' = Dt$ we obtain the dimensionless form

$$\frac{\partial p}{\partial t'} = \frac{\partial}{\partial x}\left[\left(1-x^2\right)\left(\frac{\partial p}{\partial x} - \beta p\right)\right] \tag{B1-4}$$

of the Smoluchowski-Debye equation, which we solve numerically in order to reproduce PDRM acquisition and decay (i.e., $\beta = 0$) experiments. The associated magnetization is obtained by intergrating the magnetic moment components along the direction of B, i.e.:

$$\frac{M\left(t\right)}{M_0} = 2\pi\int_{\theta=0}^{\pi} p\left(t,\theta\right)\cos\theta\sin\theta d\theta \tag{B1-5}$$

where M_0 is the magnetization corresponding to full alignment of the magnetization carriers.

A general analytical solution of the equation (B1-4) exists only for $\beta = 0$. In this case

$$p(t,\theta) = \frac{1}{4\pi} + \frac{1}{4\pi}\sum_{l=1}^{\infty} a_l e^{-Dl(l+1)t} P_l(\cos\theta), \tag{B1-6}$$

where P_l are the Legendre polynomials of order l, and a_l are coefficients determined by the initial distribution $p(0, \theta)$. Insertion of this solution into equation (B1-5) gives:

$$\frac{M(t)}{M_0} = \frac{1}{2} a_l e^{-2Dt} \int_{\theta=0}^{\pi} P_l(\cos\theta)\cos\theta\sin\theta d\theta = \frac{a_l}{3} e^{-2Dt} \tag{B1-7}$$

[Perrin, 1934]. This means that any initial magnetization decays exponentially in zero field, regardless of how it was acquired (i.e., regardless of the initial distribution of magnetic moment orientations).

On the other hand, PDRM acquisition curves can be obtained only by numerical solution of equation (B1-4). Acquisition curves originating from a fully randomized initial state (i.e. $p(0, \theta) = 1/4\pi$) have been calculated with Wolfram Mathematica® using the following command:

$$\text{NDSolve}[\{D[p[t,x],t] == D[(1-x\text{^}2)*(D[p[t,x],x] - \text{beta}*p[t,x]),x],$$
$$p[0,x] == 1/(4*\text{Pi})\}, p, \{t,0,\text{ta}\}, \{x,-1,1\}]$$

and given values of beta for β and ta for the maximum acquisition time $t_a^{'} = Dt_a$. In the limit case of $\beta \rightarrow 0$, numerical solutions converge to

$$\frac{M(t)}{M_0} = L(\beta)\left[1 - e^{-2Dt}\right] \tag{B1-8}$$

where $L(\beta) = \coth\beta - 1/\beta$ is the Langevin function. Equation (B1-8) holds with a maximum error of 0.03 for $\beta \leq 1$. Above this limit, magnetizations are acquired faster than their decay in zero field, due to the increasingly strong aligning torques associated with $\beta > 1$ (Figure B1).

In case of PDRM acquired in weak fields (i.e. $\beta < 1$), the following relationship holds between the acquisition curve M_a and the zero-field decay curve M_d:

$$M_a = M_{eq} - M_{eq}\frac{M_d}{M_f} \tag{B1-9}$$

where $M_{eq} = M_a$ (t $\rightarrow\infty$) is the equilibrium magnetization in the applied field, and $M_f = M_a(t_a)$ is the "final" PDRM acquired during a time t_a. Solution of equation (B1-9) with respect to M_d gives:

$$\frac{M_d}{M_f} = 1 - \frac{M_a}{M_{eq}} = 1 - s\frac{M_a}{M_f} \tag{B1-10}$$

with the "saturation coefficient" $s = M_f / M_{eq}$. This coefficient is estimated using an appropriate model of acquisition/decay curves based on a distribution of rotational diffusion coefficients.

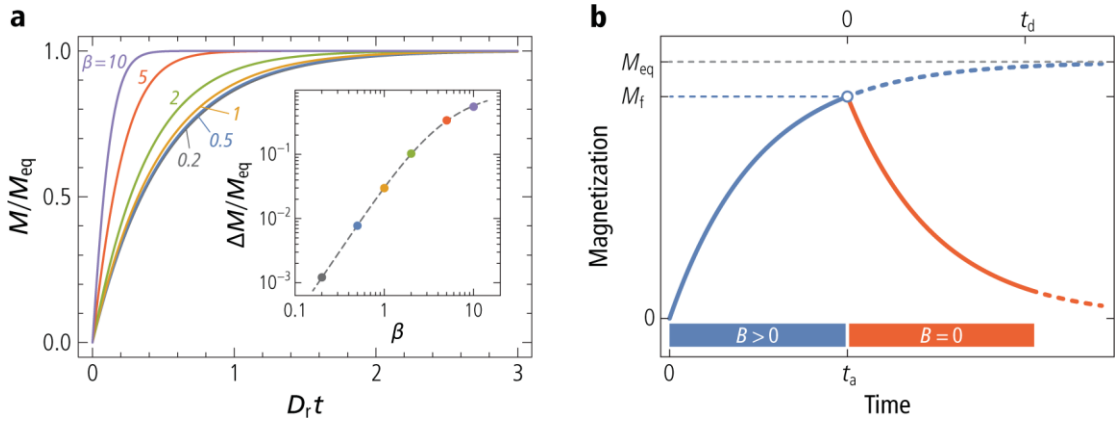

Figure B1 PDRM acquisition and decay curves. **a**, calculated acquisition curves for β = 0.2, 0.5, 1, 2, 5,and 10. All curves are normalized by the equilibrium magnetization M_{eq} =$M(t = \infty)$. The maximum difference ΔM to the limit case given by $\beta \rightarrow 0$ is shown in the insert. **b**, Incomplete acquisition curve in a field $B > 0$ (blue), followed by zero-field decay (orange). M_f is the magnetization acquired during the acquisition time t_a.

B2. Modeling of acquisition/decay curves

As shown in the previous section, weak-field PDRM acquisition and decay curves inside a mixed sediment layer characterized by a rotational diffusion coefficient D are given by:

$$\frac{M_a(t)}{M_{eq}} = 1 - e^{-2Dt}$$
$$\frac{M_d(t)}{M_d(t=0)} = e^{-2Dt} \quad \text{(B2-1)}$$

where M_{eq} is the equilibrium magnetization in the applied field. Because D is controlled by many factors, including particle size, bioturbated sediment is modeled by a distribution of D values, represented by the probability density function $p_r(D)$. Accordingly, each magnetized grain is subjected to its own rotational diffusion process that produces a small exponential acquisition and decay of the form given by equation (B2-1). Integration of $(1\text{-}e^{-2Dt})p_r$ over D gives the normalized acquisition curve:

$$\frac{M_a(t)}{M_{eq}} = \int_0^\infty p_r(D)\left(1 - e^{-2Dt}\right)dD = 1 - \int_0^\infty p_r(D)e^{-2Dt}dD \quad \text{(B2-2)}$$

In real PDRM acquisition experiments, acquisition is interrupted at a time t_a before full equilibrium with the applied field is reached (i.e. $M_a(t_a)/M_{eq} = s < 1$), so that the PDRM contribution of grains subjected to rotational diffusion with coefficient D is proportional to $p_r(D)((1\text{-}e^{-2Dt})$. The decay of the total PDRM in zero field is thus given by:

$$\frac{M_d(t)}{M_{eq}} = \int_0^\infty p_r(D)\left(1 - e^{-2Dt_a}\right)e^{-2Dt}dD \quad \text{(B2-3)}$$

Equations (B2-2 and B2-3) can be rewritten as:

$$\frac{M_a(t)}{M_{eq}} = 1 - f_d(t)$$
$$\frac{M_d(t)}{M_{eq}} = f_d(t) - f_d(t_a + t) \quad \text{(B2-4)}$$

where

$$f_d(t) = \int_0^\infty p_r(D) e^{-2Dt} dD \quad \text{(B2-5)}$$

is the normalized decay curve of the equilibrium PDRM (i.e. the magnetization acquired with $t_a \rightarrow \infty$). In mathematical terms, $f_d(2t)$ is the Laplace transform of $p_r(D)$. Conversely, the probability distribution p_r is uniquely determined by the inverse Laplace transform

$$p_r(D) = \frac{1}{2\pi i} \lim_{T\to\infty} \int_{\omega - iT}^{\omega + iT} f_d(2t) e^{Dt} dt \quad \text{(B2-6)}$$

where ω is a real parameter chosen to avoid singularities of f_d in the complex plane.

In principle, equations (B2-4 to B2-6) can be used to reconstruct p_r from a set of PDRM acquisition/decay experiments, provided that $p_r(D)$, does not change significantly over the experiment duration. In order to test the validity of this condition, acquisition and decay curves are fitted independently from each other using a suitable parameterized approximation $\tilde{f}_d$ of f_d for which the inverse Laplace transform is known. The model function $\tilde{f}_d$ must provide a good fit of all experimental data with a minimum number of paramters; ideally a single one representing the mean or median of $p_r(D)$. In order to guess a suitable analytical expression for $\tilde{f}_d$ we plotted the logarithm of normalized decay curves vs. the square root of decay time, obtaining straight lines with different slopes (Figure B2). These lines are described by $\tilde{f}_d = e^{-b\sqrt{t}}$, where b is the slope on the logarithmic plot. The inverse Laplace transform of $\tilde{f}_d$ is the probability density function

$$p_r(D, D_0) = \sqrt{\frac{\xi D_0}{\pi}} D^{-3/2} e^{-\xi D_0 / D} \quad \text{(B2-7)}$$

with $\xi = 0.227$, cumulative distribution

$$P_r(D, D_0) = 1 - \mathrm{erf}\left[\sqrt{\frac{\xi D_0}{D}}\right] \quad \text{(B2-8)}$$

and median D_0. This probability function yields the decay curve:

$$\tilde{f}_d = e^{-2\sqrt{2\xi D_0 t}} \quad \text{(B2-9)}$$

which is used to fit all experimental data.

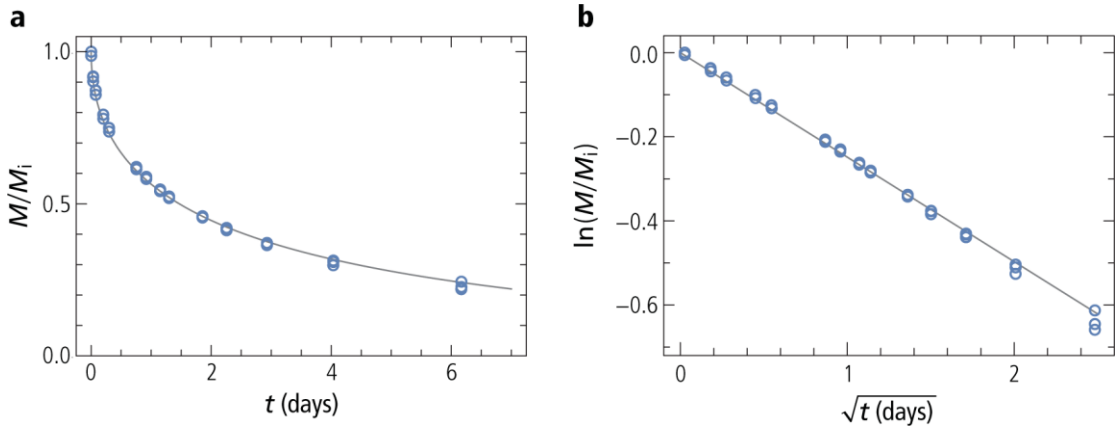

Figure B2 Rescaling of PDRM decay curves. a, PDRM decay curves for three samples of group A (blue circles), normalized by the initial value M_i , and least squares fit with $\tilde{f}_d = e^{-b\sqrt{t}}$ (gray line). b, Same as (a) for the logarithm of M/M_i vs. the square root of decay time.

Since M_{eq} is unknown, acquisition and demagnetization curves are normalized by the maximum PDRM, i.e. $M_f = M_a(t_a)$, instead of M_{eq}, and models include an (unknown) "saturation" factor $s = M_f/M_{eq}$, so that

$$f_a = \frac{M_a(t)}{M_f} = \frac{1}{s}\left[1 - \tilde{f}_d\left(t, D_a\right)\right]$$
$$f_d = \frac{M_d(t)}{M_f} = \frac{1}{s}\,\tilde{f}_d\left(t, D_0\right) - \frac{1}{s}\,\tilde{f}_d\left(\frac{D_a}{D_d}t_a + t, D_d\right) \qquad \text{(B2-10)}$$

where D_a and D_d represent the parameter D_0 during PDRM acquisition and decay, respectively. In case of stationary conditions, $D_a = D_d = D_0$. Each experiment is thus described by three unknown parameters: s, D_a, and D_d. Because of the high sensitivity of these parameters on measurement errors, additional information is used to constrain the model, using the fact that all experiments share the same total acquisition time t_a. In this case, the saturation factor s depends only on D_a and, at least in principle, on the intensity of the field applied during acquisition. As discussed previously, strong applied fields speed up the acquisition process and are equivalent to an apparent increase of D_a. Therefore, D_a-values obtained from equation (B2-10) need to be corrected a-posteriori, as it will be described later in this section. Finally, s is sensitive to large variations in the rotational diffusion coefficient, such as those existing between sample groups A-E, while samples belonging to the same groups are characterized by minor differences of D_a and are conveniently modeled with a single value of s, i.e., s_A for group A, s_B for gourp B, and so on. Small corrections of s can be applied a-posteriori once the modeled acquisition curves have been calculated. The model parameters $D_{a,i}$, $D_{b,i}$ and s_l for the i-th sample belonging to group l are determined by minimization of the sum of squared model residuals, i.e.:

$$\varepsilon = \sum_{i,k}\left[f_{a,k}\left(t_{ik}\right) - 1 + \frac{1}{s_l}\,\tilde{f}_d\left(t_{ik}, D_{a,i}\right)\right]^2 +$$
$$\sum_{i,k}\left[f_{d,k}\left(t_{ik}\right) - \frac{1}{s_l}\,\tilde{f}_d\left(t_{ik}, D_{d,i}\right) + \frac{1}{s_l}\,\tilde{f}_d\left(\frac{D_{a,i}}{D_{d,i}}t_a + t_{ik}, D_{d,i}\right)\right]^2 \qquad \text{(B2-11)}$$

where t_{ik} is the time corresponding to the k-th measurement of the i-th decay or acquisition curve, respectively, and l = A, B, C, D, and E. The model is subsequently refined by calculating the saturation factors

$$s_i = 1 - \tilde{f}_{\mathrm{d}}\left(t_{\mathrm{a}}, D_{\mathrm{a},i}\right) \tag{B2-12}$$

and minimizing

$$\varepsilon = \sum_{i,k}\left[f_{\mathrm{a},k}\left(t_{ik}\right) - 1 + \frac{1}{s_i}\,\tilde{f}_{\mathrm{d}}\left(t_{ik}, D_{\mathrm{a},i}\right)\right]^2 + \sum_{i,k}\left[f_{\mathrm{d},k}\left(t_{ik}\right) - \frac{1}{s_i}\,\tilde{f}_{\mathrm{d}}\left(t_{ik}, D_{\mathrm{d},i}\right) + \frac{1}{s_i}\,\tilde{f}_{\mathrm{d}}\left(\frac{D_{\mathrm{a},i}}{D_{\mathrm{d},i}} t_{\mathrm{a}} + t_{ik}, D_{\mathrm{d},i}\right)\right]^2 \tag{B2-13}$$

with respect to $D_{\mathrm{a},i}$ and $D_{\mathrm{d},i}$. Stationary conditions are expected to yield $D_{\mathrm{a},i} = D_{\mathrm{d},i}$ after correcting $D_{\mathrm{a},i}$ for the effect of the acquisition field intensity. The correction factors have been determined from numerical solutions of the Smoluchowski-Debye equation, and are shown in Figure B3 for the 20, 40, 60, 80, 100, and 150 μT fields used in the experiments.

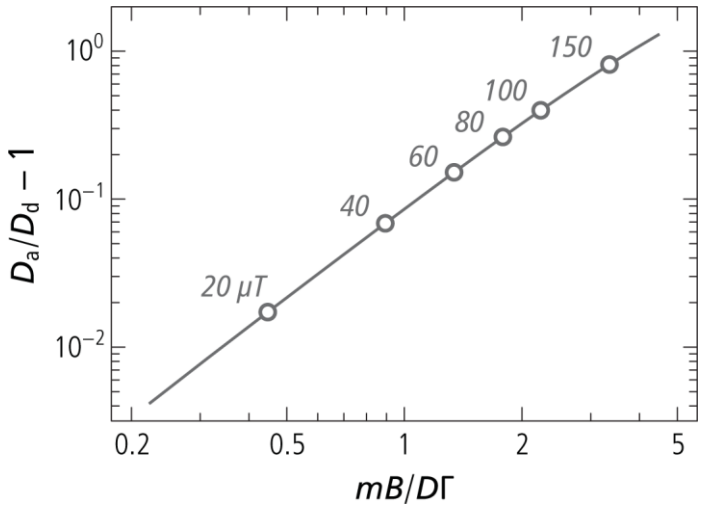

Figure B3 Difference between acquisition and decay curves. Ratio between the rotational diffusion constants deduced from acquisition curves (D_{a}) and decay curves (D_{d}), as a function of the Boltzmann factor $mB/D\Gamma$, calculated from numerical solutions of the Smoluchowski-Debye equations as described in note of Appendix B1. Values corresponding to fields used in PDRM experiments have been deduced from the Langevin fit of PDRM vs. applied field shown in Figure 5-3, i.e. $M_{\mathrm{eq}} \propto L\left(B / B_0\right)$ with B_0 = 44.8 μT.

Bibliography

Acton, G. D. and R. G. Gordon (1994). "Paleomagnetic Tests of Pacific Plate Reconstructions and Implications for Motion Between Hotspots." Science **263**(5151): 1246-1254.

Aitken, M., A. Allsop, et al. (1988). "Determination of the intensity of the Earth's magnetic field during archaeological times: reliability of the Thellier technique." Reviews of Geophysics **26**(1): 3-12.

Alexiewicz, W. (2000). "Ensemble averages for Smoluchowski–Debye rotational diffusion in the presence of a two-angle-dependent reorienting force." Chemical Physics Letters **320**(5–6): 582-586.

Aller, R. C. (1982). "The Effects of Macrobenthos on Chemical Properties of Marine Sediment and Overlying Water." Animal-sediment relations, Springer US**:** 53-102.

Amiotte Suchet, P., J.-L. Probst, et al. (2003). "Worldwide distribution of continental rock lithology: Implications for the atmospheric/soil CO2uptake by continental weathering and alkalinity river transport to the oceans." Global Biogeochemical Cycles **17**(2).

Anderson, R. F., R. F. Bopp, et al. (1988). "Mixing of particles and organic constituents in sediments from the continental shelf and slope off Cape Cod: SEEP—I results." Continental Shelf Research **8**(5–7): 925-946.

Arason, P. and S. Levi (1990). "Models of inclination shallowing during sediment compaction." Journal of Geophysical Research: Solid Earth **95**(B4): 4481-4499.

Barnes, H. A. (1997). "Thixotropy—a review." Journal of Non-Newtonian Fluid Mechanics **70**(1–2): 1-33.

Barraclough, D. R. (1976). "Spherical harmonic analysis of the geomagnetic secular variation — A review of methods." Physics of the Earth and Planetary Interiors **12**(4): 365-382.

Barton, C. E., M. W. McElhinny, et al. (1980). "Laboratory studies of depositional DRM." Geophysical Journal International **61**(2): 355-377.

Bazylinski, D. A., R. B. Frankel, et al. (1988). "Anaerobic magnetite production by a marine, magnetotactic bacterium." Nature **334**(6182): 518-519.

Bellini, S. (2009a). "Further studies on “magnetosensitive bacteria”." Chinese Journal of Oceanology and Limnology **27**(1): 6-12.

Bellini, S. (2009b). "On a unique behavior of freshwater bacteria." Chinese Journal of Oceanology and Limnology **27**(1): 3-5.

Bentley, S. J., A. Sheremet, et al. (2006). "Event sedimentation, bioturbation, and preserved sedimentary fabric: Field and model comparisons in three contrasting marine settings." Continental Shelf Research **26**(17–18): 2108-2124.

Berg, H. C. (1983). Random walks in biology. New Jersey, Princeton University Press.

Berner, R. A. (1980). Early diagenesis: A theoretical approach, Princeton University Press.

Bertani, G. (1951). "STUDIES ON LYSOGENESIS I.: The Mode of Phage Liberation by Lysogenic Escherichia coli1." Journal of bacteriology **62**(3): 293.

Biggin, A. J. (2010). "Are systematic differences between thermal and microwave Thellier-type palaeointensity estimates a consequence of multidomain bias in the thermal results?" Physics of the Earth and Planetary Interiors **180**(1-2): 16-40.

Bilardello, D., J. Jezek, et al. (2013). "Role of spherical particles on magnetic field recording in sediments: Experimental and numerical results." Physics of the Earth and Planetary Interiors **214**(0): 1-13.

Black, D. I. (1967). "Cosmic ray effects and faunal extinctions at geomagnetic field reversals." Earth and Planetary Science Letters **3**(0): 225-236.

Blakely, R. J. (1996). Potential theory in gravity and magnetic applications, Cambridge University Press.

Blakemore, R. (1975). "Magnetotactic bacteria." Science **190**(4212): 377-379.

Blakemore, R. P., D. Maratea, et al. (1979). "Isolation and pure culture of a freshwater magnetic spirillum in chemically defined medium." Journal of bacteriology **140**(2): 720-729.

Bleil, U. and T. von Dobeneck (1999). Geomagnetic Events and Relative Paleointensity Records — Clues to High-Resolution Paleomagnetic Chronostratigraphies of Late Quaternary Marine Sediments? Use of Proxies in Paleoceanography. G. Fischer and G. Wefer, Springer Berlin Heidelberg**:** 635-654.

Boudreau, B. P. (1986a). "Mathematics of tracer mixing in sediments; I, Spatially-dependent, diffusive mixing." American Journal of Science **286**(3): 161-198.

Boudreau, B. P. (1986b). "Mathematics of tracer mixing in sediments; II, Nonlocal mixing and biological conveyor-belt phenomena." American Journal of Science **286**(3): 199-238.

Boudreau, B. P. (1994). "Is burial velocity a master parameter for bioturbation?" Geochimica et Cosmochimica Acta **58**(4): 1243-1249.

Boudreau, B. P. (1998). "Mean mixed depth of sediments: The wherefore and the why." Limnology and Oceanography **43**(3): 524-526.

Buck, J. D. and R. C. Cleverdon (1960). "The spread plate as a method for the enumeration of marine bacteria." Limnology and Oceanography **5**(1): 78-80.

Butler, R. F. (1992). Paleomagnetism: magnetic domains to geologic terranes, Blackwell Scientific Publications Boston.

Cain, J. C. (1971). "Geomagnetic models from satellite surveys." Reviews of Geophysics **9**(2): 259.

Cande, S. C. and D. V. Kent (1992). "A new geomagnetic polarity time scale for the Late Cretaceous and Cenozoic." Journal of Geophysical Research **97**(B10): 13917.

Cande, S. C. and D. V. Kent (1995). "Revised calibration of the geomagnetic polarity timescale for the Late Cretaceous and Cenozoic." Journal of Geophysical Research **100**(B4): 6093.

Channell, J. E. T. and Y. Guyodo (2004). The Matuyama Chronozone at ODP Site 982 (Rockall Bank): Evidence for Decimeter-Scale Magnetization Lock-In Depths. Timescales Of The Paleomagnetic Field, American Geophysical Union**:** 205-219.

Channell, J. E. T., D. A. Hodell, et al. (2013). "Biogenic magnetite, detrital hematite, and relative paleointensity in Quaternary sediments from the Southwest Iberian Margin." Earth and Planetary Science Letters **376**(0): 99-109.

Channell, J. E. T., C. Xuan, et al. (2009). "Stacking paleointensity and oxygen isotope data for the last 1.5 Myr (PISO-1500)." Earth and Planetary Science Letters **283**(1–4): 14-23.

Chen, A. P., R. Egli, et al. (2007). "First-order reversal curve (FORC) diagrams of natural and cultured biogenic magnetic particles." Journal of Geophysical Research: Solid Earth **112**(B8)

Cisowski, S. (1981). "Interacting vs. non-interacting single domain behavior in natural and synthetic samples." Physics of the Earth and Planetary Interiors **26**(1–2): 56-62.

Coe, R. S. (1967). "Paleo-intensities of the Earth's magnetic field determined from Tertiary and Quaternary rocks." Journal of Geophysical Research **72**(12): 3247-3262.

Cole, J. J., M. L. Pace, et al. (1993). "Bacterial biomass and cell size distributions in lakes: More and larger cells in anoxic waters." Limnology and Oceanography **38**(8): 1627-1632.

Constable, C. G. and R. L. Parker (1988). "Statistics of the geomagnetic secular variation for the past 5 m.y." Journal of Geophysical Research: Solid Earth **93**(B10): 11569-11581.

Dekkers, M. J. and H. N. Böhnel (2006). "Reliable absolute palaeointensities independent of magnetic domain state." Earth and Planetary Science Letters **248**(1–2): 508-517.

Dorgan, K. M., P. A. Jumars, et al. (2005). "Burrowing mechanics: Burrow extension by crack propagation." Nature **433**(7025): 475-475.

Dunlop, D. J. (2002). "Theory and application of the Day plot (Mrs/Ms versus Hcr/Hc) 1. Theoretical curves and tests using titanomagnetite data." Journal of Geophysical Research: Solid Earth **107**(B3): EPM 4-1-EPM 4-22.

Eder, S. H. K., H. Cadiou, et al. (2012). "Magnetic characterization of isolated candidate vertebrate magnetoreceptor cells." Proceedings of the National Academy of Sciences **109**(30): 12022-12027.

Egli, R. (2004). "Characterization of Individual Rock Magnetic Components by Analysis of Remanence Curves, 1. Unmixing Natural Sediments." Studia Geophysica et Geodaetica **48**(2): 391-446.

Egli, R. (2013). "VARIFORC: An optimized protocol for calculating non-regular first-order reversal curve (FORC) diagrams." Global and Planetary Change **110, Part C**(0): 302-320.

Egli, R., A. P. Chen, et al. (2010). "Detection of noninteracting single domain particles using first-order reversal curve diagrams." Geochemistry, Geophysics, Geosystems **11**(1): Q01Z11.

Egli, R. and W. Lowrie (2002). "Anhysteretic remanent magnetization of fine magnetic particles." Journal of Geophysical Research: Solid Earth **107**(B10): 2209.

Egli, R. and X. Zhao (2015). "Natural remanent magnetization acquisition in bioturbated sediment: General theory and implications for relative paleointensity reconstructions." Geochemistry, Geophysics, Geosystems: n/a-n/a.

Elsasser, W., E. P. Ney, et al. (1956). "Cosmic-Ray Intensity and Geomagnetism." Nature **178**(4544): 1226-1227.

Faivre, D. and D. Schüler (2008). "Magnetotactic Bacteria and Magnetosomes." Chemical Reviews **108**(11): 4875-4898.

Farina, M., D. M. S. Esquivel, et al. (1990). "Magnetic iron-sulphur crystals from a magnetotactic microorganism." Nature **343**(6255): 256-258.

Fenchel, T. (2001). "Eppur si muove: many water column bacteria are motile." Aquatic Microbial Ecology **24**(2): 197-201.

Fisher, R. (1953). "Dispersion on a Sphere." Proceedings of the Royal Society A: Mathematical, Physical and Engineering Sciences **217**(1130): 295-305.

Flies, C. B., J. Peplies, et al. (2005). "Combined Approach for Characterization of Uncultivated Magnetotactic Bacteria from Various Aquatic Environments." Applied and Environmental Microbiology **71**(5): 2723-2731.

Frankel, R. (2009). "The discovery of magnetotactic/magnetosensitive bacteria." Chinese Journal of Oceanology and Limnology **27**(1): 1-2.

Frankel, R. B. and R. P. Blakemore (1980). "Navigational compass in magnetic bacteria." Journal of Magnetism and Magnetic Materials **15–18, Part 3**(0): 1562-1564.

Galindo-Gonzalez, C., J. M. Feinberg, et al. (2009). "Magnetic and microscopic characterization of magnetite nanoparticles adhered to clay surfaces." American Mineralogist **94**(8-9): 1120-1129.

Geibert, W., M. M. Rutgers van der Loeff, et al. (2005). "Quantifying the opal belt in the Atlantic and southeast Pacific sector of the Southern Ocean by means of 230Th normalization." Global Biogeochemical Cycles **19**(4).

Gilder, S., Y. Chen, et al. (2001). "Oligo-Miocene magnetostratigraphy and rock magnetism of the Xishuigou section, Subei (Gansu Province, western China) and implications for shallow inclinations in central Asia." Journal of Geophysical Research **106**(B12): 30505.

Griffiths, D. H., R. F. King, et al. (1960). " The Remanent Magnetism of Some Recent Varved Sediments. " Proceedings of the Royal Society of London A: Mathematical, Physical and Engineering Sciences 256(1286): 359-383.

Guyodo, Y. and J.-P. Valet (1996). "Relative variations in geomagnetic intensity from sedimentary records: the past 200,000 years." Earth and Planetary Science Letters **143**(1–4): 23-36.

Guyodo, Y. and J.-P. Valet (1999). "Global changes in intensity of the Earth's magnetic field during the past 800[thinsp]kyr." Nature **399**(6733): 249-252.

Hammond, D. E., J. McManus, et al. (1996). "Early diagenesis of organic material in equatorial Pacific sediments: stpichiometry and kinetics." Deep Sea Research Part II: Topical Studies in Oceanography **43**(4–6): 1365-1412.

Hanzlik, M., M. Winklhofer, et al. (2002). "Pulsed-field-remanence measurements on individual magnetotactic bacteria." Journal of Magnetism and Magnetic Materials **248**(2): 258-267.

Hays, J. D. (1971). "Faunal Extinctions and Reversals of the Earth's Magnetic Field." Geological Society of America Bulletin **82**(9): 2433-2447.

Henshaw, P. C. and R. T. Merrill (1979). "Characteristics of drying remanent magnetization in sediments." Earth and Planetary Science Letters **43**(2): 315-320.

Heslop, D. (2007). "Are hydrodynamic shape effects important when modelling the formation of depositional remanent magnetization?" Geophysical Journal International **171**(3): 1029-1035.

Heslop, D., A. P. Roberts, et al. (2014). "Characterizing magnetofossils from first-order reversal curve (FORC) central ridge signatures." Geochemistry, Geophysics, Geosystems **15**(6): 2170-2179.

Heslop, D., A. P. Roberts, et al. (2013). "Quantifying magnetite magnetofossil contributions to sedimentary magnetizations." Earth and Planetary Science Letters **382**(0): 58-65.

Irving, E. (1957). "The Origin of the Palaeomagnetism of the Torridonian Sandstones of North-West Scotland." Philosophical Transactions of the Royal Society of London. Series A, Mathematical and Physical Sciences **250**(974): 100-110.

Irving, E. and A. Major (1964). "Post-Depositional Detrital Remanent Magnetization in a Synthetic Sediment." Sedimentology **3**(2): 135-143.

Jabbari-Farouji, S., G. H. Wegdam, et al. (2012). "Aging of rotational diffusion in colloidal gels and glasses." Physical Review E **86**(4): 041401.

Jarvis, P., B. Jefferson, et al. (2005). "A review of floc strength and breakage." Water Research **39**(14): 3121-3137.

Jezek, J., S. Gilder, et al. (2012). "Numerical simulation of inclination shallowing by rolling and slipping of spherical particles." Computers & Geosciences **49**(0): 270-277.

Jogler, C., M. Niebler, et al. (2010). "Cultivation-independent characterization of 'Candidatus Magnetobacterium bavaricum' via ultrastructural, geochemical, ecological and metagenomic methods." Environmental Microbiology **12**(9): 2466-2478.

Johnson, B., M. Barry, et al. (2012). "In situ tensile fracture toughness of surficial cohesive marine sediments." Geo-Marine Letters **32**(1): 39-48.

Johnson, E. A., T. Murphy, et al. (1948). "Pre-history of the Earth's magnetic field." Terrestrial Magnetism and Atmospheric Electricity **53**(4): 349-372.

Jonkers, A. R. T., A. Jackson, et al. (2003). "Four centuries of geomagnetic data from historical records." Reviews of Geophysics **41**(2).

Jonkers, A. T. (2007). Geomagnetism, History of. Encyclopedia of Geomagnetism and Paleomagnetism. D. Gubbins and E. Herrero-Bervera, Springer Netherlands**:** 355-360.

Kallmeyer, J., R. Pockalny, et al. (2012). "Global distribution of microbial abundance and biomass in subseafloor sediment." Proceedings of the National Academy of Sciences **109**(40): 16213-16216.

Karlin, R. (1990). "Magnetic mineral diagenesis in suboxic sediments at Bettis Site W-N, NE Pacific Ocean." Journal of Geophysical Research: Solid Earth **95**(B4): 4421-4436.

Katari, K. and L. Tauxe (2000). "Effects of pH and salinity on the intensity of magnetization in redeposited sediments." Earth and Planetary Science Letters **181**(4): 489-496.

Katari, K., L. Tauxe, et al. (2000). "A reassessment of post-depositional remanent magnetism: preliminary experiments with natural sediments." Earth and Planetary Science Letters **183**(1–2): 147-160.

Kent, D. V. (1973). "Post-depositional Remanent Magnetisation in Deep-sea Sediment." Nature **246**(5427): 32-34.

Kent, D. V. (1982). "Apparent correlation of palaeomagnetic intensity and climatic records in deep-sea sediments." Nature **299**(5883): 538-539.

Kim, M., S. M. Anthony, et al. (2011). "Colloidal rotation near the colloidal glass transition." The Journal of Chemical Physics **135**(5).

King, R. F. (1955). " The remanent magnetism of artificially deposited sediments.." Geophysical Journal International **7**: 115-134.

Kirschvink, J. L. and S.-B. R. Chang (1984). "Ultrafine-grained magnetite in deep-sea sediments: Possible bacterial magnetofossils." Geology **12**(9): 559-562.

Klootwijk, C. T., J. S. Gee, et al. (1992). "An early India-Asia contact: paleomagnetic constraints from Ninetyeast ridge, ODP Leg 121." Geology **20**(5): 395-398.

Kobayashi, A., J. L. Kirschvink, et al. (2006). "Experimental observation of magnetosome chain collapse in magnetotactic bacteria: Sedimentological, paleomagnetic, and evolutionary implications." Earth and Planetary Science Letters **245**(3–4): 538-550.

Koenderink, G. H., H. Zhang, et al. (2003). "On the validity of Stokes-Einstein-Debye relations for rotational diffusion in colloidal suspensions." Faraday Discussions **123**(0): 335-354.

Kono, M. (2007). 5.01 - Geomagnetism in Perspective. Treatise on Geophysics. G. Schubert. Amsterdam, Elsevier**:** 1-31.

Kuterbach, D. A., B. Walcott, et al. (1982). "Iron-Containing Cells in the Honey Bee (Apis mellifera)." Science **218**(4573): 695-697.

Løvlie, R. (1976). "The intensity pattern of post-depositional remanence acquired in some marine sediments deposited during a reversal of the external magnetic field." Earth and Planetary Science Letters **30**(2): 209-214.

Laj, C., C. Kissel, et al. (2000). "North Atlantic palaeointensity stack since 75ka (NAPIS–75) and the duration of the Laschamp event." Philosophical Transactions of the Royal Society of London. Series A: Mathematical, Physical and Engineering Sciences **358**(1768): 1009-1025.

Langel, R. A. and W. J. Hinze (1998). The magnetic field of the Earth's lithosphere: the satellite perspective, Cambridge University Press.

Larrasoaña, J. C., Q. Liu, et al. (2014). "Paleomagnetic and paleoenvironmental implications of magnetofossil occurrences in late Miocene marine sediments from the Guadalquivir Basin, SW Spain." Frontiers in Microbiology **5**: 71.

Leslie, B. W., S. P. Lund, et al. (1990). "Rock magnetic evidence for the dissolution and authigenic growth of magnetic minerals within anoxic marine sediments of the California continental borderland." Journal of Geophysical Research: Solid Earth **95**(B4): 4437-4452.

Levi, S. and S. K. Banerjee (1976). "On the possibility of obtaining relative paleointensities from lake sediments." Earth and Planetary Science Letters **29**(1): 219-226.

Li, J., Y. Pan, et al. (2010). "Biomineralization, crystallography and magnetic properties of bullet-shaped magnetite magnetosomes in giant rod magnetotactic bacteria." Earth and Planetary Science Letters **293**(3–4): 368-376.

Locat, J., H. Lee, et al. (2002). "Shear Strength Development with Burial in Eel River Margin Slope Sediments." Marine Georesources & Geotechnology **20**(2): 111-135.

Lowe, D. A. J., R. L. Parker, et al. (2001). "Estimating the crustal power spectrum from vector Magsat data." Journal of Geophysical Research **106**(B5).

Ludwig, P., R. Egli, et al. (2013). "Characterization of primary and secondary magnetite in marine sediment by combining chemical and magnetic unmixing techniques." Global and Planetary Change **110, Part C**(0): 321-339.

Lundin, R. (2001). "Erosion by the Solar Wind." Science **291**(5510).

Lundin, R., S. Barabash, et al. (2004). "Solar Wind-Induced Atmospheric Erosion at Mars: First Results from ASPERA-3 on Mars Express." Science **305**(5692): 1933-1936.

Mao, X., R. Egli, et al. (2014a). "Magneto-Chemotaxis in Sediment: First Insights." PLoS ONE **9**(7): e102810.

Mao, X., R. Egli, et al. (2014b). "Magnetotaxis and acquisition of detrital remanent magnetization by magnetotactic bacteria in natural sediment: First experimental results and theory." Geochemistry, Geophysics, Geosystems **15**(1): 255-283.

Martinez, Vincent A., R. Besseling, et al. (2012). "Differential Dynamic Microscopy: A High-Throughput Method for Characterizing the Motility of Microorganisms." Biophysical Journal **103**(8): 1637-1647.

McCormac, B. M. and J. E. Evans (1969). "Consequences of Very Small Planetary Magnetic Moments." Nature **223**(5212): 1255-1255.

McNeill, D. F. and J. L. Kirschvink (1993). "Early dolomitization of platform carbonates and the preservation of magnetic polarity." Journal of Geophysical Research: Solid Earth **98**(B5): 7977-7986.

Meadows, P. S. and J. Tait (1989). "Modification of sediment permeability and shear strength by two burrowing invertebrates." Marine Biology **101**(1): 75-82.

Meysman, F. J. R., B. P. Boudreau, et al. (2003). "Relations between local, nonlocal, discrete and continuous models of bioturbation." Journal of Marine Research **61**(3): 391-410.

Mitchell, J. G. and K. Kogure (2006). "Bacterial motility: links to the environment and a driving force for microbial physics." FEMS Microbiology Ecology **55**(1): 3-16.

Mitra, R. and L. Tauxe (2009). "Full vector model for magnetization in sediments." Earth and Planetary Science Letters **286**(3–4): 535-545.

Moskowitz, B. M., R. B. Frankel, et al. (1989). "A comparison of magnetite particles produced anaerobically by magnetotactic and dissimilatory iron-reducing bacteria." Geophysical Research Letters **16**(7): 665-668.

Muxworthy, A., W. Williams, et al. (2003). "Effect of magnetostatic interactions on the hysteresis parameters of single-domain and pseudo-single-domain grains." Journal of Geophysical Research: Solid Earth **108**(B11): n/a-n/a.

Muxworthy, A. R. and D. J. Dunlop (2002). "First-order reversal curve (FORC) diagrams for pseudo-single-domain magnetites at high temperature." Earth and Planetary Science Letters **203**(1): 369-382.

Néel, L. (1949). "Théorie du traînage magnétique des ferromagnétiques en grains fins avec applications aux terres cuites." Ann. géophys **5**(2): 99-136.

Nagata, T. (1961). Rock magnetism. Tokyo, Maruzen Co.

Needham, J., W. Ling, et al. (1962). Science and Civilisation in China. Vol. 4: Physics and Physical Technology. Part. 1: Physics. Cambridge, Cambridge University Press.

Neubert, T., M. Mandea, et al. (2001). "Ørsted satellite captures high-precision geomagnetic field data." Eos, Transactions American Geophysical Union **82**(7): 81-88.

Newell, A. J. (2005). "A high-precision model of first-order reversal curve (FORC) functions for single-domain ferromagnets with uniaxial anisotropy." Geochemistry, Geophysics, Geosystems **6**(5).

Opdyke, M. D. and J. E. Channell (1996). Magnetic stratigraphy, Academic Press.

Ouyang, T., D. Heslop, et al. (2014). "Variable remanence acquisition efficiency in sediments containing biogenic and detrital magnetites: Implications for relative paleointensity signal recording." Geochemistry, Geophysics, Geosystems **15**(7): 2780-2796.

Paterson, G. A., Y. Wang, et al. (2013). "The fidelity of paleomagnetic records carried by magnetosome chains." Earth and Planetary Science Letters **383**(0): 82-91.

Payne, M. A. and K. L. Verosub (1982). "The acquisition of post-depositional detrital remanent magnetization in a variety of natural sediments." Geophysical Journal International **68**(3): 625-642.

Pemberton, G. S., M. J. Risk, et al. (1976). "Supershrimp: Deep Bioturbation in the Strait of Canso, Nova Scotia." Science **192**(4241): 790-791.

Perrin, F. (1934). "Mouvement brownien d'un ellipsoide - I. Dispersion diélectrique pour des molécules ellipsoidales." J. Phys. Radium **5**(10): 497-511.

Petermann, H. and U. Bleil (1993). "Detection of live magnetotactic bacteria in South Atlantic deep-sea sediments." Earth and Planetary Science Letters **117**(1–2): 223-228.

Petersen, N., T. von Dobeneck, et al. (1986). "Fossil bacterial magnetite in deep-sea sediments from the South Atlantic Ocean." Nature **320**(6063): 611-615.

Pisias, N. G., L. A. Mayer, et al. (1995). "Paleoceanography of the eastern equatorial Pacific during the Neogene: synthesis of Leg 138 drilling results." Proceedings of the Ocean Drilling Program. Scientific results **138**.

Rabouille, C. and J. F. Gaillard (1991). "A coupled model representing the deep-sea organic carbon mineralization and oxygen consumption in surficial sediments." Journal of Geophysical Research: Oceans **96**(C2): 2761-2776.

Raup, D. M. (1985). "Magnetic reversals and mass extinctions." Nature **314**(6009): 341-343.

Reed, D. C., K. Huang, et al. (2006). "Steady-state tracer dynamics in a lattice-automaton model of bioturbation." Geochimica et Cosmochimica Acta **70**(23): 5855-5867.

Richter, R. (1952). "Fluidal-texture in Sediment-Gesteinen und ober Sedifluktion überhaupt." Notizbl. Hess. L.-Amt. Bodenforsch **3**: 67-81.

Roberts, A. P., L. Chang, et al. (2012). "Searching for single domain magnetite in the “pseudo-single-domain” sedimentary haystack: Implications of biogenic magnetite preservation for sediment magnetism and relative paleointensity determinations." Journal of Geophysical Research: Solid Earth **117**(B8): B08104.

Roberts, A. P., C. R. Pike, et al. (2000). "First-order reversal curve diagrams: A new tool for characterizing the magnetic properties of natural samples." Journal of Geophysical Research: Solid Earth **105**(B12): 28461-28475.

Roberts, A. P., L. Tauxe, et al. (2013). "Magnetic paleointensity stratigraphy and high-resolution Quaternary geochronology: successes and future challenges." Quaternary Science Reviews **61**: 1-16.

Roberts, A. P. and M. Winklhofer (2004). "Why are geomagnetic excursions not always recorded in sediments? Constraints from post-depositional remanent magnetization lock-in modelling." Earth and Planetary Science Letters **227**(3–4): 345-359.

Sagnotti, L., F. Budillon, et al. (2005). "Evidence for a variable paleomagnetic lock-in depth in the Holocene sequence from the Salerno Gulf (Italy): Implications for “high-resolution” paleomagnetic dating." Geochemistry, Geophysics, Geosystems **6**(11).

Sarmiento, J. L. and N. Gruber (2006). Ocean Biogeochemical Dynamics. Princeton, N. J., Princeton Univ. Press.

Seki, K., R. C. Elphic, et al. (2001). "On Atmospheric Loss of Oxygen Ions from Earth Through Magnetospheric Processes." Science **291**(5510): 1939-1941.

Šestanović, S., M. Šolić, et al. (2005). "Volume, abundance and biomass of sediment bacteria in the eastern mid Adriatic Sea." Acta adriatica **46**(2): 177-191.

Shcherbakov, V. and N. Sycheva (2010). "On the mechanism of formation of depositional remanent magnetization." Geochemistry, Geophysics, Geosystems **11**(2).

Shcherbakov, V. P. and V. V. Shcherbakova (1983). "On the theory of depositional remanent magnetization in sedimentary rocks." Geophysical surveys **5**(4): 369-380.

Shcherbakov, V. P. and V. V. Shcherbakova (1987). "On the physics of acquisition of post-depositional remanent magnetization." Physics of the Earth and Planetary Interiors **46**(1–3): 64-70.

Shcherbakov, V. P., N. K. Sycheva, et al. (1996). "Monte Carlo modelling of TRM and CRM acquisition and comparison of their properties in an ensemble of interacting SD grains." Geophysical Research Letters **23**(20): 2827-2830.

Shull, D. H. (2001). "Transition-matrix model of bioturbation and radionuclide diagenesis." Limnology and Oceanography **46**(4): 905-916.

Simpson, E. T., T. Kasama, et al. (2005). "Magnetic induction mapping of magnetite chains in magnetotactic bacteria at room temperature and close to the Verwey transition using electron holography." Journal of Physics: Conference Series **17**: 108-121.

Smith, C. R. and C. Rabouille (2002). "What controls the mixed-layer depth in deep-sea sediments? The importance of POC flux." Limnology and Oceanography **47**(2): 418-426.

Solan, M., B. D. Wigham, et al. (2004). "In situ quantification of bioturbation using time-lapse fluorescent sediment profile imaging (f-SPI), luminophore tracers and model simulation." Marine Ecology Progress Series **271**: 1-12.

Spassov, S. and J.-P. Valet (2012). "Detrital magnetizations from redeposition experiments of different natural sediments." Earth and Planetary Science Letters **351–352**(0): 147-157.

Spring, S., R. Amann, et al. (1995). "Phylogenetic Analysis of Uncultured Magnetotactic Bacteria from the Alpha-Subclass of Proteobacteria." Systematic and Applied Microbiology **17**(4): 501-508.

Stacey, F. (1972). "On the role of Brownian motion in the control of detrital remanent magnetization of sediments." pure and applied geophysics **98**(1): 139-145.

Steinberger, B., N. Petersen, et al. (1994). "Movement of magnetic bacteria in time-varying magnetic fields." Journal of Fluid Mechanics **273**: 189-211.

Stolz, J. F., S.-B. R. Chang, et al. (1986). "Magnetotactic bacteria and single-domain magnetite in hemipelagic sediments." Nature **321**(6073): 849-851.

Stott, L., C. Poulsen, et al. (2002). "Super ENSO and Global Climate Oscillations at Millennial Time Scales." Science **297**(5579): 222-226.

Suganuma, Y., J. i. Okuno, et al. (2011). "Post-depositional remanent magnetization lock-in for marine sediments deduced from 10Be and paleomagnetic records through the Matuyama–Brunhes boundary." Earth and Planetary Science Letters **311**(1–2): 39-52.

Sverdrup, H. U., M. W. Johnson, et al. (1942). The Oceans: Their physics, chemistry, and general biology, Prentice-Hall New York.

Tarduno, J. A., W. Tian, et al. (1998). "Biogeochemical remanent magnetization in pelagic sediments of the western equatorial Pacific Ocean." Geophysical Research Letters **25**(21): 3987-3990.

Tarduno, J. A. and S. L. Wilkison (1996). "Non-steady state magnetic mineral reduction, chemical lock-in, and delayed remanence acquisition in pelagic sediments." Earth and Planetary Science Letters **144**(3–4): 315-326.

Tauxe, L. (1993). "Sedimentary records of relative paleointensity of the geomagnetic field: Theory and practice." Reviews of Geophysics **31**(3): 319.

Tauxe, L. (1998). Paleomagnetic principles and practice, Springer Science & Business Media.

Tauxe, L. and D. V. Kent (1984). "Properties of a detrital remanence carried by haematite from study of modern river deposits and laboratory redeposition experiments." Geophysical Journal International **76**(3): 543-561.

Tauxe, L. and D. V. Kent (2004). A Simplified Statistical Model for the Geomagnetic Field and the Detection of Shallow Bias in Paleomagnetic Inclinations: was the Ancient Magnetic Field Dipolar? Timescales Of The Paleomagnetic Field, American Geophysical Union**:** 101-115.

Tauxe, L. and H. Staudigel (2004). "Strength of the geomagnetic field in the Cretaceous Normal Superchron: New data from submarine basaltic glass of the Troodos Ophiolite." Geochemistry, Geophysics, Geosystems **5**(2).

Tauxe, L., J. L. Steindorf, et al. (2006). "Depositional remanent magnetization: Toward an improved theoretical and experimental foundation." Earth and Planetary Science Letters **244**(3-4): 515-529.

Tauxe, L. and T. Yamazaki (2007). 5.13 - Paleointensities. Treatise on Geophysics. G. Schubert. Amsterdam, Elsevier**:** 509-563.

Teal, L. R., M. T. Bulling, et al. (2008). "Global patterns of bioturbation intensity and mixed depth of marine soft sediments." Aquatic Biology **2**(3): 207.

Thellier, E. and O. Thellier (1959). "Sur l'intensité du champ magnétique terrestre dans le passé historique et géologique." Ann. Geophys. **15**: 285-376.

Torquato, S. (1995). "Nearest-neighbor statistics for packings of hard spheres and disks." Physical Review E **51**(4): 3170-3182.

Trauth, M. H., M. Sarnthein, et al. (1997). "Bioturbational mixing depth and carbon flux at the seafloor." Paleoceanography **12**(3): 517-526.

Tucker, P. (1979). "Selective post-depositional realignment in a synthetic sediment." Physics of the Earth and Planetary Interiors **20**(1): p11-p14.

Tucker, P. (1980). "A grain mobility model of post-depositional realignment." Geophysical Journal International **63**(1): 149-163.

Valet, J.-p. and L. Meynadier (1993). "Geomagnetic field intensity and reversals during the past four million years." Nature **366**(6452): 234-238.

van Vreumingen, M. J. (1993). "The influence of salinity and flocculation upon the acquisition of remanent magnetization in some artificial sediments." Geophysical Journal International **114**(3): 607-614.

Verosub, K. L., R. A. Ensley, et al. (1979). "The role of water content in the magnetization of sediments." Geophysical Research Letters **6**(4): 226-228.

Wack, M. R. and S. A. Gilder (2012). "The SushiBar: An automated system for paleomagnetic investigations." Geochemistry, Geophysics, Geosystems **13**(3): Q12Z38.

Walker, M. M., T. E. Dennis, et al. (2002). "The magnetic sense and its use in long-distance navigation by animals." Current Opinion in Neurobiology **12**(6): 735-744.

Weitz, D. (2011). Colloidal Glasses. Glasses and Grains. B. Duplantier, T. C. Halsey and V. Rivasseau, Springer Basel. **61:** 25-39.

Wilson, L. G., V. A. Martinez, et al. (2011). "Differential Dynamic Microscopy of Bacterial Motility." Physical Review Letters **106**(1): 018101.

Wiltschko, W. and R. Wiltschko (2005). "Magnetic orientation and magnetoreception in birds and other animals." Journal of Comparative Physiology A **191**(8): 675-693.

Winch, D. E., D. J. Ivers, et al. (2005). "Geomagnetism and Schmidt quasi-normalization." Geophysical Journal International **160**(2): 487-504.

Won, J. (2013). "Anisotropic strength ration and plasticity index of natural clays." Proceedings of the 18th international conference on soil mechanics and geotechnical engineering, Paris, pp. 445-448.

Yamazaki, T., Y. Yamamoto, et al. (2013). "Rock-magnetic artifacts on long-term relative paleointensity variations in sediments." Geochemistry, Geophysics, Geosystems **14**(1): 29-43.

Yu, Y., L. Tauxe, et al. (2004). "Toward an optimal geomagnetic field intensity determination technique." Geochemistry, Geophysics, Geosystems **5**(2).

Zhu, R. X., K. A. Hoffman, et al. (2001). "Earliest presence of humans in northeast Asia." Nature **413**(6854): 413-417.

Zhu, R. X., R. Potts, et al. (2004). "New evidence on the earliest human presence at high northern latitudes in northeast Asia." Nature **431**(7008): 559-562.

Acknowledgments

Every road comes to an end. I would like to thank people who helped me along the way in the past four years:

- My supervisor Ramon Egli. I benefit from his rigorous thinking and wide knowledge of science all the time. He is amazingly fast in learning new things, yet he is always patient when I struggle to follow.
- Stuart Gilder, both for his encouragement and criticism. Without his critical opinions in the initial stage of the experiments, I may never be determined to perform redeposition experiments with unprecedented amount of samples.
- Nikolai Petersen. He is a real gentleman. His love in science is inspiring. I am impressed by his knowledge, patience and kindness. I appreciate his advice during my difficult time when Ramon just left LMU.
- Qingsong Liu. He supported my decision to pursue PhD study in LMU. His advice and encouragement helped me through the difficult time when I encountered setbacks in the early stage of the PhD study.
- Manuela Weiss for her cares in Niederlippach and heartwarming birthday greetings.
- Colleagues in the paleomagnetism group in Munich for their helps and discussions, e.g. Xuegang Mao and Qingguo Wei, Kuang He, Yanjun Cheng, all Michaeles, Pieter Smid, Valerian Bachtadse, Uwe Kirscher, Edoardo Dallanave, Florian Lhuillier.
- Moritz Bernauer, Lorenzo Colli, Thomas Chust, Maria Nader-Nieto, Lion Krischer for creating a pleasant working environment in Room 417.
- Other colleagues, e.g., Jens Weismüller and Kasra Hosseini Zad, for interesting conversations.
- Christoph Moder and roommates (Federico Benetti, Noppadol Mekareeya, Yue You) for their friendships.
- Former colleagues in Beijing for their helps over the years.
- Mike Jackson and Dario Bilardello at IRM (Institute for rock magnetism, University of Minnesota) for their kind help in measurements. IRM visiting fellowship is acknowledged for supporting me to perform rock magnetic measurements at IRM.
- DFG (Deutsche Forschungsgemeinschaft) for funding my PhD study. (Grant Nr. EG294/2-1)
- Owners of Warmi Nudeln Bar. I enjoyed their food and friendship very much, which can warm bitter winters.
- Xiang Zhao, Yong Wei and Youwei Xu for their inspiring academic discussions.
- Friends in Trier. I had a very relaxing time with them, making foods, playing volleyball, jogging and taking photos. Pleasant memory!
- My family. Thanks for your unconditional supports all the time!